AN ABSTRACT OF THE THESIS OF

Adin Berberović for the degree of
Master of Science in
Wood Science presented
on May 24, 2007
Title: Numerical Simulation of Wood Drying

Abstract approved:

_____

Michael R. Milota

A mathematical and then a numerical model were developed for simulating a convective batch lumber drying process. The model incorporates mass and heat transfer relationships within the lumber stack, as well as thermodynamic properties of the wood and drying air. It takes into account a change of air properties along the stack and its effect on the mass and heat transfer parameters. Kiln and individual board properties as well as a drying schedule are the input parameters that are defined and entered by a user. The model relies on the drying rate functions which are empirical correlations based on single-board tests.

The drying rate function for hemlock was obtained based on experiment results from 23 small charges dried over a range of conditions used in industry. Three larger batches of hemlock were also dried using three different industrial schedules.

The change of average moisture content with time predicted by the model was verified by weighing a kiln charge with load cells during drying. The change of board temperatures and temperature drop along the stack were verified by measuring the actual temperatures in the kiln during drying.

The model was first validated against data available in the literature. Then the experimentally-determined drying function for hemlock was used as the model input and the model output was compared to the larger hemlock batches. Validated variables for both cases were board temperatures, temperature drop through the package and average moisture content of the package.

Numerical Simulation of Wood Drying

by
Adin Berberović

A THESIS

submitted to

Oregon State University

in partial fulfillment of
the requirements for the
degree of

Master of Science

Presented May 24, 2007
Commencement June 2008

Master of Science thesis of Adin Berberović presented on May 24, 2007

APPROVED:

_____

Major Professor, representing Wood Science

_____

Head of the Department of Wood Science and Engineering

_____

Dean of the Graduate School

I understand that my thesis will become part of the permanent collection of Oregon State University libraries. My signature below authorizes release of my thesis to any reader upon request.

_____

Adin Berberović, Author

ACKNOWLEDGMENTS

Without the great support that I had it would not be possible to accomplish this work and therefore I would like to thank:

Professor Mike Milota, from Oregon State University, who was my major professor and my main support throughout this whole project.

Professor Jim Funck, from Oregon State University, who helped me reveal how to relate computer electronics and wood sciences which was an important aspect of the project.

Professor Ron Metoyer, from Oregon State University, whose class on computer graphics I took was my guide in making a visualization part of the simulation.

Milo Clauson, from Oregon State University, who helped me in conducting the experiments for the model validation.

Professor Bogosav Vasiljević, from the Faculty of Mechanical Engineering in Belgrade, whose lectures and classes I took gave me a strong background in thermodynamics.

My family, as my most important support to which I dedicate all my work.

THANK YOU ALL !

TABLE OF CONTENTS

	Page
1. Introduction…….	1
2. Literature Review……	5
2.1 Introduction……..…….	5
2.2 Single-board drying models based on a drying rate function……...	13
2.3 Single-board drying models describing a movement of each phase of moisture in wood…….....	14
2.4 Determinant stack drying models ……..	24
2.5 Stochastic stack drying models……	31
2.6 Conclusion……...	40
2.6.1 Single-board drying models……	40
2.6.2 Stack drying models……	42
3. Mathematical description of the model……...	45
3.1 Surface temperature (Energy conservation)……..	49
3.2 Air temperature (Energy conservation)…….	51
3.3 Board temperature (Energy conservation)……	54
3.4 Absolute humidity of air (Mass conservation)…….....	55
3.5 Moisture content of a board (Mass conservation)…….	57
3.6 Thermophysical properties of air, water and wood……...	59

TABLE OF CONTENTS (Continued)

Page

3.6.1 Thermophysical properties of air and water……. 59

3.6.2 Thermophysical properties of wood…… 63

4. A general algorithm used in the model……... 64

5. Materials and methods…… 70

5.1 Introduction…… 70

5.2 Obtaining a drying rate function…… 70

5.2.1 Experiments……. …… 70

5.2.2 Data analysis……. ……... 79

5.3 Experiments for validation…….. 82

5.3.1 Experiments…. …….. 82

5.3.2 Analysis…….. 86

6. Results and validation…… 88

6.1Experimental……..……... 88

6.1.1 Drying rate function……..... 88

6.1.2 Package drying…… 96

TABLE OF CONTENTS (Continued)

Page

6.1.2.1 Charge 1…….…….. 96
6.1.2.2 Charge 2……. 99
6.1.2.3 Charge 3……. 103
6.1.2.4 Comparisons……. 107

6.2 Validation…….. 107

6.2.1 Loblolly pine…….. 107

6.2.1.1 Mass transfer……..... 110
6.2.1.2 Heat transfer……. 111

6.2.2 Hemlock……. 112

6.2.2.1 Mass transfer……..... 114
6.2.2.2 Heat transfer…….. 116

7. Discussion……... 119

8. Conclusions……. 129

Nomenclature……..... 132

Bibliography…… 136

LIST OF FIGURES

Figure Page

2.1.1 Typical drying rate curve under constant drying conditions (Mujumdar and Devahastin 2000)……...…….. 10

2.1.2 A generalized form of drying rate curve (Milota and Tschernitz 1990) 13

2.3.1 Schematic drawing of steady state flow between two different boundary conditions (Hart 1964)….……...……... 16

2.3.2 Moisture concentration distribution during period A (solid curves) and period B (dashed curves) (Hart 1964)……. 18

2.3.3 Moisture content of southern pine lumber during drying (model and experimental data) (Stanish et al. (1986))……..... 20

2.3.4 Temperature and moisture distribution in southern pine lumber with time (model and experimental data) (Stanish et al. (1986))…….. 21

2.3.5 Temperature and moisture distribution in Douglas fir lumber with time (model and experimental data) (Stanish et al. (1986))…….. 22

2.3.6 Temperature and moisture distribution in brick with time (model and experimental data) (Stanish et al. (1986))……..... 23

LIST OF FIGURES (Continued)

Figure Page

2.3.7 Temperature and moisture profiles and the predicted position of evaporation plane as a function of time for 100mm x 50mm boards of heartwood (Pang et al. (1992))……..... 23

2.3.8 Temperature and moisture profiles and the predicted position of evaporation plane as a function of time for 100mm x 50mm boards of mixed wood (Pang et al. (1992))…….. 23

2.3.9 Temperature and moisture profiles and the predicted position of evaporation plane as a function of time for 100mm x 50mm boards of heartwood (Pang et al. (1992))…….. 24

2.4.1 Measured centerline temperature and predicted temperature from model for center board in the uninterrupted drying experiment (Milota and Tschernitz 1994)……. 25

2.4.2 Temperature drop through the package as measured and as predicted by the model for the uninterrupted drying experiment (Milota and Tschernitz 1994)……..... 26

2.4.3 Average moisture content of the package as measured and predicted by the model(Milota and Tschernitz 1994)…… 26

2.4.4 Average moisture content during drying (measured and from the model) (Sun et al. 1996)……. 28

LIST OF FIGURES (Continued)

Figure	Page
2.4.5 Average moisture content during drying (Awadalla et al.2003)……	29
2.4.6 The moisture content variation for a stack of mixed sapwood/heartwood boards……	30
2.5.1 Moisture change using a single set point schedule (Cronin et al. 2003)	32
2.5.2 Moisture change using a double set point schedule (Cronin et al. 2003)…….	33
2.5.3. (a) Mean moisture content vs, time for a single set point schedule (b) standard deviation in moisture content vs. time for a single set point schedule (Cronin et al. 2003)……	35
2.5.4. (a) Mean moisture content vs. time for a double set point schedule (b) standard deviation in moisture content vs. time for a double set point schedule (Cronin et al. 2003)……	36
2.5.5 Green moisture content distribution (Kayihan 1984)……	39
2.5.6 Drying curve of the charge (Kayihan 1984)……..	39
2.5.7 Dry moisture content distribution (Kayihan 1984)……	40
3.1 Illustration of a stack and a close look at a pair of boards and air between them on which the mass and energy balances are applied…….	46

LIST OF FIGURES (Continued)

Figure	Page
3.1.1 Parameters for calculating a surface and board centerline temperature (T_s and T_m)……	51
3.2.1 Parameters for calculating an air temperature T_g……..	53
3.4.1 Parameters for calculating air humidity Y…….	57
3.5.1 Parameters for calculating board moisture content X ……...	58
4.1 The algorithm used in modeling……...	65
4.1 (Continued) The algorithm used in modeling…….....	66
4.1 (Continued)The algorithm used in modeling…….....	67
4.2 The algorithm used for reading data from an Excel sheet……	68
4.2 The algorithm used for reading data from an Excel sheet……	69
5.2.1.1 Dry- and wet-bulb temperatures and drying time used for small charges of hemlock (Charge 1 and 2)…….	73
5.2.1.2 Dry- and wet-bulb temperatures and drying time used for small charges of hemlock (Charge 3)……...	73

LIST OF FIGURES (Continued)

Figure Page

5.2.1.3 Dry- and wet-bulb temperatures and drying time used for small charges of hemlock (Charge 4)……... 74

5.2.1.4 Dry- and wet-bulb temperatures and drying time used for small charges of hemlock (Charge 5)……..... 74

5.2.1.5 Dry- and wet-bulb temperatures and drying time used for small charges of hemlock (Charge 6)……... 75

5.2.1.6 Dry- and wet-bulb temperatures and drying time used for small charges of hemlock (Charge 7)……... 75

5.2.1.7 Dry- and wet-bulb temperatures and drying time used for small charges of hemlock (Charge 8 and 9)……. 76

5.2.1.8 Dry- and wet-bulb temperatures and drying time used for small charges of hemlock (Charge 10)……..... 76

5.2.1.9 Dry- and wet-bulb temperatures and drying time used for small charges of hemlock (Charge 11)……. 77

5.2.1.10 Dry- and wet-bulb temperatures and drying time used for small charges of hemlock (Charge 12)……. 77

5.2.1.11 Dry- and wet-bulb temperatures and drying time used for small charges of hemlock (Charge 13, 14, and 15)…….. 78

LIST OF FIGURES (Continued)

Figure Page

5.2.1.12 Dry- and wet-bulb temperatures and drying time used for small charges of hemlock (Charge 16, 17, and 18)……... 78

5.2.1.13 Dry- and wet-bulb temperatures and drying time used for small charges of hemlock (Charge 19, 20, 21, 22, and 23)…..……. 79

5.2.2.1 End view of stack with numbered boards and TDAL thermocouple placement ( )…….. 83

5.2.2.2 Side and end view of board with mounted thermocouples …… 84

6.1.1.1 Fluxes divided by wet-bulb depression versus moisture content…... 88

6.1.1.2 Drying fluxes versus wet-bulb depression for a constant rate period. 89

6.1.1.3 Drying fluxes versus difference between moisture and equilibrium moisture content for a falling rate period (Tdb=224.6ºF)…….. 90

6.1.1.4 Drying fluxes versus difference between moisture and equilibrium moisture content for a falling rate period (Tdb=199.4ºF)……... 91

6.1.1.5 Drying fluxes versus difference between moisture and equilibrium moisture content for a falling rate period (Tdb=181.4ºF)……... 91

6.1.1.6 Drying fluxes versus difference between moisture and equilibrium moisture content for a falling rate period (Tdb=176ºF)…….. 92

LIST OF FIGURES (Continued)

Figure	Page
6.1.1.7 Predicted versus actual fluxes for the falling rate period……..	93
6.1.1.8 Impact of the variable n on the shape of the drying function curve....	94
6.1.1.9 Comparison of drying fluxes for both drying periods predicted by drying function to that measured……	95
6.1.2.1.1 Temperature drop through the package as measured and as predicted by the model (Charge 1)……..	97
6.1.2.1.2 Average moisture content of the package as measured and as predicted by the model (Charge 1)……..	98
6.1.2.1.3 Board-by-board comparison of ending moisture content distribution predicted by the model to that measured (Charge 1)…	98
6.1.2.2.1 Centerline temperature for a board (10, C) as measured and as predicted by the model (Charge 2)……	100
6.1.2.2.2 Centerline temperature for a board (10, F) as measured and as predicted by the model (Charge 2)……..	101
6.1.2.2.3 Temperature drop through the package as measured and as predicted by the model (Charge 2)……..	101

LIST OF FIGURES (Continued)

Figure Page

6.1.2.2.4 Average moisture content of the package as measured and as predicted by the model (Charge 2)…….. 102

6.1.2.2.5 Board-by-board comparison of ending moisture content distribution predicted by the model to that measured (Charge 2)… 102

6.1.2.3.1 Centerline temperature for a board (10, A) as measured and as predicted by the model (Charge 3)…….. 104

6.1.2.3.2 Centerline temperature for a board (10, B) as measured and as predicted by the model (Charge 3)…….. 105

6.1.2.3.3 Temperature drop through the package as measured and as predicted by the model (Charge 3)…….. 105

6.1.2.3.4 Average moisture content of the package as measured and as predicted by the model (Charge 3)…….. 106

6.1.2.3.5 Board-by-board comparison of ending moisture content distribution predicted by the model to that measured (Charge 3)… 106

6.2.1.1 Average moisture content of the package as measured (Milota and Tschernitz 1994) and as predicted by the model…… 109

LIST OF FIGURES (Continued)

Figure Page

6.2.1.2 Centerline temperature for center board in the uninterrupted drying experiment as measured (Milota and Tschernitz 1994) and as predicted by the model……..... 109

6.2.1.3 Temperature drop through the package for the uninterrupted drying experiment as measured (Milota and Tschernitz 1994) and as predicted by the model ……..…….. 110

7.1 Effect of the condensation coefficient on average moisture content prediction…….. 120

7.2 Influence of the time step on accuracy of the average moisture content prediction……. 123

7.3 Influence of the time step on accuracy of the board temperature prediction…….. 124

7.4 Effect of the velocity on average moisture content of the package during drying……..... 125

7.5 Effect of fan reversal times on average moisture content from one side of the package to the other. Initial airflow was from left to right…… 126

LIST OF TABLES

Table	Page
2.1.1 Overview of mathematical models made to date……..	7
2.1.1 (Continued) Overview of mathematical models made to date……..	8
2.1.1 (Continued) Overview of mathematical models made to date……..	9
2.3.1 Calculated time required to dry one-inch thick wood of 0.5 specific gravity (green volume basis) to ten percent average moisture content at 150°F (Hart 1964)…….....	19
5.2.1.1 Drying schedules for 23 charges of hemlock for obtaining the drying function……	72
5.2.2.1 Schedule for the first charge used for the model validation……	85
5.2.2.2 Schedule for the second charge used for the model validation……..	85
5.2.2.3 Schedule for the third charge used for the model validation……..	85
6.1.2.1.1 Parameters of the boards measured before and after drying (Charge 1)…….....	96
6.1.2.2.1 Parameters of the boards measured before and after drying (Charge 2)……...	100

LIST OF TABLES (Continued)

Table	Page
6.1.2.3.1 Parameters of the boards measured before and after drying (Charge 3)……	104
6.2.1.1 Values of the parameters used in the simulation (Loblolly pine)…..	108
6.2.2.1 Values of the parameters used in the simulation (Charge 1)…….	113
6.2.2.2 Values of the parameters used in the simulation (Charge 2)……..	113
6.2.2.3 Values of the parameters used in the simulation (Charge 3)……..	114

Numerical Simulation of Wood Drying

1. Introduction

The operation of drying reduces the moisture content of wood. The liquid evaporates into a vapor phase by the application of heat. It is one of the oldest and most common chemical engineering unit operations. There are over four hundred reported types of dryers in use.

Drying is an essential operation in the wood processing industries and is needed for the following reasons:

a) Preservation and storage

b) Reduction in cost of transportation by a weight reduction

c) Increased mechanical properties

d) Dimensional stability

e) Increased specific heat of combustion

f) Achieving an appropriate color of the wood product

g) Ability to be painted or finished

National energy consumption for industrial drying operations ranges from 10-25% for highly developed countries **(**Mujumdar and Devahastin 2000**)** which makes the drying process important not only in terms of wood product quality but also in terms of energy consumption.

Convective lumber drying not only consumes a lot of energy, it also requires one to several tens of days. For example, the energy consumption for convective drying of 6/4 red oak boards from 80% to 7% moisture content is 6.09 million

Btu/thousand fbm and the whole drying process takes approximately 36 days **(**Forest Products Laboratory 1999**)**.

The structure of wood limits how fast water can move through wood. In addition, the sensitivity of the structure to stresses set up in drying limits the drying rate. Very fast drying causes defects such as surface and internal checks, splits, collapse, and warp. The variability of wood properties in different directions makes the drying process more complicated. Each species has different properties, and even within the same species, the variability in drying rate and properties imposes limitations on the development of standard drying procedures. In many cases, improper drying may lead to inferior product quality and therefore a non-salable product.

One of the main challenges in wood drying is choosing an optimal drying regime. The optimal drying regime means the values of temperature, humidity, air velocity, and stacking geometry for which the best quality, shortest drying time, and lowest energy consumption are achieved. A numerical simulation can be beneficial in choosing the optimal drying schedule by predicting drying variables, such as final moisture content, very quickly and accurately without running a kiln. Given sets of predicted output drying variables for different input drying parameters makes it easier to choose the most optimal drying regime.

The interactions of wood, water, heat, and stress during drying are very complex. The moisture content and temperature of wood as well as humidity and temperature of drying air along with all their thermophysical properties and transfer coefficients change during drying.

Even though the majority of processes taking place during drying can be described by differential equations, there are parameters and coefficients that can not

be described by equations. In these cases, experiments are used for obtaining the parameters' behavior. Experiments are also used for validating results calculated by the numerical simulation. Therefore, the best approach in describing a drying process is using an integration of mathematical modeling using a system of coupled differential equations and results and conclusions obtained from experiments.

The purpose of this work was to create and validate a model that simulates the processes taking place within a lumber stack during kiln drying and predicts the values of the main drying variables such as temperature of the wood and air, moisture content of the wood, humidity of the air, and the temperature drop along the stack. A further purpose of the work was to develop a drying rate function so the model can be applied to western hemlock lumber. Based on the steps necessary to create and validate the model, the objectives of this work are:

1) Make a valid mathematical model that describes the heat and mass transfer processes occurring in a stack of lumber during drying.

2) Develop drying rate function for hemlock which will be used in the mathematical model to describe how fast moisture moves through wood.

3) Validate the model by comparing the experimental results obtained by drying a stack of hemlock boards to the results obtained from the simulation.

Even though there are many simulations dealing with wood drying already made, there are several advantages in making an original simulation:

1) All the assumptions made in deriving the mathematical and numerical model are known which is important in terms of accuracy and range of use of the simulation.

2) Unlike other simulations, this simulation incorporates an input programming module which communicates with Excel enabling the simulation to import all the input parameters from an Excel sheet. It gives the simulation a greater range of use and also makes it easier for a user to enter input drying parameters.

3) It can also export all the output drying parameters into an Excel sheet which enables a user to do statistics or other analyses on the data, draw various charts and thereby get a better insight into the drying process, and share the data more easily with other users.

4) It takes advantage of Visual Basic environment by using graphical tools for showing parameters such as temperature, moisture content, humidity of boards, and air channels between boards. All the current values of these parameters can be easily checked by selecting the board and air elements by right-clicking a mouse.

The impact of this work will be to integrate wood drying and computer science in a simulation that can predict the values of the drying variables and help a user to gain insight into wood drying behavior.

2. Literature Review

2.1 Introduction

The structural complexity of wood is one of the difficulties in mathematical modeling. Structural changes, such as shrinkage and pit aspiration, take place during drying which makes wood behavior even harder to simulate. A capillary-porous structure causes a capillary pressure to emerge. There is also a chemical interaction between wood and bound water. These factors lead to the conclusion that moisture movement in wood may not be attributable to a single physical phenomenon.

A summary of some of the models in the literature is given in the Table 2.1.1. The wood drying models in the literature can be divided into two groups:

a) Single-board drying models

b) Stack drying models that simulate the drying of a stack of lumber consisting of many boards by using a single-board drying model applied on each board

The mathematical models describing a single-board drying process can be categorized into two groups:

a) Models based on a drying rate function that describes how the average moisture content of a board changes with drying parameters

b) Models based on thermodynamic relations describing how each form of moisture (free water, water vapor and bound water) moves through wood under certain drying conditions

Stack models can be further classified as deterministic or stochastic. Deterministic stack models are based on the laws of energy and mass conservation. In these models, a single-board drying model is applied on each board in a stack. Calculations are also made of the temperature and humidity change of the drying air flowing through the stack using energy and mass conservation equations.

Stochastic models use relationships between the dependent variables, such as air temperature and initial wood moisture content, and the independent variables, such as final wood moisture content.

The stochastic relations are obtained by observing and measuring their values during drying. In these models, the stack is considered as a system and boards as different elements. Stochastic relationships between the drying variables and the independent variables are applied on each board (element). This may change with position in the stack (system).

Table 2.1.1 Overview of mathematical models made to date.

Author	Year	Drying Material		Drying Object		Type of Model	
		Wood	Any porous media	Single board	Stack	Characteristic function	Modeling of each phase of moisture
Alvear et al	2003	x			x	x	
Awadalla et al	2004	x			x	x	
Baronas et al.	1999	x		x			x
Baronas et al.	2001	x		x			x
Belhanri	2003		x	x			x
Berger and Pei	1972	x	x	x			x
Bramhall	1978	x			x		x
Cronin et al.	2002	x			x	Stochastic Modeling	
Davis et al.	2002	x		x			x
Dedic et al.	2003	x		x			x
Elustondo and Avramidis	2005	x			x	Stochastic Modeling	
Erriguible et al.	2005		x	x			x
Hart C. Arthur	1964	x		x		Analytical model based on Fickian Diffusion	
Hashimoto et al.	2003		x	x			x
Kanevce et al.	2002	x		x		x	
Chen et al.	1996	x		x			x
Kayihan	1982	x		x			x
Kayihan	1985	x			x	Stochastic Modeling	
Keey and Ashworth	1979	x			x	x	
Liu et al.	2000	x		x			x

Table 2.1.1 (Continued) Overview of mathematical models made to date.

Author	Year	Drying Material		Drying Object		Type of Model	
		Wood	Any porous media	Single board	Stack	Characteristic function	Modeling of each phase of moisture
Luikov	1975		x	x			x
Meel	1958		x	x		x	
Meroney	1969	x			x	Analytical diffusion model	
Milota and Tschernitz	1990	x		x		x	
Milota and Tschernitz	1994	x			x	x	
Pang	2002	x			x	x	
Pang	2005	x		x	x	x	x
Pang and Haslett	1997	x		x	x	x	x
Pang et al.	1992	x		x			x
Perre et al.	1999	x		x			x
Perre and Turner	1997		x	x			x
Perre and Turner	1999		x	x			x
Perre and Turner	2002		x	x			x
Pinheiro et al.	1998	x		x			x
Plumb and Gong	1996	x		x			x
Raisul et al.	2003	x		x			x
Souza and Nebra	1996	x		x			x
Spencer H.	1969		x	Grain material			x
Stamm and Nelson	1961	x		x		Analytical diffusion model	
Stanish et al.	1986		x	x			x
Sun et al	2005	x			x	x	

Table 2.1.1 (Continued) Overview of mathematical models made to date.

Author	Year	Drying Material		Drying Object		Type of Model	
		Wood	Any porous media	Single board	Stack	Characteristic function	Modeling of each phase of moisture
Slade W.	1996	x		x			x
Thomas et al.	1980	x		x			x
Yrjola and Saastamoinen	2002	x		x			x
Zhang and Datta	2004		x	x			x
Zhang et al.	1999		x	x			x

Most of the models simulating the drying of a stack of lumber are based on a drying rate function. The drying rate function describes how moisture content changes with time given a set of drying conditions (Mujumdar and Devahastin 2000). Under constant drying conditions, this function consists of three drying periods: the initial, constant rate, and falling rate drying periods (Fig. 2.1.1). The initial period is much shorter than the constant and falling and therefore it is usually neglected.

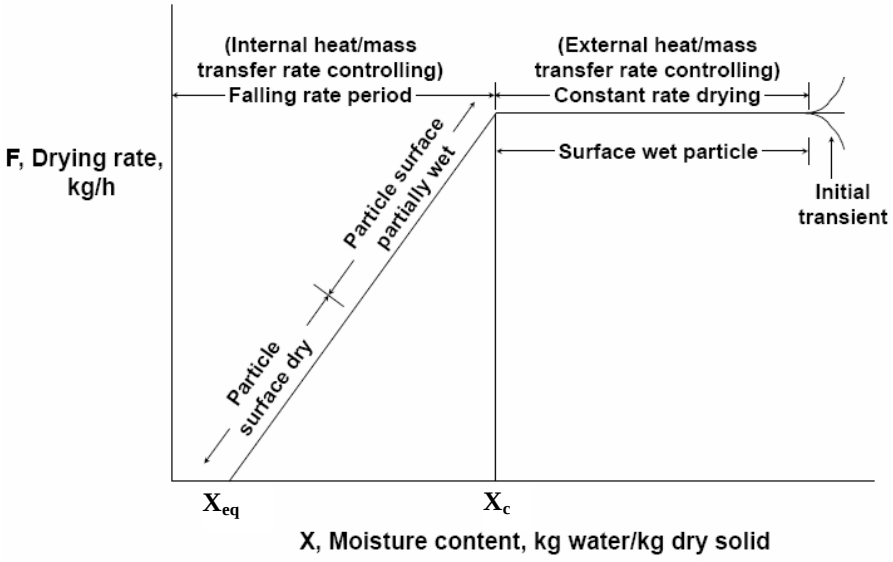

Fig. 2.1.1 Typical drying rate curve under constant drying conditions (Mujumdar and Devahastin 2000).

The drying rate during the constant drying rate period is controlled by external heat and mass transfer between the drying air and wood. The drying rate during this period is proportional to the wet-bulb depression (Milota and Tschernitz 1990). It is also dependent on the square root of velocity (Welty et al 1984). This period may or may not be observed depending on the initial moisture content, intensity of drying, and

the heat-up period (Milota and Tschernitz 1990). The evaporation plane is at the surface of a board. When all the water evaporates from the surface, the falling rate period starts. The moisture content at which this happens is called a critical moisture content (X_c).

The drying rate during the falling rate period is controlled by internal heat and mass parameters. The evaporation plane recedes into the interior of a board and diffusion is the controlling mechanism for moisture movement. More advanced drying theory predicts two falling rate periods (Bogner and Vasiljević 1986). Since the two falling rate periods are difficult to describe mathematically, it is usually approximated by just one drying period. This period was found to be dependent on the difference between the moisture content of the board and the equilibrium moisture content (X_{eq}) and also dependent on board temperature (Milota and Tschernitz 1990).

According to (Treybal 1980), diffusion through polymers is an activated process that follows a temperature-dependent, Arrhenius-type expression where the rate of diffusion is defined by a diffusion coefficient (Eq. 2.1.1),

$$D=D_0 \cdot \exp[-Ea/(R \cdot T)] \qquad (2.1.1)$$

where Ea is the activation energy (J/mol), R is the universal gas constant (8.314 J/mol K), and D_0 is a constant.

For wood, slope of the drying rate function during the constant rate period depends on the value of the diffusion coefficient. Therefore, the slope of the drying rate curve in the falling rate period can be described in the same way as the diffusion coefficient (Eq. 2.1.2),

$$St=S_0 \cdot \exp[-Ea/(R \cdot T_{db})] \qquad (2.1.2)$$

where S_0 and Ea can be found from experiments. Dry-bulb temperature is selected instead of wet-bulb temperature for the slope calculation because as the boards approach equilibrium moisture content, the internal board temperature will approach the dry-bulb temperature (Milota and Tschernitz 1990).

So, the drying rate function for both the constant and falling rate periods is mathematically defined by Equations 2.1.3 and 2.1.4, respectively:

$$\text{Flux}_{cr} = w_{D_{cr}} = f(T_{db} - T_{wb}, v) \text{ , for } X > X_c \tag{2.1.3}$$

$$\text{Flux}_{fr} = St \cdot (X - X_{eq}) \text{ , for } X_c > X > X_{eq} \tag{2.1.4}$$

where the function $f(T_{db}\text{-}T_{wb}, v)$ and St can be found from experiments. In practice, the exact value for the critical moisture content, X_c, is difficult to determine and the transition between the two functions can be smoothly accomplished using the function (Milota and Tschernitz 1990),

$$w_D = \{[St \cdot (X - X_{eq})]^{-n} + (w_{D_{cr}})^{-n}\}^{-\frac{1}{n}} \tag{2.1.5}$$

where parameter n can be found from experiments. This function approaches two asymptotes (Fig. 2.1.2), $St\cdot(X\text{-}X_{eq})$ at moisture contents near the EMC and w_{Dcr} at high moisture contents.

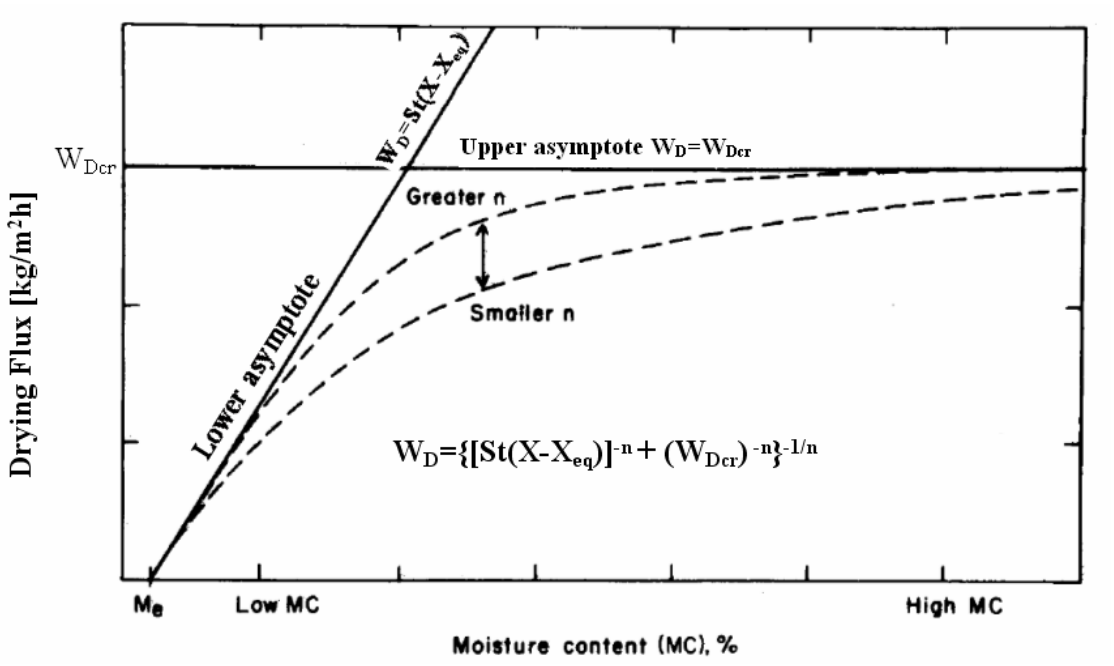

Fig. 2.1.2 A generalized form of drying rate curve (Milota and Tschernitz 1990).

2.2 Single-board drying models based on a drying rate function

These models do not treat the behavior of free and bound water and water vapor separately, but use a drying rate function to calculate the change of the average board moisture content based on the drying conditions. The drying rate function represents the overall contribution of all the mechanisms involved in a transfer of moisture through wood and is obtained experimentally. There are two types of the drying rate functions:

1) Those that express an absolute drying rate or flux (w_D). In this case, the flux is correlated to temperature, air velocity, board moisture content, board geometry, and wood structural properties (Milota and Tschernitz 1990)

2) Those that express a functional relationship between a dimensionless relative drying rate (f) and a dimensionless normalized moisture content (Φ). Here, f is defined as the ratio of the current drying rate to the drying rate at the critical moisture content (X_c). The value of Φ is defined as $(X-X_{eq})/(X_c- X_{eq})$ **(**Pang and Haslett 1997**,** Sun et al. 2005**)** where X_{eq} is the equilibrium moisture content. An actual relationship is also correlated and based on the same parameters as with the absolute drying rate or flux **(**Pang and Haslett 1997, Sun et al. 2005**)**

Depending on the type of characteristic function used, there are two ways it is implemented into a mathematical model. The absolute rate or flux is directly used and the mass transfer between a board and air can be described as

$$\rho_S \cdot V_S \cdot \frac{\partial X}{\partial t} = -F \tag{2.2.1}$$

where F is expressed as a drying rate or as:

$$\rho_S \cdot V_S \cdot \frac{\partial X}{\partial t} = -w_D \cdot A \tag{2.2.2}$$

where w_D is a flux and A is a surface area over which the mass transfer occurs.

When the dimensionless relationships are used, the mass transfer between the board and air can be described as follows:

$$\rho_S \cdot V_S \cdot \frac{\partial X}{\partial t} = -\beta \cdot (\rho_{v,s} - \rho_{v,g}) \cdot A \cdot f \tag{2.2.3}$$

Single board drying models based on a drying rate function do not take a large amount of processor time to calculate a change in a board average moisture content because the board is not divided into many elements, but is treated as a single body. They are usually used in stack drying models that simulate a lumber stack drying where the drying rate function is recalculated for all the boards for every time step.

2.3 Single-board drying models describing a movement of each phase of moisture in wood

The equations for these models are derived based on the thermodynamic relationships for each phase of moisture in wood. The movement of the free and bound water and water vapor is described and simulated separately. Some of the coefficients may be obtained by experiments. The equations for each phase are coupled.

These models utilize the static and capillary pressure gradients as the driving force for free water. The transfer of water vapor is driven by the static pressure gradient and the difference in the partial pressure of water vapor. The former causes bulk flow while the latter is responsible for diffusion. The flow of bound water is governed by diffusion with the chemical potential gradient of the bound water as the driving force. All these models assume that water vapor, bound water, and free water are in a local equilibrium.

A board is usually divided into many elements in the models based on the thermodynamic relationships for each phase of moisture. All the governing equations are applied on each element. This results in a long calculation time and it is difficult to apply these models to the drying of a stack of lumber consisting of many boards. Therefore, they are usually used for an accurate prediction of temperature and moisture profiles within a board.

One of the earliest analyses of the principles of moisture movement in wood was made by Hart (1964). He integrated Fick's first law (Eq. 2.3.1) describing a process of diffusion and the anatomy of wood to explain how moisture moves through wood. The solutions he obtained were analytical. The graphical interpretation of Equation 2.3.1 is shown on the Figure 2.3.1.

$$J = D \cdot \frac{dC}{dx} \tag{2.3.1}$$

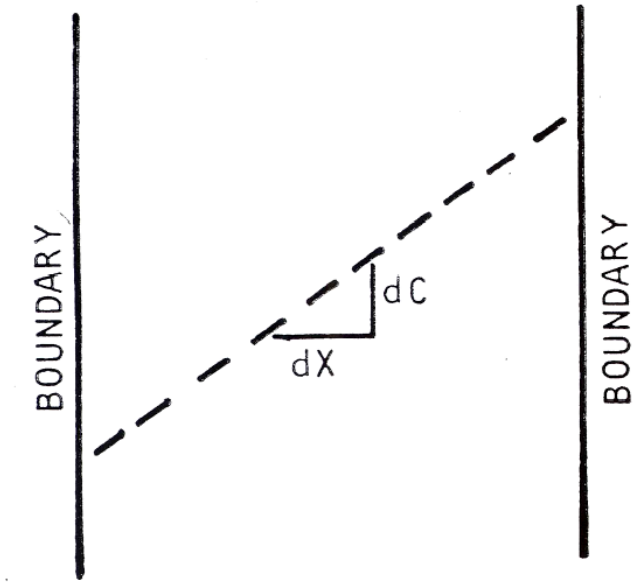

Figure 2.3.1 Schematic drawing of steady state flow between two different boundary conditions (Hart 1964).

When Fickian diffusion is applied to the unsteady state movement of moisture through wood, two distinct periods exist (Figure 2.3.2). During the first period (period A), the moisture gradient advances from the surface to the center of the specimen but no moisture change occurs at the center.

During the second period (period B), the moisture gradient has reached the center and the moisture content at the center is decreasing. If the diffusion coefficient is assumed to be constant with moisture content, then the drying times for the first (A) and the second (B) periods, respectively, are:

$$t = \frac{\pi}{4} \cdot \frac{a^2}{D} \cdot E^2 \tag{2.3.2}$$

$$t = \frac{4}{\pi^2} \cdot \frac{a^2}{D} \cdot [\ln \frac{8}{\pi^2} - \ln(1 - E)] \tag{2.3.3}$$

where

t - Total elapsed time since the beginning of drying[s]
a - Specimen half-thickness [cm]
D - Diffusion coefficient [cm^2/s]
E - Fraction of the total water removed [-]

This approach is in accordance with the advanced drying theory which predicts two falling rate periods instead of one (Bogner and Vasiljević 1986).

The first equation (2.3.2) applies to approximately the first one-third of the moisture desorbed (or absorbed), while the second equation applies to the remaining two-thirds. In the derivation of these two equations, it was assumed that movement occurred through two opposite plane surfaces but no movement occurred through the specimen edges.

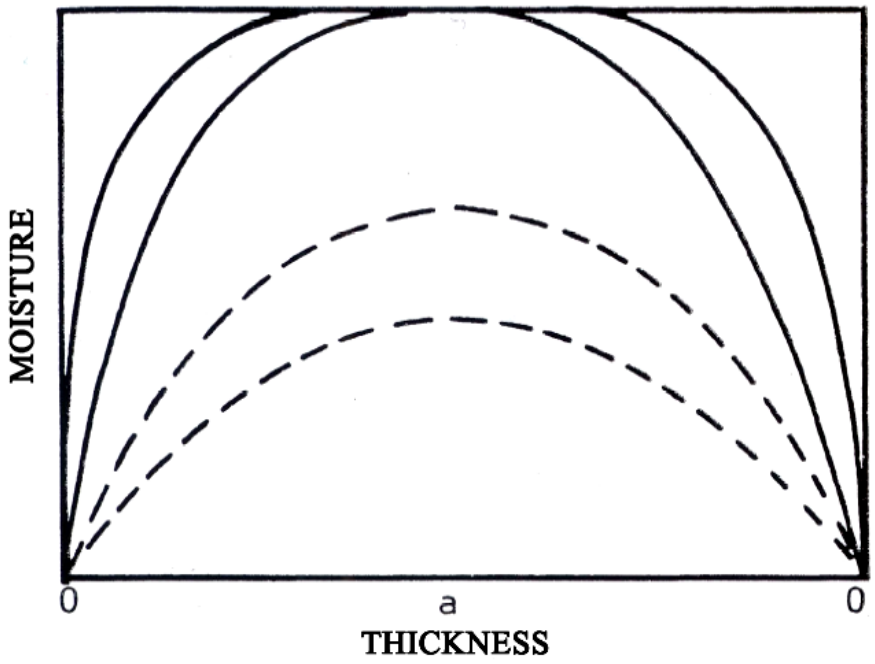

Figure 2.3.2 Moisture concentration distribution during period A (solid curves) and period B (dashed curves) (Hart 1964)

Hart found it useful to consider that the rate of movement through a given surface is the product of the surface diffusion coefficient and the surface concentration gradient where the surface concentration gradient depended upon the particular shape of the moisture gradient throughout the piece. Using this approach with the rate of movement, the drying times for the period A and period B, respectively, are:

$$t = (\text{constant})\frac{\rho_S \cdot a^2}{D_s} \cdot E^2 \qquad (2.3.4)$$

$$t = b_1 - b_2 \cdot \frac{\rho_S \cdot a^2}{D_s} \ln(1 - E) \qquad (2.3.5)$$

where ρ_S is the density of bone-dry wood [kg/m^3] and b_1 and b_2 are constants.
The values of b_1 and b_2 depend upon the curve employed for the period B, and b_1 also depends upon the time involved in the period A. A moisture gradient for the period B can be described with the following equation:

$$\frac{X_x - X_s}{X_a - X_s} = \sin\left(\frac{\pi}{2} \cdot \frac{x}{a}\right)$$

where X_x, X_a, and X_s are the moisture contents at depth x, the center (depth a) and the surface, respectively.

Drying times predicted using Hart's equations for one-inch thick wood with a 0.5 specific gravity (green volume basis) dried from green to 10 % average moisture content at 150°F are given in table 2.3.1.

Table 2.3.1 Calculated time required to dry one-inch thick wood of 0.5 specific gravity (green volume basis) to ten percent average moisture content at 150°F (Hart 1964).

Initial Moisture Content (percent)	Equilibrium Moisture Content (percent)	Time (hours)		
		Highly Permeable	Moderately Permeable	Impermeable
55	5	-	47.6	56.6
55	15/5*	-	58.8	81.7
155	5	59.2	72.5	174.8

*E.M.C reduced from 15 to 5 only after the center moisture content reaches 30 %

Stanish et al. (1986), made a model whose equations were frequently used by many researchers who were modeling the process of wood drying. This model is a simulation of the drying of hygroscopic porous media. Besides using continuity equations for air and water flow and energy balance equations for the system wood-moisture, phase equilibrium equations were used to obtain the density of water vapor at any time and place in wood during simulation. Comparison of model simulation results with the experimental data are given in Figures 2.3.3, 2.3.4, 2.3.5, and 2.3.6.

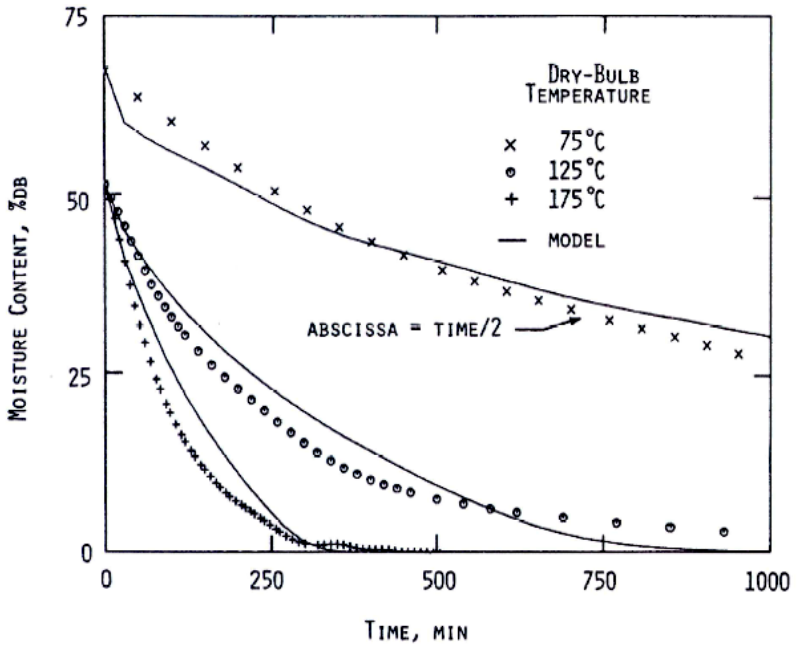

Figure 2.3.3 Moisture content of southern pine lumber during drying (model and experimental data) (Stanish et al. 1986).

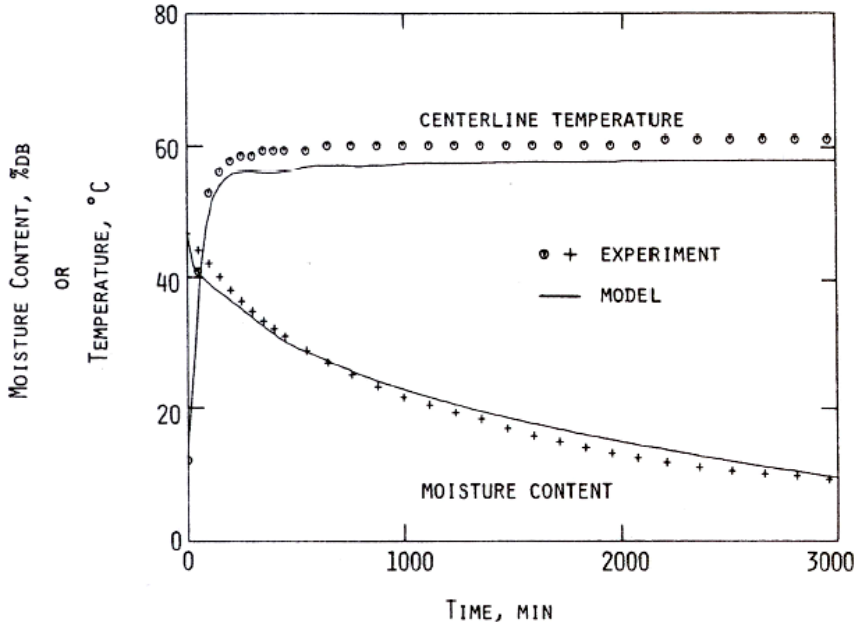

Figure 2.3.4 Temperature and moisture distribution in southern pine lumber with time (model and experimental data) (Stanish et al. 1986).

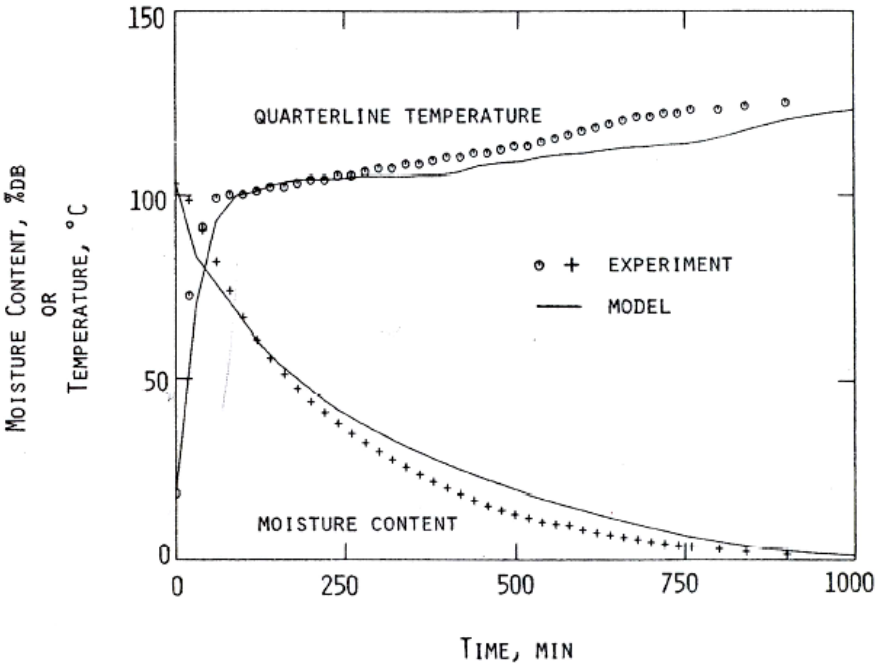

Figure 2.3.5 Temperature and moisture distribution in Douglas fir lumber with time (model and experimental data) (Stanish et al. 1986).

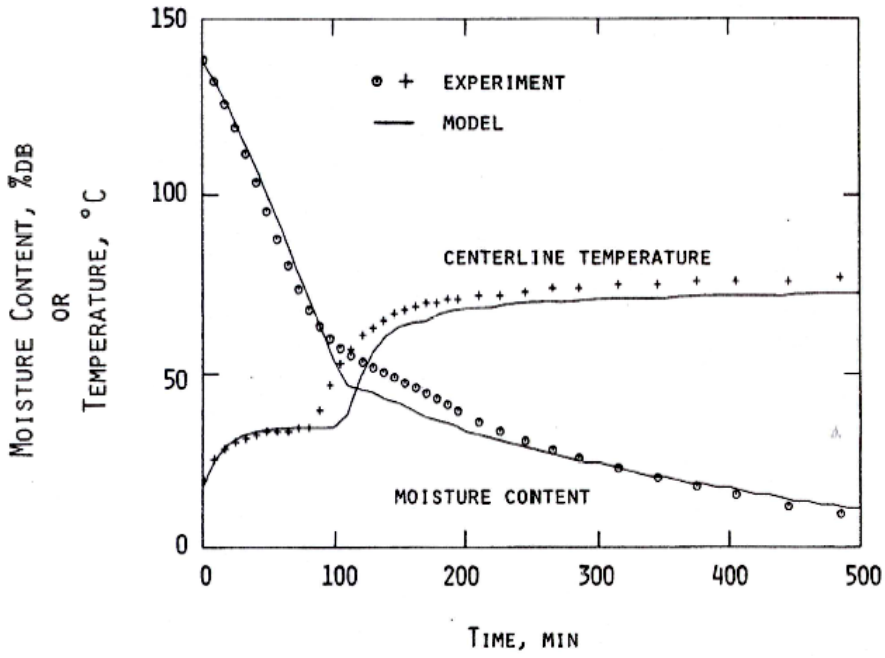

Figure 2.3.6 Temperature and moisture distribution in brick with time (model and experimental data) (Stanish et al. 1986).

The model showed a good agreement with the experimental results. The various materials shown in the figures demonstrate that once a good mathematical model of a drying of porous media is written, it can be applied for different materials just by changing the coefficients used in the equations.

Pang et al. (1992), modeled the high-temperature drying of *Pinus radiata* using the same thermodynamic relations as Stanish et al. (1986). One of the differences is that the mass balance equations are applied around the evaporative plane for obtaining the properties and position of it. Therefore, besides moisture and temperature profiles, this model is able to predict the position of evaporative plane in wood during drying. Simulation and experimental results are given in Figures 2.3.7, 2.3.8, and 2.3.9.

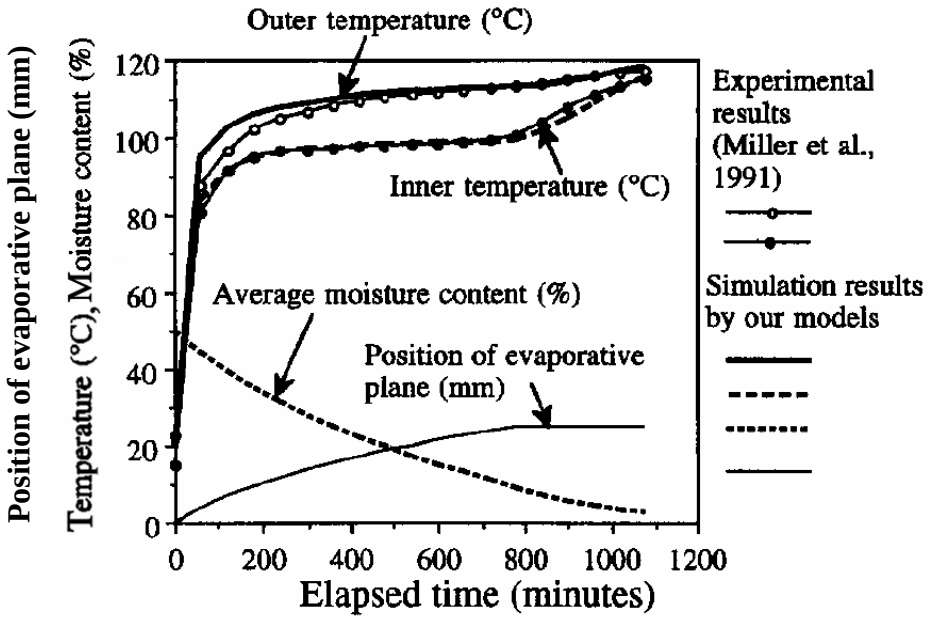

Figure 2.3.7 Temperature and moisture profiles and the predicted position of evaporation plane for 100mm x 50mm boards of heartwood (Pang et al. 1992).

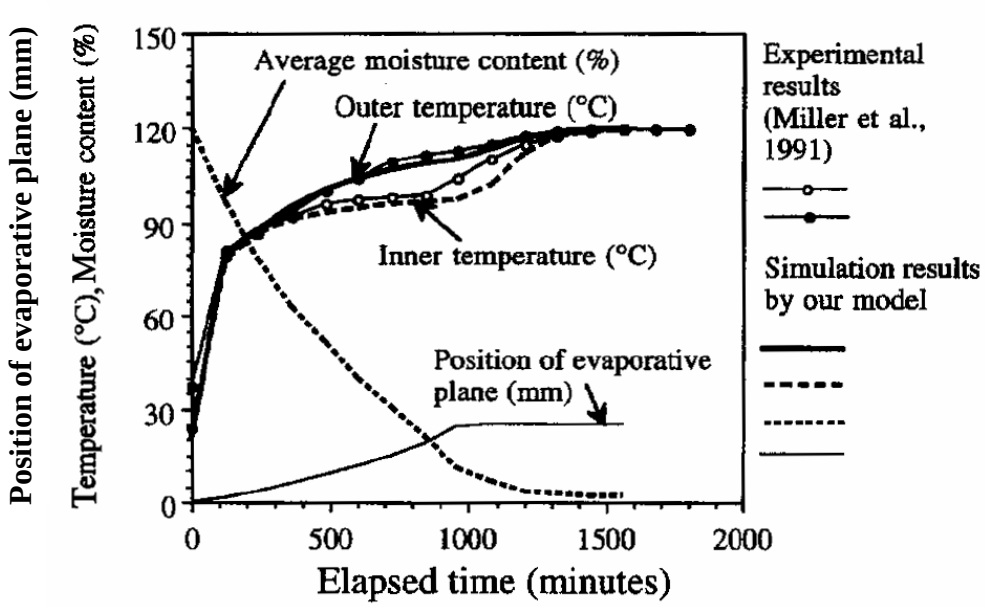

Figure 2.3.8 Temperature and moisture profiles and the predicted position of evaporation plane for 100mm x 50mm boards of mixed wood (Pang et al. 1992).

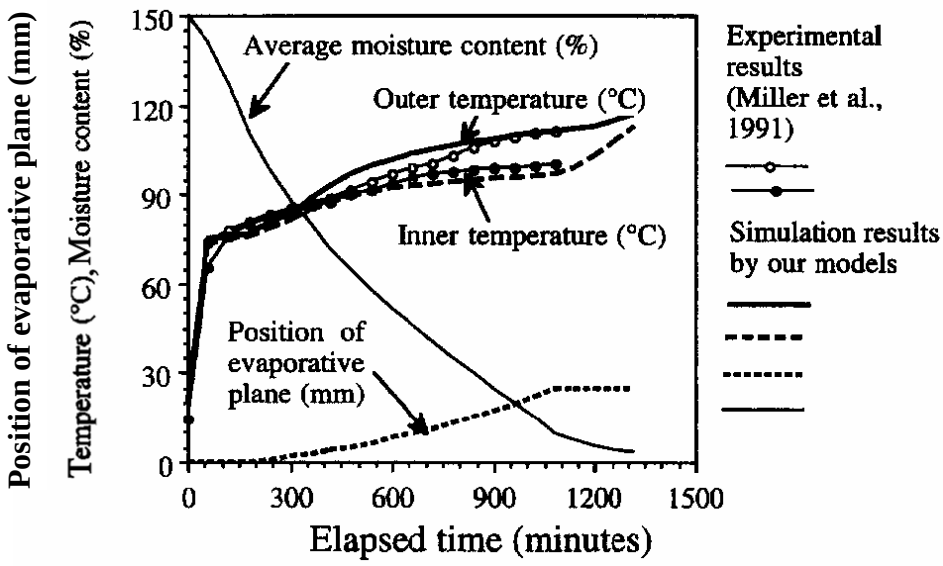

Figure 2.3.9 Temperature and moisture profiles and the predicted position of evaporation plane for 100mm x 50mm boards of sapwood (Pang et al. 1992).

2.4 Determinant stack drying models

In determinant stack drying models, a single board drying model based on a drying rate function is applied on each board in the stack. Each board can have a different drying rate due to the changing drying conditions across the stack or in different airflow paths.

Milota and Tschernitz (1994), developed a model that simulates drying in a batch lumber kiln. The drying rate function was implemented directly into the mathematical model. It was obtained from single-board laboratory tests (Milota and Tschernitz 1990). The characteristic function was expressed as:

$$w_D = \left(\left(St\left(X - X_{eq}\right) \right)^{-N} + \left(w_{D_{cr}} \right)^{-N} \right)^{-\frac{1}{N}} \qquad (2.4.4)$$

where

$$St = 0.204 \cdot e^{(-3980.83/T_{g,IN})}$$

$$w_{D_{cr}} = (16.42 + 16.56 \cdot (T_{g,IN} - T_{W,IN}) - 0.1087 \cdot (T_{g,IN} - T_{W,IN})^2) \cdot (v/6.75)^n \cdot 10^{-6}$$

$$N = 0.75 + 0.167 \cdot (T_{g,IN} - T_{W,IN}) \text{ for } (T_{g,IN} - T_{W,IN}) < 25.5$$

$$N = 5 \text{ for } (T_{g,IN} - T_{W,IN}) \geq 25.5$$

All the parameters and coefficients were obtained from the single-board experiments.

This drying rate function was applied on each board to obtain the variables such as temperature and moisture content of a board temperature and humidity of air. The simulation results compared to the experimental results are shown in Figures 2.4.1, 2.4.2, and 2.4.3.

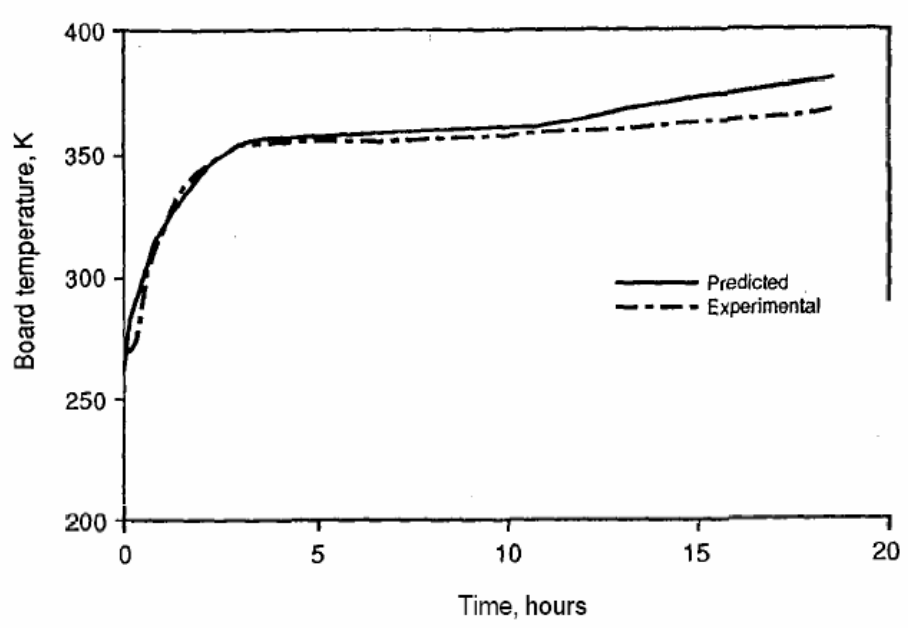

Figure 2.4.1 Measured centerline temperature and predicted temperature from model for center board in the uninterrupted drying experiment (Milota and Tschernitz 1994)

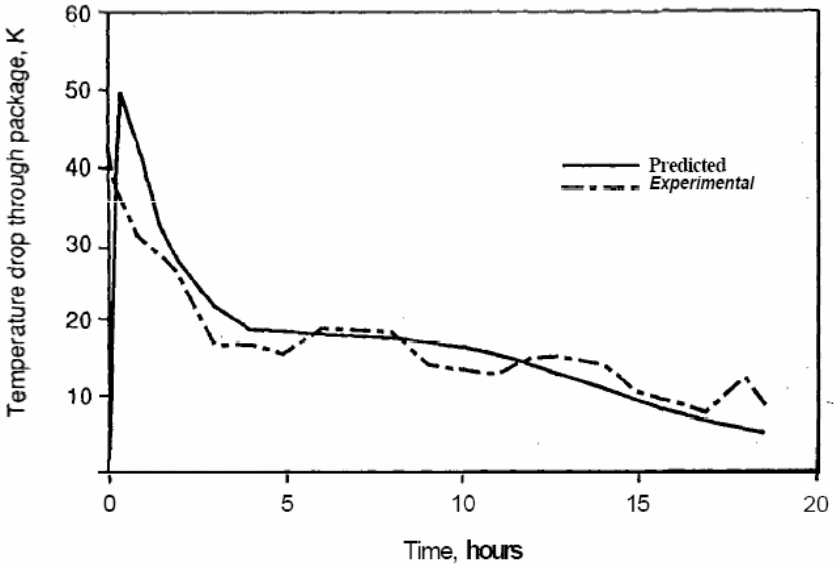

Figure 2.4.2 Temperature drop through the package as measured and as predicted by the model for the uninterrupted drying experiment (Milota and Tschernitz 1994)

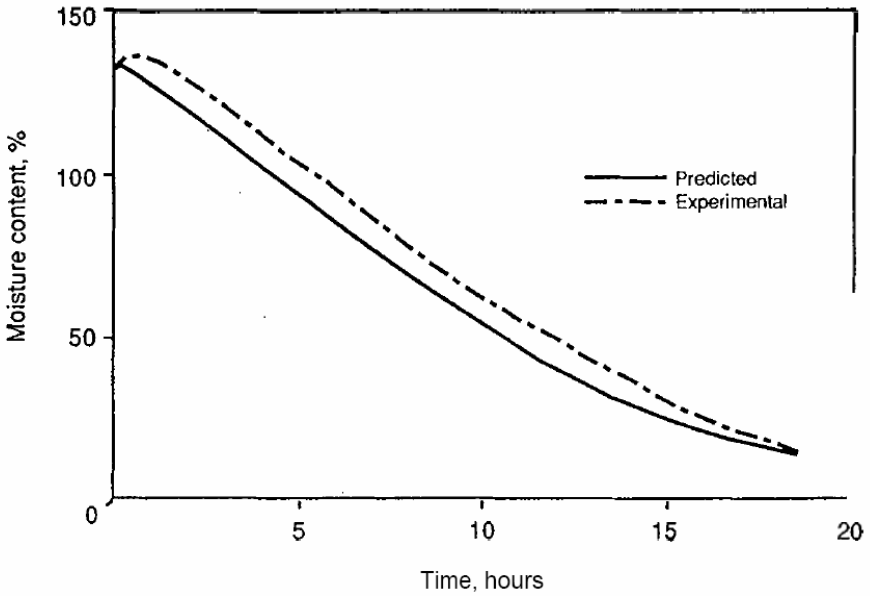

Figure 2.4.3 Average moisture content of the package as measured and predicted by the model (Milota and Tschernitz 1994)

Sun et al. (1996), made a model that simulates the drying of *Pinus radiata* timber in a kiln-wide stack. The drying rate function method was adopted for the description of the moisture transfer processes inside wood boards. In contrast to the model of Milota and Tschernitz (1994), the characteristic drying curve was used to obtain a relative drying rate function (f) which was then used in the mass transfer equation (Eq. 2.4.5). This curve was then used to account for a decrease in moisture flow due the evaporative plane receding into the wood.

The equation describing moisture movement was defined as follows:

$$W_v = \frac{\omega_v \cdot W_B}{(1-\omega_v)} + \frac{f \cdot k_W \cdot A(\omega_{v,sat} - \omega_v)}{(1-\omega_{v,sat})} \qquad (2.4.5)$$

where

ω- mass fraction [-]

f - normalized drying rate [-]

k_W - mass transfer coefficient [$kg/m^2 \cdot s$]

For the constant rate period the value of the relative drying rate function (f) is one because the evaporation plane is still at the board surface and therefore there is no flow resistance. For the falling rate period, when the evaporation plane starts receding into the wood thereby decreasing the moisture flow rate, the function f is defined as follows:

$$f = \Phi^{A - B\Phi_{fsp}} \qquad (2.4.6)$$

where

$$\Phi = \frac{X - X_{eq}}{X_c - X_{eq}} \tag{2.4.7}$$

and

$$\Phi_{fsp} = \frac{X - X_{fsp}}{X_c - X_{fsp}} \tag{2.4.8}$$

where A and B are the constants obtained for *Pinus radiata*.

The normalized drying rate function (f) accounts for the different stages of drying. The comparison of calculated and measured data is given on the Figure 2.4.4.

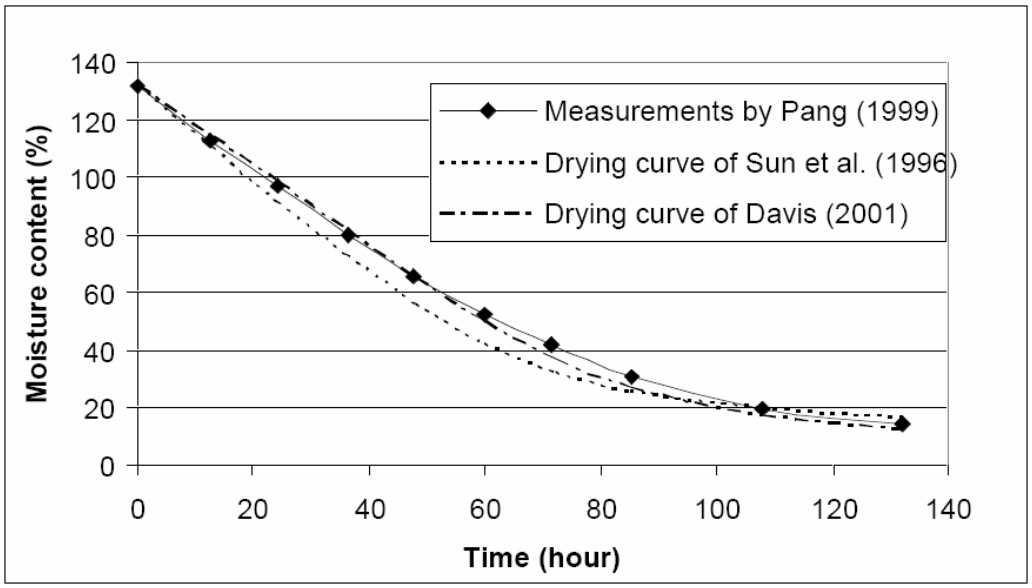

Figure 2.4.4 Average moisture content during drying (measured and from the model) (Sun et al. 1996).

The model of Awadalla et al. (2003) is also based on a characteristic function. One difference compared to the previous two models is that it did not use the drying rate function but the sorption isotherms of wood to obtain the partial pressure of the

water vapor at the surface of the wood. The model also simulates the drying of a lumber stack. The driving force for moisture movement is the difference between the partial pressure of water vapor at the wood surface and in the air flowing over the boards (Eq. 2.4.9). The value of $p_{v,s}$ is determined from the sorption isotherms of wood.

$$W_v = \frac{\beta}{R_v T_s}\left(p_{v,s} - p_{v,g}\right)\cdot A \tag{2.4.9}$$

This moisture flow rate is then used in the energy and mass conservation equations to obtain other relevant parameters. The comparison of calculated and measured data is given on the Figure 2.4.5.

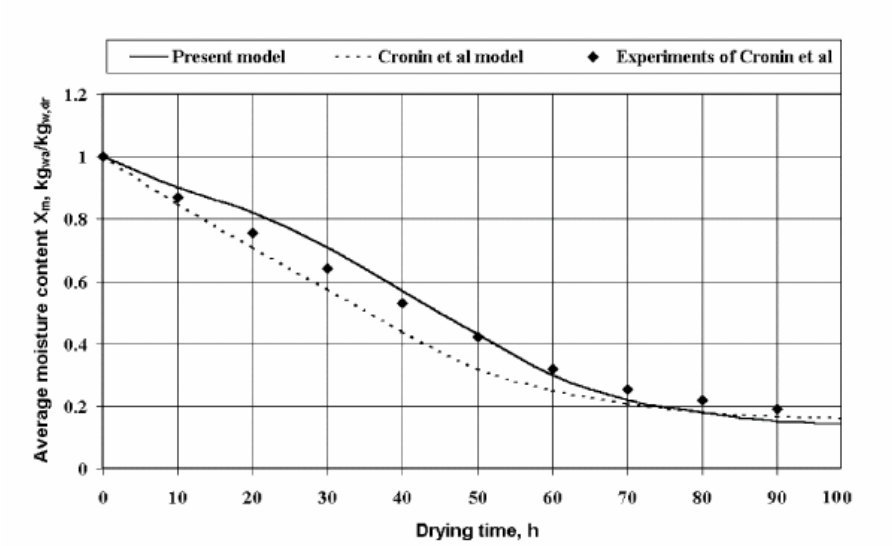

Figure 2.4.5 Average moisture content during drying (Awadalla et al.2003).

Pang (2002) developed a kiln-wide drying model and investigated the effects of wood variability and rheological properties on lumber drying. He used the drying rate function in the form of a relative drying rate function which was also used in the

mass and heat transfer equations. As in the previous models the mass and energy balance equations were used for obtaining the main drying parameters such as the moisture content and temperature of the wood and the temperature and humidity of the air.

For modeling purposes, the mixed sapwood/heartwood boards were classified into three categories based on their cross-section composition: (1) a board with approximately half sapwood and half heartwood; (2) a board with more mostly sapwood; and (3) a board of mostly heartwood. The predicted results obtained by this model are shown in Figure 2.4.6

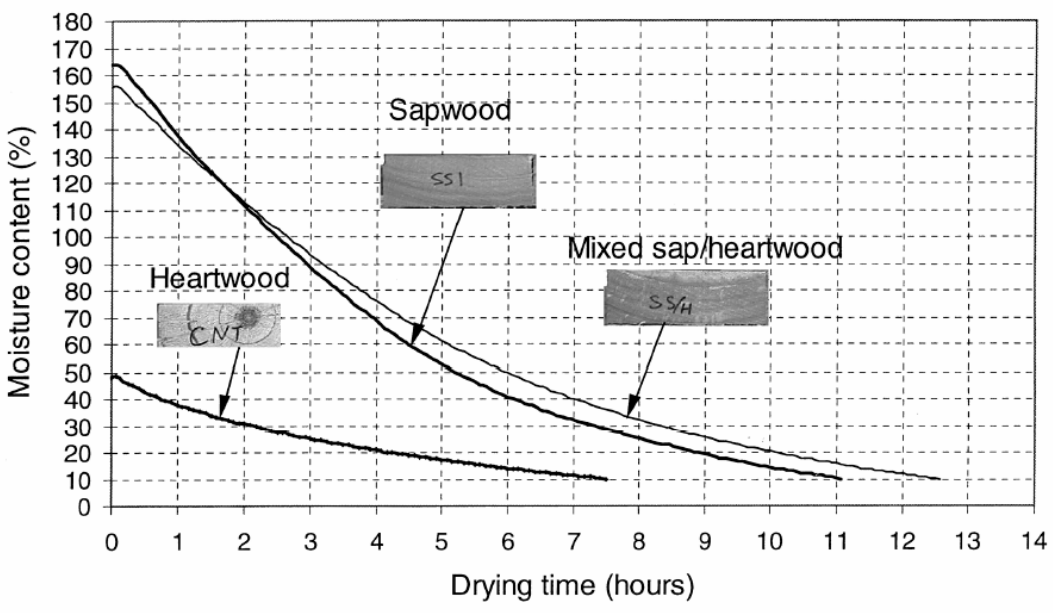

Figure 2.4.6 Predicted drying-rate curves for sapwood, heartwood and mixed sapwood/heartwood boards (Pang 2002).

2.5 Stochastic stack drying models

Cronin et al. (2003) derived a probabilistic drying model and then applied different drying schedules to test it and examine the effect of timber drying schedules on variability in board-by-board moisture content distribution. They started with the assumption that the rate of drying at any time is a linear function of the difference between current board moisture content and the equilibrium moisture content for the kiln climate. They also assumed that there are no separate phenomenological phases (constant and falling rate periods) that can exist in drying. This assumption makes this function different than the function defined by the Equation 2.1.4. The following expression for board moisture content was obtained (Eq. 2.5.1):

$$X(t) = (X_i - X_{eq}) \cdot e^{-kt} + X_{eq} \tag{2.5.1}$$

where k reflects a number of internal and external thermo-physical drying mechanisms and therefore must be found by experiment. In this model, k was correlated with the diffusivity of water in the timber and hence exhibited a strong sensitivity to the kiln dry-bulb temperature.

Equation 2.5.1 is valid over the entire drying process. However, the equilibrium moisture content must remain constant with respect to time (implying that the drying schedule wet- and dry-bulb temperatures are not changed during the schedule). This drying schedule is called a single set point drying schedule. Figure 2.5.1 illustrates such a single set point schedule.

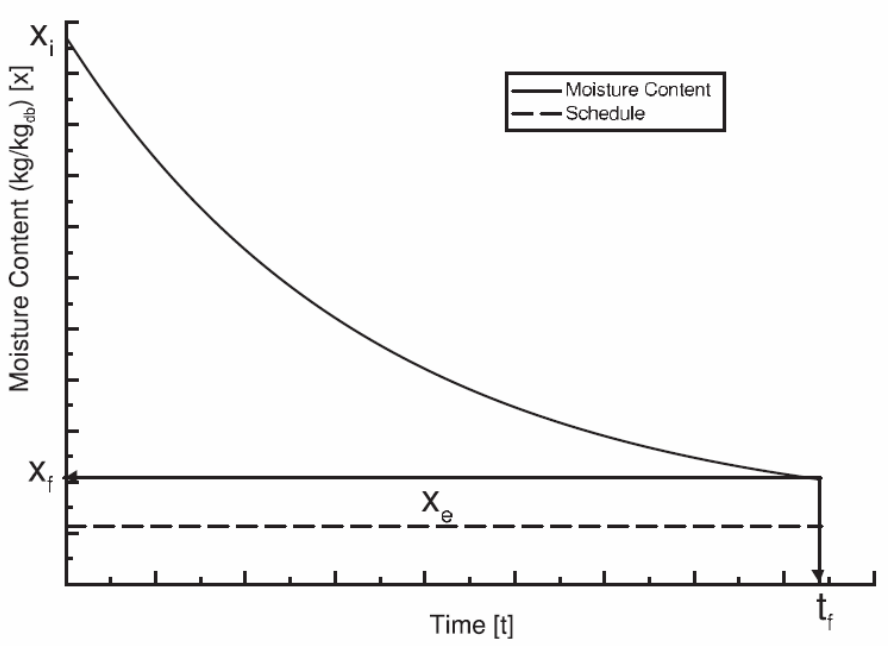

Figure 2.5.1 Moisture change using a single set point schedule (Cronin et al. 2003).

While equilibrium moisture content is calculated from the wet-bulb depression (the difference between the dry- and wet-bulb temperatures), the parameters X_i and k were considered as random variables governed by corresponding probability density functions. Each distribution was characterized by having a mean and standard deviation, μ_{xi} and σ_{xi} and μ_k and σ_k, respectively. Both the initial moisture content and the drying rate constant were represented by the normal distribution. The following expressions were used from the theory of functions of random variables:

$$\mu_x = (\mu_{xi} - X_{eq}) \cdot e^{-\mu_k \cdot t + (1/2)\sigma^2_k \cdot t^2} + X_{eq} \tag{2.5.2}$$

$$\sigma^2_x = e^{-2 \cdot \mu_k \cdot t + \sigma^2_k \cdot t^2} [\sigma^2_{xi} \cdot e^{\sigma^2_k \cdot t^2} + (\mu_{xi} - X_{eq})^2 (e^{\sigma^2_k \cdot t^2} - 1)] \tag{2.5.3}$$

A double set point schedule model was developed as well. It could predict the mean and dispersion in moisture content where the equilibrium moisture content was changed (in a stepwise fashion) during the drying process. A moisture change for this case is shown in Figure 2.5.2.

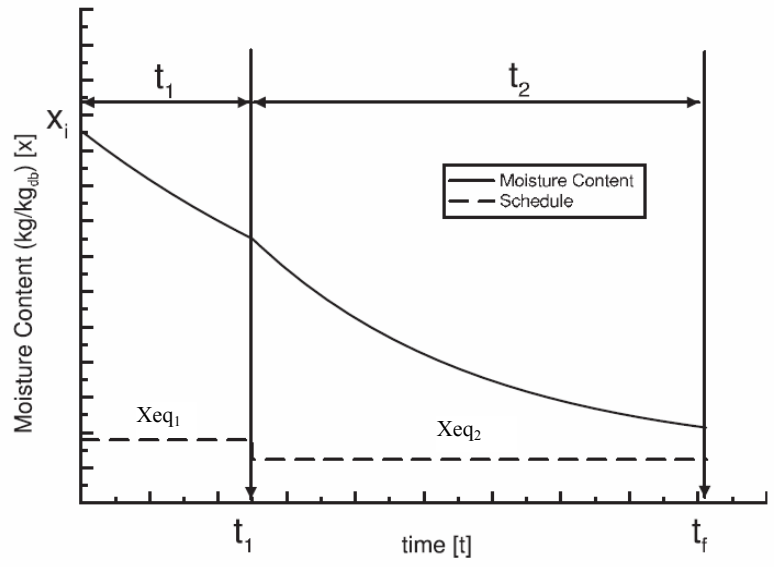

Figure 2.5.2 Moisture change using a double set point schedule (Cronin et al. 2003)

For a schedule consisting of two distinct equilibrium moisture contents, the deterministic drying model will be:

$$X(t) = (X_i - X_{eq_1}) \cdot e^{-k_1 t} + X_{eq_1},\ 0 \le t \le t_1 \tag{2.5.4}$$

$$\begin{aligned} X(t) = {} & (X_i - X_{eq_1}) \cdot e^{-k_1 t_1} \cdot e^{-k_2 (t - t_1)} + \\ & + (X_{eq_1} - X_{eq_2}) \cdot e^{-k_2 (t - t_1)} + X_{eq_2}, t_1 \le t \le t_f \end{aligned} \tag{2.5.5}$$

At times less than t_1, the mean and standard deviation in moisture content will be given by Eqs. 2.5.2 and 2.5.3. For times greater than t_1, the mean and variance of moisture content X at any time t can be derived using the theory of functions of random variables as:

$$\mu_x = [(\mu_{xi} - X_{eq_1})e^{-\mu_{k1}\cdot t_1 + (1/2)\sigma^2_{k1}\cdot t_1^2} + \\ +(X_{eq_1} - X_{eq_2})]e^{-\mu_{k2}\cdot(t-t_1)+(1/2)\sigma^2_{k2}\cdot(t-t_1)^2} + X_{eq_2} \tag{2.5.6}$$

$$\sigma^2_x = e^{-2\cdot\mu_{k2}\cdot(t-t_1)+\sigma^2_{k2}\cdot(t-t_1)^2}[Ae^{\sigma^2_{k2}(t-t_1)^2} + B(e^{\sigma^2_{k2}\cdot(t-t_1)^2} - 1)] + \\ + (X_{eq_1} - X_{eq_2})^2 e^{-2\cdot\mu_{k2}\cdot(t-t_1)+\sigma^2_{k2}\cdot(t-t_1)^2}[e^{\sigma^2_{k2}\cdot(t-t_1)^2} - 1)] \tag{2.5.7}$$

where the constants A and B were given as:

$$A = e^{-2t_1\cdot\mu_{k1}+\sigma^2_{k1}\cdot t_1^2}[\sigma^2_{xi}\cdot e^{\sigma^2_{k1}t_1^2} + (\mu_{xi} - X_{eq_1})(e^{\sigma^2_{k1}\cdot t_1^2} - 1)]$$

$$B = (\mu_{xi} - X_{eq_1})e^{-\mu_{k1}\cdot t_1 + (1/2)\sigma^2_{k1}\cdot t_1^2}$$

The comparative charts of the model and experimental results using a single and double set point drying schedule are shown in Figures 2.5.3 and 2.5.4, respectively.

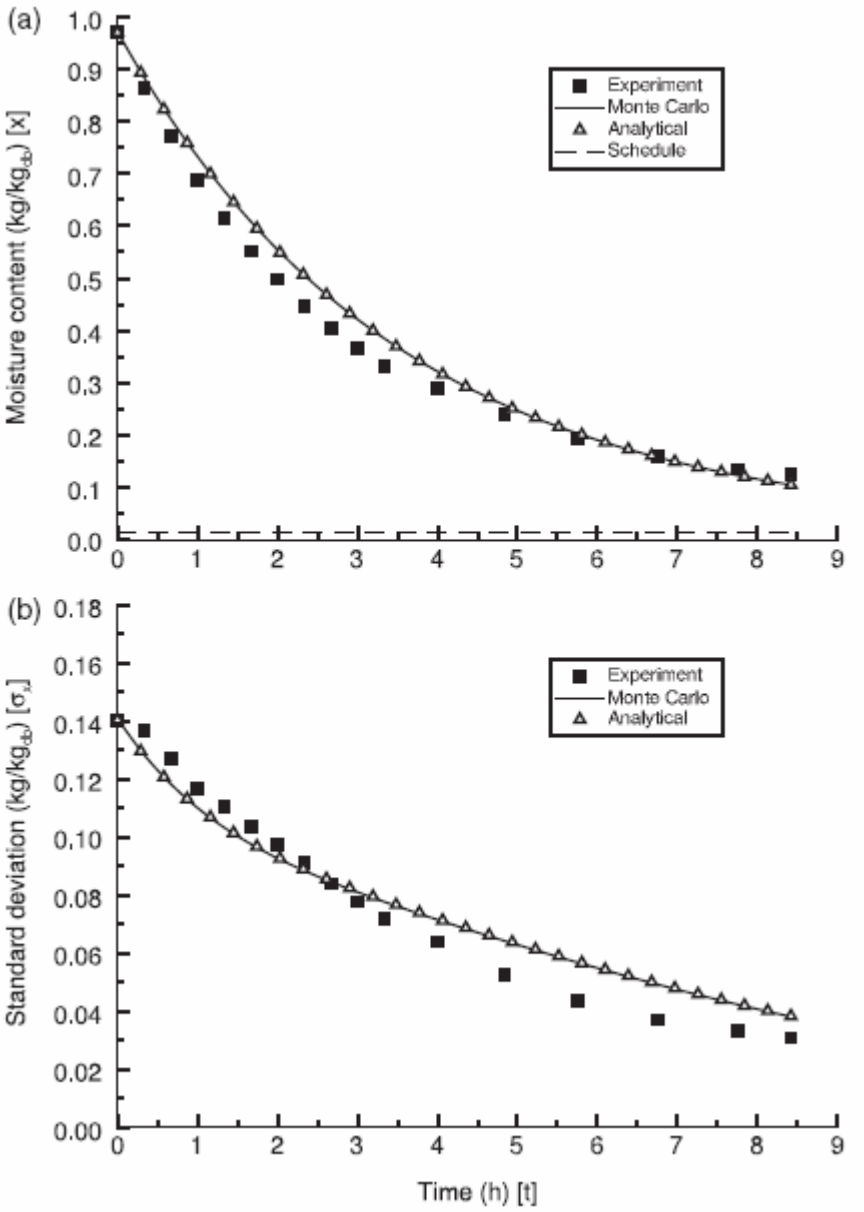

Figure 2.5.3. (a) Mean moisture content vs, time for a single set point schedule (b) standard deviation in moisture content vs. time for a single set point schedule (Cronin et al. 2003).

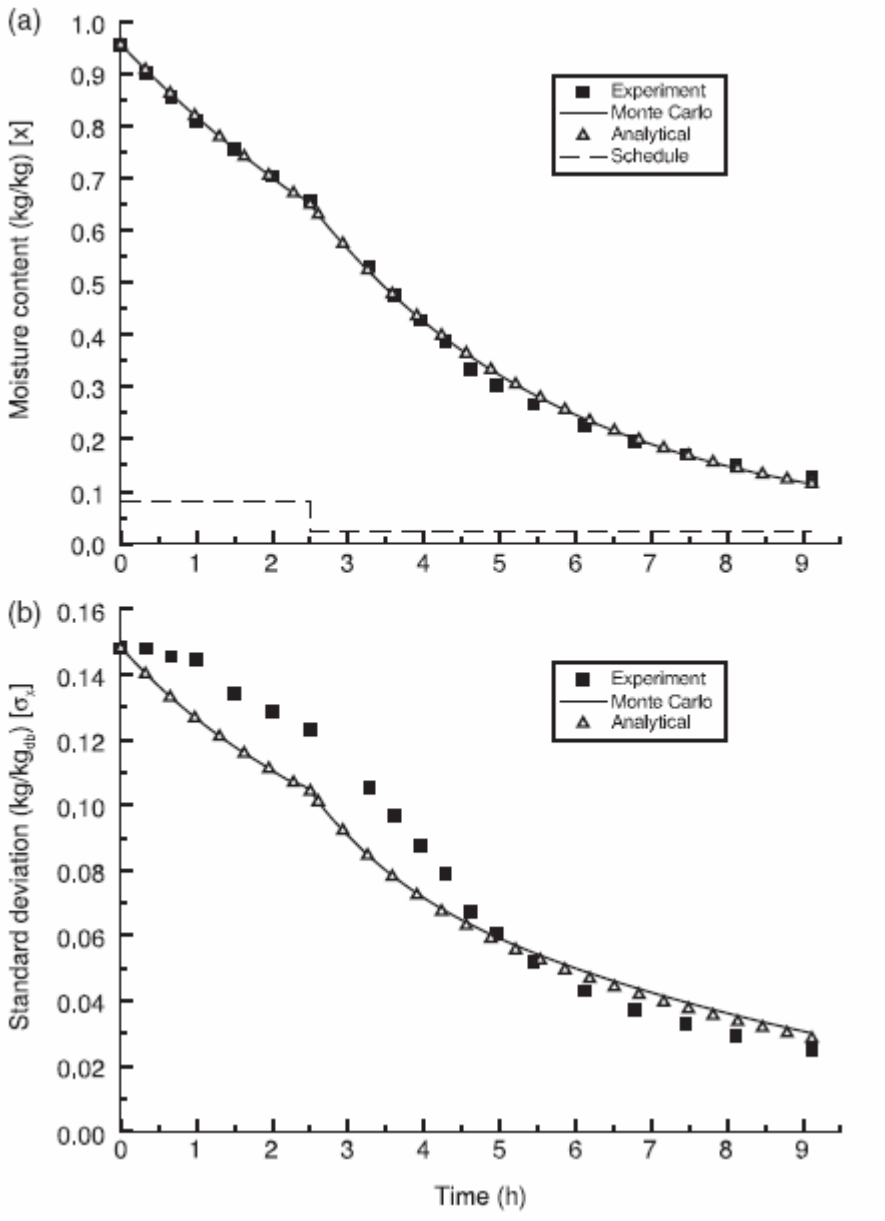

Figure 2.5.4. (a) Mean moisture content vs. time for a double set point schedule (b) standard deviation in moisture content vs. time for a double set point schedule (Cronin et al. 2003).

Kayihan (1985) made a stochastic model of lumber drying in batch kilns. It was based on energy and mass balances but, variables such as a drying flux and initial moisture content were calculated using stochastic parameters.

The drying flux was correlated as a function of the dry-basis moisture content X. It was assumed that at high moisture levels drying was controlled by external resistances and occurs at a constant flux. This flux was called a. At low moisture levels the drying flux is controlled by internal diffusion which can be approximated by $b\cdot(X-X_{eq})$ where X_{eq} is the equilibrium moisture content at the drying conditions and b is a drying flux parameter. Using these asymptotes the correlation form was expressed as:

$$(\frac{dX}{dt})/A = -\frac{b(X-X_{eq})}{[1+(\frac{b(X-X_{eq})}{a})^n]^{1/n}} \qquad (2.5.8)$$

The value of a was correlated as a function of the physical parameters such as T_{db}, T_{wb}, $p_{v,sat}$, p_g , and β. The value of b was correlated as an Arrhenius type of function of ambient temperature (T_a) since it describes diffusion. One additional stochastic term was introduced for each variable to account for wood structural variations, board dimensions, and a dynamic kiln behavior [$\varepsilon(\sigma^2_a)$ and $\varepsilon(\sigma^2_{\ln b})$]. Dynamic kiln behavior results in non-repetitive dryer performance. This is dependent on its size, load, heat exchange equipment, the air circulation rate and direction, heat losses, and the physical arrangement of the stacks and boards. With the addition of these additional terms, the fluxes a and b were defined as follows:

$$a = f(T_{db},\ T_{wb},\ p_{v,sat},\ p_g,\ \beta) + \varepsilon(\sigma^2{}_a) \tag{2.5.9}$$

$$\ln b = \ln b_0 - f(T_a) + \varepsilon(\sigma^2{}_{\ln b}) \tag{2.5.10}$$

where $\varepsilon(\sigma^2{}_a)$ is a random error with zero mean and $\sigma^2{}_a$ variance and $\varepsilon(\sigma^2{}_{\ln b})$ is also a random error with zero mean and $\sigma^2{}_{\ln b}$ variance.

The variables a and b change with the operating conditions. At the beginning of the simulation each board is assigned initial values for a and b including random errors according to the designated variances. These become the base values for each board for the rest of the simulation. The actual parameters representing current operating behavior are then computed from the base values.

Board green moisture contents are entered as a Weibull distribution for which the density and the cumulative distribution functions are respectively:

$$f(X_G) = \left(\frac{X_G - c}{b}\right)^{a-1}\left(\frac{a}{b}\right)e^{\left(-\left(\frac{X_G - c}{b}\right)^a\right)} \tag{2.5.11}$$

$$F(X_G) = 1 - e^{\left[-\left(\frac{X_G - c}{b}\right)^a\right]} \tag{2.5.12}$$

where a, b, and c are parameters obtained from experiments.

By using the equations 2.5.11 and 2.5.12, variations in board green moisture content among the boards in a stack were taken into account. The comparative charts of the model and experimental results are shown in the Figures 2.5.5, 2.5.6 and 2.5.7.

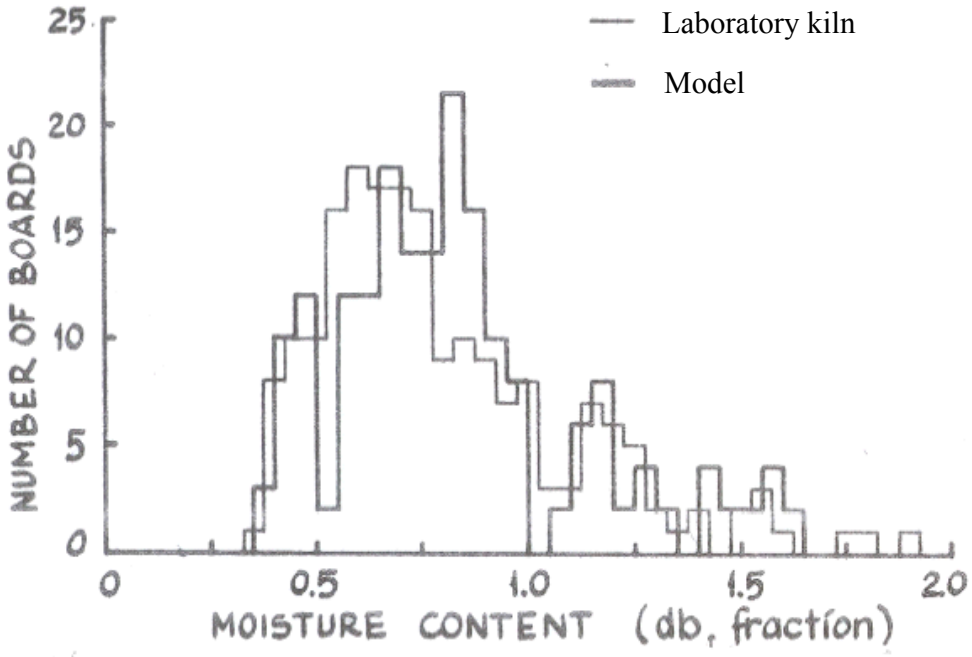

Figure 2.5.5 Green moisture content distribution (Kayihan 1984)

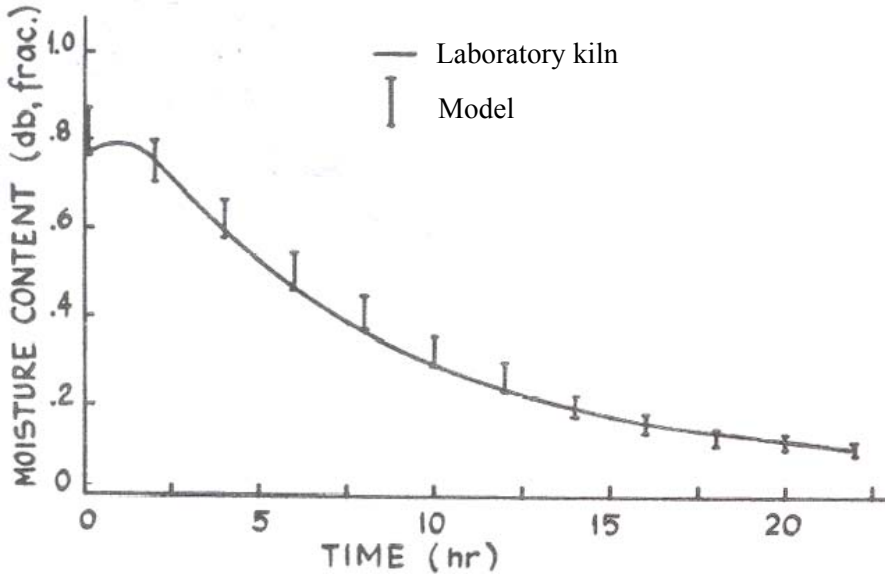

Figure 2.5.6 Drying curve of the charge (Kayihan 1984)

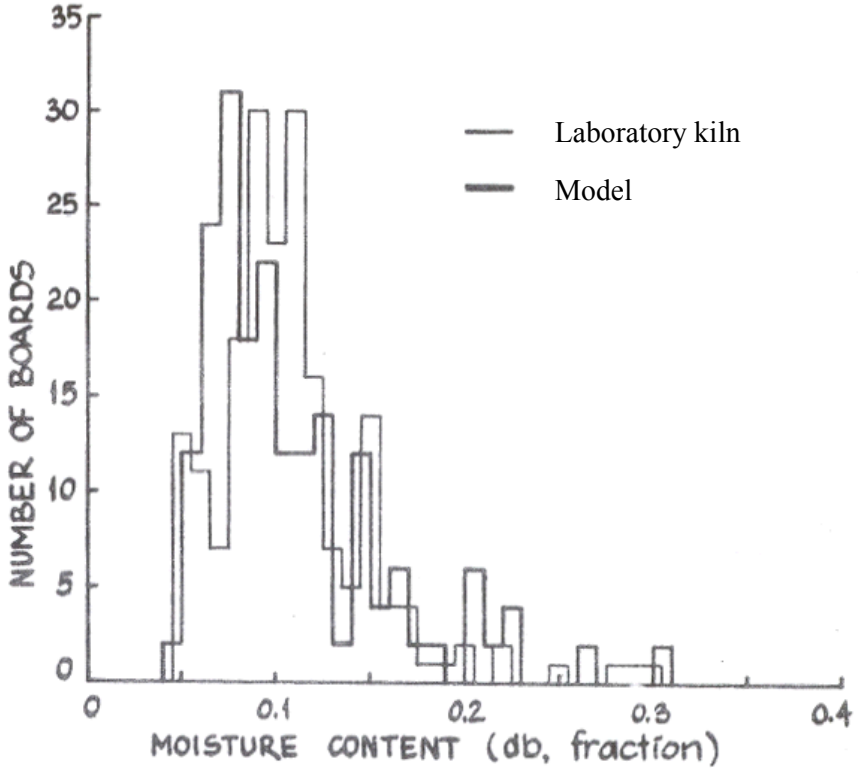

Figure 2.5.7 Dry moisture content distribution (Kayihan 1984)

2.6 Conclusion

2.6.1 Single-board drying models

Both approaches to creating single-board drying models, using a drying rate function and thermodynamic relationships, gave the results which were in good agreement with experimental results. Regardless, there are still advantages and disadvantages for both modeling approaches.

Mathematical models based on the drying rate function present a somewhat simplified approach to simulating the drying process because the moisture movement

is described using only one equation, a drying rate function. In contrast, models based on thermodynamic relations use equations for every phase of moisture. The accuracy of models based on the drying rate function is preserved by real experiments conducted to obtain the function. The simplicity of the model makes the numerical solution much easier and quicker. This makes them suitable for using in simulations dealing with drying of stack of lumber consisting of a large number of boards. Only the differences in the mass and heat transfer coefficients and drying air occurring from board to board across the stack must be taken into account.

With this approach, however, there is a difficulty in choosing an appropriate surface condition on which to base the calculation of the amount of energy transferred from the drying medium to the board. This problem can be solved by applying energy conservation over the surface (Incropera and Dewitt 1996). It is done by taking a sum of all the energy terms contributing to determine the surface temperature. This is an iterative process because the energy transfer depends on the surface temperature. When the surface temperature is obtained, the energy transferred from the drying air to the board by convection is calculated as the heat transferred from the surface to the interior of board by conduction.

Mathematical models based on thermodynamic relations provide a more realistic simulation of wood drying. They provide more accurate temperature and moisture profiles within the wood board because in this approach a board is usually divided into a certain number of elements in two or three different directions enabling us to solve two problems very efficiently. The first is solving the boundary conditions for calculating the heat transfer from the drying medium to the board and the second is to simulate a movement of the evaporation plane within a wood board during the drying process.

On the other hand, numerical models used for solving these kind of problems are more complicated and harder to implement. It also takes a long time to obtain the numerical solution which makes them unsuitable for simulating drying of a lumber stack consisted of many boards. To use those models in the drying of a stack of lumber, they would still have to be modified to account for differences in the mass and heat transfer coefficients and the drying air condition from board to board across the stack. Also, the right choices of the values of coefficients such as diffusivity, permeability, and mass and heat transport are essential for obtaining the results that are in good agreement with the experimental results.

It can be concluded that there is a trade-off in choosing which single board drying model will be used for simulating the drying process. If the heat and mass transfer within just one board is to be simulated, thereby simulating temperature and moisture profiles within the wood during drying, the mathematical model based on thermodynamics relations is most likely to be used. But, if the drying of a whole stack is to be simulated, a single board mathematical model based on the drying rate function should be used.

2.6.2 Stack drying models

There are two different approaches in modeling the drying of a stack of lumber. The first is called deterministic and is purely physical, using mathematical tools for obtaining solutions. The second is called stochastic and uses experimental observations and mathematical tools from the theory of probability and random numbers to obtain solutions.

The deterministic models try to describe all the physical processes, such as heat and mass transfer, occurring during drying. They are based on exact sciences such

as physics, thermodynamics, fluid mechanics, and material science. Capturing the physics of the drying process ensures solutions that match experimental results. Once the model results are in agreement with experimental results, it can be used then to simulate the drying process using different drying scenarios.

A disadvantage of this approach, though, is that all the parameters are considered as fixed values rather than as distributions. This is especially important for wood because variability is one of the most important wood features (Bowyer et al. 2003). It even exists within the same species coming from the same region and therefore all the properties are subject to variations. The deterministic models do not account for variations in properties and therefore they do not treat each board within a stack differently. Therefore this approach cannot account for the variability in drying parameters within a stack and is more suitable for calculating the averaged values of drying parameters.

The stochastic drying models are based on experimental observations and mathematical tools from the theory of probability and random numbers. Observations and experimental measurements are key things in using these models. A disadvantage of this approach is that no physical process equations are included in describing a drying process. It is based more on mathematical approximations of conclusions made from observations and experimental results. Even though they don't use energy and mass conservation equations which are essential in a drying process, they still can capture the physics of drying process by approximations of curves and dependences obtained experimentally or by deterministic models.

An advantage of stochastic stack models over the deterministic models is that they can account for variations in drying parameters between boards in a stack. They do that by considering the drying parameters as distributions using mathematical tools

from the theory of probability and random numbers. To use this approach, mean and standard deviation of certain drying parameters must be obtained experimentally.

Stochastic models account not only for variations in drying parameters of each board but also for a dynamic kiln behavior. A dynamic kiln behavior results in non-repetitive dryer performance.

Besides drying parameters and dynamic kiln behavior, green moisture content also varies among boards which further affects board drying behavior. The stochastic models can also capture this property using a mean and a deviation of green moisture content of certain species obtained experimentally.

What seems to be a problem with the stochastic models, considering that they don't use a physical model to describe a drying process, is that they are not so adaptive to changes in the drying conditions. From the paper on probabilistic analysis of timber drying schedules (Cronin, 2003) it can be seen that a different and much more complex equation than that for the single set point drying schedule had to be derived for the double set point schedule to describe a drying process (Eq. 2.5.4 - 2.5.7). In industrial practice a drying schedule is changed much more than two times, and often continuously during a drying process.

There is also one more concern emerging from the fact that the stochastic models do not use a physics model and it is how easy and if they can be adapted to the change of parameters that affect heat and mass transfer processes. Those parameters may be the geometry of the solid or the material from which it is made.

Therefore the combination of deterministic and stochastic model seems to be the best solution. Such a model was made by Kayihan (1985) and it showed an excellent agreement with experiments taking variability as well as a physical model into account. On one hand, this deterministic model takes advantage of physical model that describes a drying process faithfully and on the other hand allows the variability in drying properties, a kiln behavior, and green moisture content to be accounted for.

3. Mathematical description of the model

The mathematical model derived in this project simulates the mass and heat transfer processes taking place between wood and air during the drying of a stack of lumber (Fig. 3.1). Inputs to the model include the initial conditions for the wood, such as moisture content, temperature, and specific gravity, and air properties, such as temperature, humidity, and velocity during the drying process. The model outputs include five main drying variables:

a) Surface temperature for each board
b) Temperature of air
c) Temperature at center of boards
d) Absolute humidity of each air element
e) Moisture contents of boards

The model is based on general laws of energy (Eq. 3.1) and mass (Eq. 3.2) conservation applied on both the drying air and wood:

$$\frac{\partial E_{ACC}}{\partial t} = \dot{E}_{ACC} = \dot{E}_{IN} - \dot{E}_{OUT} + \dot{E}_{GEN} \tag{3.1}$$

$$\frac{\partial \rho}{\partial t} + \frac{\partial}{\partial x}(\rho \cdot v_x) = \Pi \tag{3.2}$$

And on the equations of conductive (Eq. 3.3) and convective (Eq. 3.4) heat transfer.

$$q_{cond} = -\lambda \frac{\partial T}{\partial x} \tag{3.3}$$

$$q_{conv} = h \cdot \Delta T \tag{3.4}$$

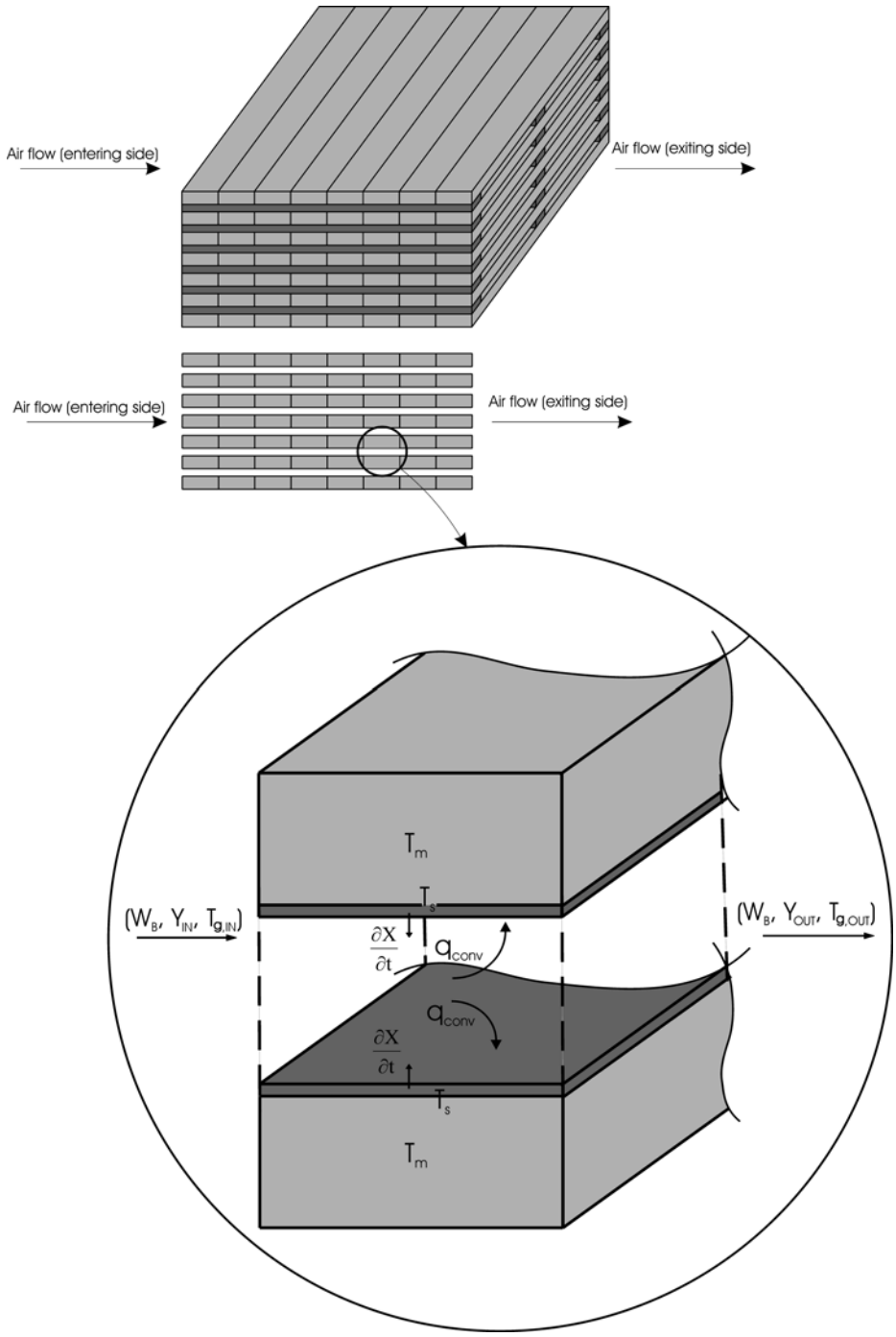

Figure 3.1 Illustration of a stack and a close look at a pair of boards and air between them on which the mass and energy balances are applied.

The drying variables for each pair of boards and the air element between them (Fig. 3.1) are calculated during an execution step. Properties of one air element at the exiting side become entering properties for the next air element in the flow direction.

The governing equations in the model are a system of coupled differential equations. The dependent variables are highly coupled and therefore all the calculations must be performed within iterations where one set of iterations is used to calculate one type of variable (temperature) and then another set of iterations is used to calculate of another type of variable (humidity, moisture content) based on the current value of the variables calculated within the first set of iterations.

The calculations or iterations are performed until all the variables are coupled where the criterion is a difference between the values of variables from the last and the current iteration. The criterion is a number small enough to ensure the accuracy of results and large enough to keep the running time short.

The model calculates a drying rate for each board using a drying rate function obtained experimentally (Chapter 5). Thus, the model does not deal with the behavior of free and bound water and water vapor separately but combines them. The drying rate function, which represents the overall contribution of all the moisture driving mechanisms, is directly used in the heat and mass transfer equations. The drying rate function provides a drying rate ($\frac{\partial X}{\partial t}$) [$kg_{H2O}/s$] or a drying flux [$kg_{H2O}/(s \cdot m^2)$] which is dependent on the properties of air flowing between the boards and the moisture content of the wood. As the properties change across the stack, the value of the drying rate changes as well.

Some assumptions were made to make to shorten the simulation run time. These were:

a) Work and kinetic and potential energy that exist in a system are neglected.

b) The process is considered to be isobaric.

c) Humid air is considered to be a mixture of two ideal gases, bone-dry air and water vapor. Each obeys the ideal gas law and Dalton's law.

d) The gas and solid are independent phases with characteristic properties.

e) Mass and energy transport are one-dimensional.

f) The evaporation plane does not recede into interior of a board but remains at the surface.

g) All the bonds between bound moisture and wood are broken before moisture reaches a surface.

h) Shrinkage is not taken into account.

Assumptions f and g are made because when using a drying rate function for describing moisture movement it is impossible to predict exact amounts of free and bound water and water vapor flowing through wood. Even though these assumptions deviate from reality, when combined with the drying rate function the wood behavior will be captured because all the removed moisture has to evaporate eventually and this energy is captured by the model equations.

3.1. Surface temperature (Energy conservation)

The surface temperature of the board must be known for other wood and air variables to be calculated. To calculate the surface temperature, the board is considered as one element with two infinitely thin surface layers. The energy conservation is applied on both layers to calculate an approximated value of T_s. In this case, the accumulation term energy in the surface layer can be neglected because $V_s \rightarrow 0$ so $\rho_S \cdot V_s \cdot (c_S + X \cdot c_v) \cdot (\frac{\partial T_s}{\partial t}) \rightarrow 0$ also. Note that even though the surfaces are considered infinitely thin, they appear with a finite thickness on all the figures used for deriving the governing equations. This was done to distinguish a surface from interior of a board.

Because a board was considered as one element, the heat between the infinitely thin surface and the rest of the board is conducted over half of board thickness (b/2). This is consistent with the finite volume approach as described by Patankar (1980). In addition, the model assumptions that all moisture evaporates from a surface layer and that all the bonds between bound moisture and wood are broken before moisture reaches a surface are important. Therefore, there is not a term describing energy for breaking bonds between bound moisture and wood in the equation for the surface temperature but only energy required for evaporation of moisture.

The following three terms determine the board surface temperature (Fig. 3.1.1):

a) Rate of energy transfer by convection from air to the surface

$$q_{conv} = h \cdot (T_g - T_s) \cdot A \Big|_{\substack{\text{upper} \\ \text{or lower} \\ \text{surface}}}$$

b) Rate of energy transfer by conduction from the surface to the interior of the board

$$q_{cond} = \left[\frac{\lambda_S}{\frac{b}{2}} \cdot (T_s - T_m) \cdot A\right]\Bigg|_{\substack{\text{upper}\\ \text{or lower}\\ \text{surface}}}$$

c) Energy required for the evaporation of moisture

$$\rho_s \cdot V_s \cdot (-\frac{\partial X}{\partial t}) \cdot (\Delta H)\Bigg|_{\substack{\text{upper}\\ \text{or lower}\\ \text{surface}}}$$

These are combined so that the energy balance applied on the surface is defined as follows:

$$h \cdot (T_g - T_s)\Big|_{\substack{\text{upper}\\ \text{or lower}\\ \text{surface}}} \cdot A - \left[\frac{\lambda_S}{\frac{b}{2}} \cdot (T_s - T_m) \cdot A\right]_{\substack{\text{upper}\\ \text{or lower}\\ \text{surface}}} - \rho_s \cdot V_s \cdot (-\frac{\partial X}{\partial t}) \cdot (\Delta H)\Big|_{\substack{\text{upper}\\ \text{or lower}\\ \text{surface}}} = 0 \quad (3.1.1)$$

From the equation (3.1.1) the temperature for the lower and upper surface can be calculated as:

$$T_{s,\,l(u)} = \frac{h \cdot T_g\Big|_{\substack{\text{upper}\\ \text{or lower}\\ \text{surface}}} + \frac{\lambda_S}{\frac{b}{2}} \cdot T_m - \rho_s \cdot b \cdot (-\frac{\partial X}{\partial t}) \cdot (\Delta H)\Big|_{\substack{\text{upper}\\ \text{or lower}\\ \text{surface}}}}{\frac{\lambda_S}{\frac{b}{2}} + h_{l(u)}} \quad (3.1.2)$$

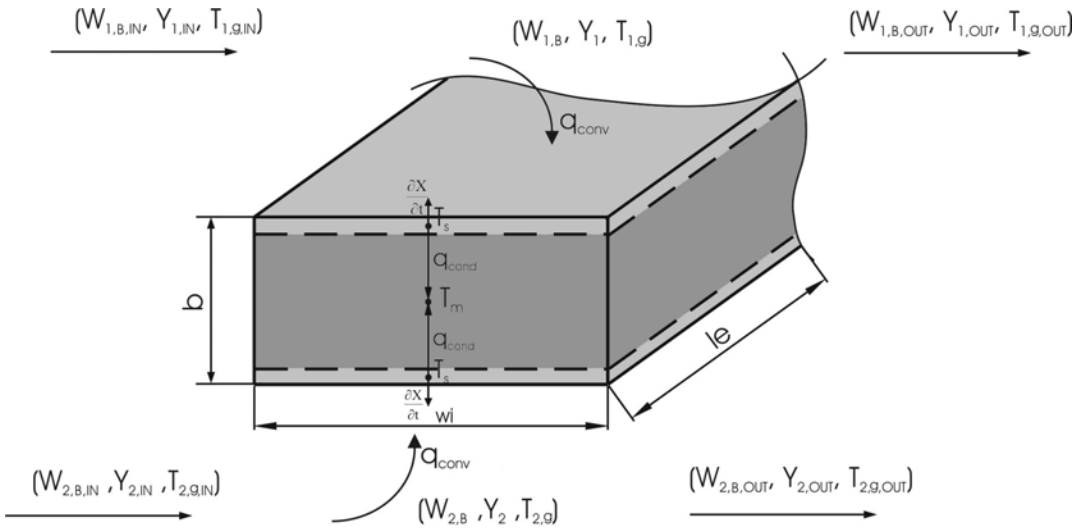

Figure 3.1.1 Parameters for calculating a surface and board centerline temperature (T_s and T_m).

3.2 Air temperature (Energy conservation)

The air temperature (Fig. 3.2.1) is calculated using the following terms:

a) Energy required due to the change of enthalpy of the air element from the input to the output side

$$v \cdot \rho_B \cdot V_g \cdot \frac{\partial i}{\partial x}$$

where enthalpy is defined as $i = c_B \cdot T_g + Y \cdot (c_v \cdot (T_g - 273.15) + \Delta H)$

b) Rate of energy transfer from air to the board surface by convection

$$q_{conv} = \sum_{\substack{\text{lower and} \\ \text{upper board}}} h \cdot (T_g - T_s) \cdot A$$

c) Energy of water vapor released off the board surface

$$\sum_{\substack{\text{upper and lower} \\ \text{board}}} \rho_S \cdot V_S \cdot (-\frac{\partial X}{\partial t}) \cdot (\Delta H + c_v \cdot (T_s - 273.15))$$

d) Energy required to change the water vapor from the surface temperature to the air temperature

$$\sum_{\substack{\text{upper and lower}\\ \text{board}}} \rho_S \cdot V_S \cdot (-\frac{\partial X}{\partial t}) \cdot (c_v \cdot (T_g - T_s))$$

The accumulation term can be neglected due to the highly convective flow. $(\rho_B \cdot V_g \cdot \frac{\partial i}{\partial t} = 0)$.

The energy balance over one air element is then defined as:

$$\begin{aligned} & v \cdot \rho_B \cdot V_g \cdot \frac{\partial i}{\partial x} = -h \cdot (T_g - T_s) \cdot A + \\ & + \sum_{\substack{\text{upper and lower}\\ \text{board}}} \rho_S \cdot V_S \cdot (-\frac{\partial X}{\partial t}) \cdot (\Delta H + c_v \cdot (T_s - 273.15) - c_v \cdot (T_g - T_s)) \end{aligned} \tag{3.2.1}$$

where the convective mass transfer coefficient (h) is obtained using equations described in the section 3.6.1.

The mass flow of dry air is:

$$W_B = \frac{v \cdot \rho_B \cdot V_g}{\Delta x} = \frac{v \cdot \rho_B \cdot V_g}{wi} \tag{3.2.2}$$

Combining equations 3.21 and 3.2.2 gives:

$$T_{g,OUT} = \frac{-h \cdot (T_g - T_s) \cdot A}{W_B \cdot (c_B + c_v \cdot Y)} + \frac{\sum_{\substack{\text{upper and lower} \\ \text{board}}} \rho_S \cdot V_S \cdot (-\frac{\partial X}{\partial t}) \cdot (c_v \cdot T_s - c_v \cdot (T_g - T_s))}{W_B \cdot (c_B + c_v \cdot Y)} + T_{g,IN} \tag{3.2.3}$$

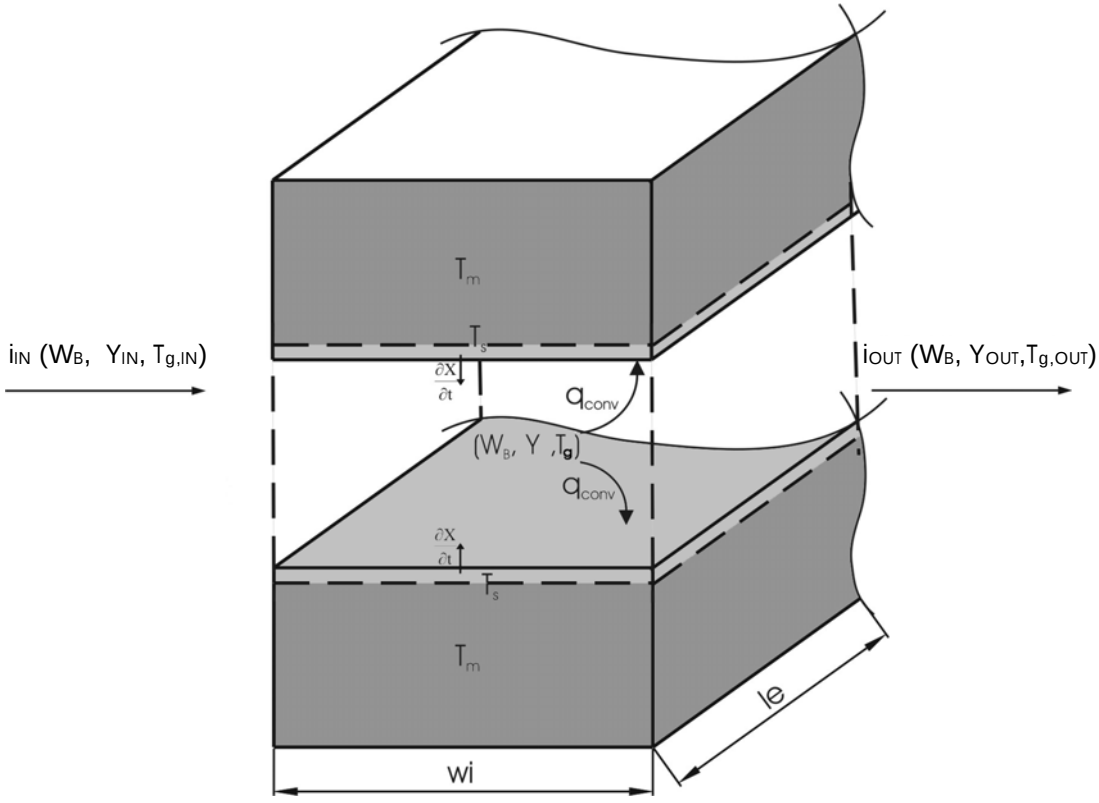

Figure 3.2.1 Parameters for calculating an air temperature T_g.

3.3 Board temperature (Energy conservation)

The equations to determine centerline temperature are applied to the entire volume of the board because the surfaces are considered infinitely thin. For the representation of the term $\partial T/\partial t$, it will be adopted that the temperature in the center of the board prevails throughout the control volume, which is consistent with the finite volume approach as described by Patankar (1980). To calculate a board centerline temperature there are several terms that are taken into consideration (Fig. 3.1.1):

a) Rate of energy accumulation within a board (accumulation term)

$$\rho_S \cdot V_S \cdot (c_S + X \cdot c_{Al}) \cdot (\frac{\partial T_m}{\partial t})$$

b) Rate of energy transfer from the surfaces to the board by conduction

$$q_{cond} = \sum_{\substack{\text{upper and lower} \\ \text{surface}}} \frac{\lambda_S}{\frac{b}{2}} \cdot (T_s - T_m) \cdot A$$

c) Rate at which energy is used for heating liquid moisture from the board to the surface temperature

$$\sum_{\substack{\text{upper and lower} \\ \text{surface}}} \rho_S \cdot V_S \cdot (-\frac{\partial X}{\partial t}) \cdot (c_{Al} \cdot (T_m - T_s))$$

d) Rate at which energy is used to break bonds between bound moisture and wood

$$\rho_S \cdot V_S \cdot (-\frac{\partial X}{\partial t}) \cdot \Delta E_w$$

This term is only applied to bound water for moisture content below the fiber saturation point of 30%.

Combining these, the energy conservation equation around a board is defined as:

$$\rho_S \cdot V_S \cdot (c_S + X \cdot c_{Al}) \cdot (\frac{\partial T_m}{\partial t}) = \sum_{\substack{\text{upper and lower} \\ \text{side of board}}} \frac{\lambda_S}{\frac{b}{2}} \cdot (T_s - T_m) \cdot A - \\ - \sum_{\substack{\text{upper and lower} \\ \text{side of board}}} \rho_S \cdot V_S \cdot (-\frac{\partial X}{\partial t}) \cdot (c_{Al} \cdot (T_s - T_m) + \Delta E_w) \quad (3.3.1)$$

After a rearrangement of the equation 3.3.1, it follows that the board centerline temperature is:

$$T^t{}_m = \frac{\sum_{\substack{\text{upper and} \\ \text{lower side} \\ \text{of board}}} [\frac{\lambda_S}{\frac{b}{2}} \cdot (T_s - T^{t-\Delta t}{}_m) \cdot A - \rho_S \cdot V_S \cdot (-\frac{\partial X}{\partial t}) \cdot (\Delta E_w + c_{Al} \cdot (T_s - T^{t-\Delta t}{}_m))]}{\rho_S \cdot V_S \cdot (c_S + X \cdot c_{Al})} \cdot \Delta t + \\ + T^{t-\Delta t}{}_m \quad (3.3.2)$$

3.4 Absolute humidity of air (Mass conservation)

The absolute humidity of an air element is obtained by using a mass conservation equation which accounts for:

a) Difference between the rate at which the humidity enters and leaves the air element

$$v \cdot \rho_B \cdot V_g \cdot \frac{\partial Y}{\partial x}$$

b) Rate at which water vapor comes out of wood

$$\sum_{\substack{\text{upper and/or lower}\\ \text{board}}} \rho_S \cdot V_S \cdot (-\frac{\partial X}{\partial t})$$

The change of the absolute humidity of the air element with time can be neglected due to the highly convective flow ($\rho_B \cdot V_g \cdot \frac{\partial Y}{\partial t} = 0$).

The mass balance over the air element is as follows:

$$v \cdot \rho_B \cdot V_g \cdot \frac{\partial Y}{\partial x} = \sum_{\substack{\text{upper and/or lower}\\ \text{board}}} \rho_S \cdot V_S \cdot (-\frac{\partial X}{\partial t}) \qquad (3.4.1)$$

The mass flow of dry air is:

$$W_B = \frac{v \cdot \rho_B \cdot V_g}{\Delta x} \qquad (3.4.2)$$

After a substitution of the equation 3.4.2 into the equation 3.4.1, it follows that

$$Y_{OUT} = \frac{\sum_{\substack{\text{upper and/or lower}\\ \text{board}}} \rho_S \cdot V_S \cdot (-\frac{\partial X}{\partial t})}{W} + Y_{IN} \qquad (3.4.3)$$

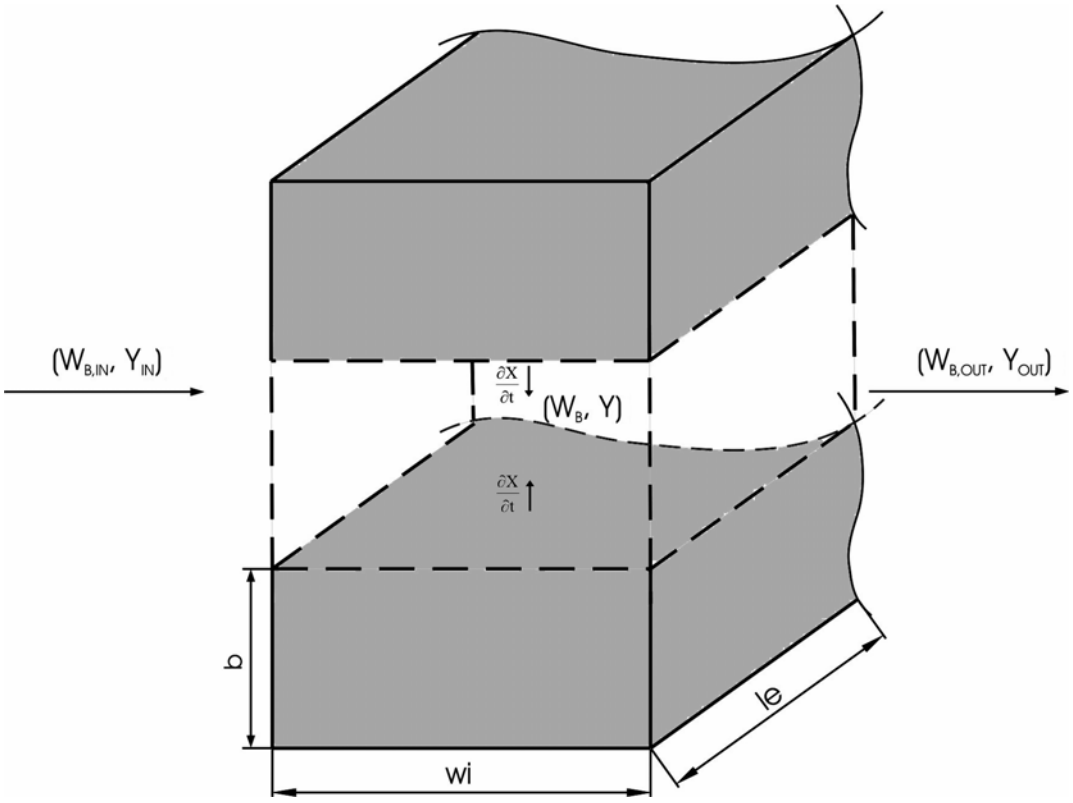

Figure 3.4.1 Parameters for calculating an absolute air humidity Y.

3.5 Moisture content of a board (mass conservation)

When there is no condensation, moisture content of boards is calculated using the following terms (Fig. 3.5.1):

a) Accumulation term or the rate at which the water content of a whole board changes

$$\rho_s \cdot V_s \cdot \frac{\partial X}{\partial t}$$

b) Amount of moisture removed per unit time

$$\sum_{\substack{\text{lower and}\\ \text{upper surface}}} w_D \cdot A$$

where w_D is calculated based on the characteristic drying rate function

The mass balance for a board can be defined as follows:

$$\rho_s \cdot V_s \cdot \frac{\partial X}{\partial t} = - \sum_{\substack{\text{lower and}\\ \text{upper surface}}} w_D \cdot A \qquad (3.5.1)$$

After a rearrangement of the equation 3.5.1 it follows that:

$$X^t = \frac{- \sum_{\substack{\text{lower and}\\ \text{upper surface}}} w_D \cdot A}{\rho_s \cdot V_s} \cdot \Delta t + X^{t-\Delta t} \qquad (3.5.2)$$

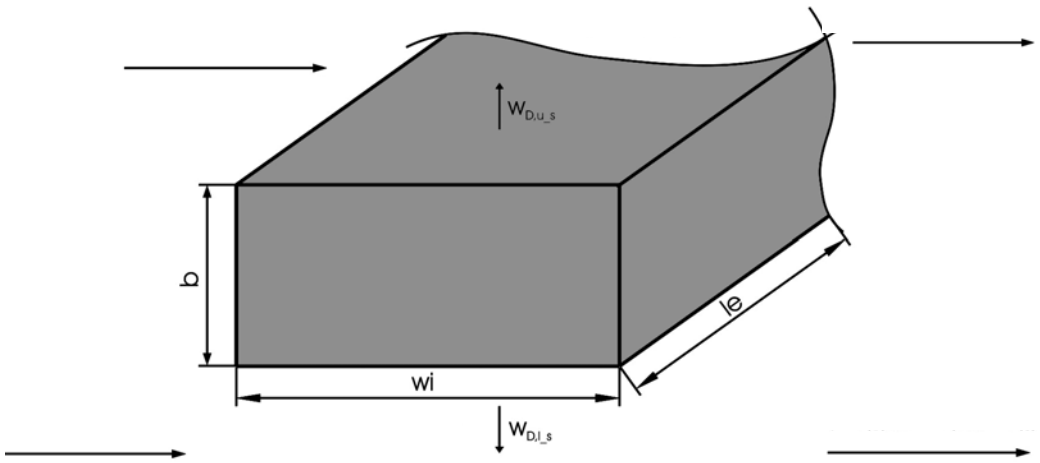

Figure 3.5.1 Parameters for calculating board moisture content X.

When a condensation occurs the following terms are used to calculate the moisture content of a board:

a) Accumulation term or the rate at which the current moisture content of a whole board changes, $\rho_s \cdot V_s \cdot \frac{\partial X}{\partial t}$

b) Amount of condensed water going to the board, $c \cdot \beta \cdot (\rho_{v,s} - \rho_{v,g}) \cdot A$

The mass balance for a board can then be defined as follows:

$$\rho_s \cdot V_s \cdot \frac{\partial X}{\partial t} = -c \cdot \beta \cdot (\rho_{v,s} - \rho_{v,g}) \cdot A \qquad (3.5.3)$$

For this work it was assumed that all the condensed water ran off the boards so c is considered to be zero.

3.6 Thermophysical properties of air, water, and wood

To solve the system of coupled equations describing the heat and mass transfer during wood drying, the thermophysical properties of the wood, water, and the drying gas have to be calculated during the simulation. Each equation was tested by comparing it with published values in literature over the full range of its use.

3.6.1 Thermophysical properties of air and water

Saturated water vapor pressure

The saturated vapor pressure must be obtained before any of the properties of air can be calculated. All the other air properties can be obtained using standard

thermodynamic relationships. The saturated water vapor pressure is obtained from the following expression (Yaws 1999):

$$p_{v,sat} = 133.3223684 \cdot 10^{\left(29.861 - \frac{3152.2}{T} - 7.3037 \cdot \frac{\mathrm{Log}(T)}{\mathrm{Log}(10)} + 0.24247 \cdot 10^{-8} \cdot T + 0.1809 \cdot 10^{-5} \cdot T^2\right)} \tag{3.6.1.1}$$

Heat capacities

The heat capacity for dry air is calculated as follows (Cadiergues 1977):

$$c_B = 1005 \tag{3.6.1.2}$$

The heat capacity of water vapor is obtained by the following equation (Mujumdar and Devastahin 2000):

$$\begin{aligned} c_v = {} & 1883 - 1673.7 \cdot 10^{-4}(T_v - 273.15) + \\ & + 8438.6 \cdot 10^{-7}(T_v - 273.15)^2 - 2696.6 \cdot 10^{10}(T_v - 273.15)^3 \end{aligned} \tag{3.6.1.3}$$

The heat capacity of water is calculated as (Mujumdar and Devastahin 2000):

$$\begin{aligned} c_{Al} = {} & 2822.3 + 1182.8 \cdot 10^{-2}(T_{Al} - 273.15) - \\ & - 3504.3 \cdot 10^{-5}(T_{Al} - 273.15)^2 + \\ & + 3601 \cdot 10^{-8}(T_{Al} - 273.15)^3 \end{aligned} \tag{3.6.1.4}$$

Latent heat of vaporization

The latent heat of vaporization is calculated as (Stanish et al. 1986):

$$\Delta H = 2792000 - 160 \cdot T_{Al} - 3.42 \cdot T_{Al}^2 \tag{3.6.1.5}$$

Convective heat and mass transfer coefficients of air flowing between two boards

The value of the convective heat transfer coefficient is a function of the Reynolds, Prandtl, and Nusselt numbers for the air between two parallel plates (Rohsenow and Hartnett 1973**,** Mujumdar and Devahastin 2000):

$$\mathrm{Re} = \frac{\rho_g \cdot \mathrm{ST} \cdot v_g}{\mu_g} \tag{3.6.1.6}$$

$$\mathrm{Pr} = \frac{c_g \cdot \mu_g}{\lambda_g} \tag{3.6.1.7}$$

$$\mathrm{Nu} = \begin{cases} 5.5, & \mathrm{Re}\cdot\mathrm{Pr} < 300 \\ 0.5029\cdot(\mathrm{Re}\cdot\mathrm{Pr})^{0.4194}, & 300 \le \mathrm{Re}\cdot\mathrm{Pr} \le 2000 \\ 0.1244\cdot(\mathrm{Re}\cdot\mathrm{Pr})^{0.6032}, & \mathrm{Re}\cdot\mathrm{Pr} > 2000 \end{cases} \tag{3.6.1.8}$$

$$h = \frac{\mathrm{Nu}\cdot\lambda_g}{\mathrm{ST}} \tag{3.6.1.9}$$

where

$$\begin{aligned} \lambda_g = {} & 2.425\cdot10^{-2} - 7.889\cdot10^{-5}(T_g - 273.15) - \\ & - 1.790\cdot10^{-8}(T_g - 273.15)^2 - \\ & - 8.570\cdot10^{-12}(T_g - 273.15)^3 \end{aligned} \tag{3.6.1.10}$$

$$c_g = 1.00926 \cdot 10^3 - 4.0403 \cdot 10^{-2}(T_g - 273.15) + \\ +6.1759 \cdot 10^{-4}(T_g - 273.15)^2 - 4.097 \cdot 10^{-7}(T_g - 273.15)^3 \quad (3.6.1.11)$$

$$\mu_g = 1.691 \cdot 10^{-5} + 4.984 \cdot 10^{-8}(T_g - 273.15) - \\ - 3.187 \cdot 10^{-11}(T_g - 273.15)^2 + \\ +1.319 \cdot 10^{-14}(T_g - 273.15)^3 \quad (3.6.1.12)$$

The value of the convective mass transfer coefficient is a function of Reynolds, Schmidt, and Sherwood number for air flow between two parallel plates where Reynolds number is calculated in the same manner as above (Eq. 3.6.1.6) (Rohsenow and Hartnett 1973**,** Mujumdar and Devahastin 2000):

$$Sc = \frac{\nu_g}{D_g} \quad (3.6.1.13)$$

$$Sh = \begin{cases} 5.5, & Re \cdot Sc < 300 \\ 0.5029 \cdot (Re \cdot Sc)^{0.4194}, & 300 \le Re \cdot Sc \le 2000 \\ 0.1244 \cdot (Re \cdot Sc)^{0.6032}, & Re \cdot Sc > 2000 \end{cases} \quad (3.6.1.14)$$

$$\beta = \frac{Sh \cdot D_g}{ST} \quad (3.6.1.15)$$

where

$$\nu_g = \frac{\mu_g}{\rho_g} \quad (3.6.1.16)$$

$$D_g = 2.20 \cdot 10^{-5} \cdot \left(\frac{101325}{p_g}\right)\left(\frac{T_g}{273.15}\right)^{1.75} \quad (3.6.1.17)$$

3.6.2 Thermophysical properties of wood

Specific heat of wood

The specific heat of bone-dry wood can be calculated from the following formula (Forest Products Laboratory, 1999):

$$c_S = 3.867 \cdot T_S + 103.1 \qquad (3.6.2.1)$$

In the governing equations, the specific heat of moist wood is calculated as a sum of the specific heats of bone dry wood and the moisture within wood.

Enthalpy of wetting

When wood moisture content drops below the fiber saturation point only bound water is present in wood. It is bound to wood matrix and therefore the additional amount of energy is required for breaking these bonds.

The enthalpy of wetting per kg of bone dry wood is calculated using the following expression (Skaar 1991):

$$\Delta E_w = \int_{X_{fsp}}^{X} 1.17 \cdot 10^6 \cdot e^{(-14 \cdot X)} dX = -\frac{1.17 \cdot 10^6}{14} \cdot (e^{-14 \cdot X_{fsp}} - e^{-14 \cdot X}) \qquad (3.6.2.2)$$

The integral of the function ($1.17 \cdot 10^6 \cdot e^{(-14 \cdot X)} dX$) was taken over a moisture range because it is dependent on moisture content. The area below this function is actually the energy required for breaking bonds between the bound water and wood at certain moisture content (X).

4. A general algorithm used in the model

The calculation algorithm used in the model is showed in Figure 4.1. The algorithm consists of several parts:

a) An input part which reads input parameters from Excel spreadsheet and places them into arrays

b) A part that selects the appropriate drying schedule based on the current time step

c) The main function which calculates the five main variables

d) An output part which both displays the current values of the main variables and exports them to an Excel spreadsheet.

In addition to the main algorithm that calculates the drying variables, a second algorithm is used to make it easier to enter input or initial data, through an Excel spreadsheet.

All the input data are entered in the spreadsheets before the simulation is run. The simulation reads the data from the spreadsheets places them into arrays and, then starts with calculations (Figure 4.2).

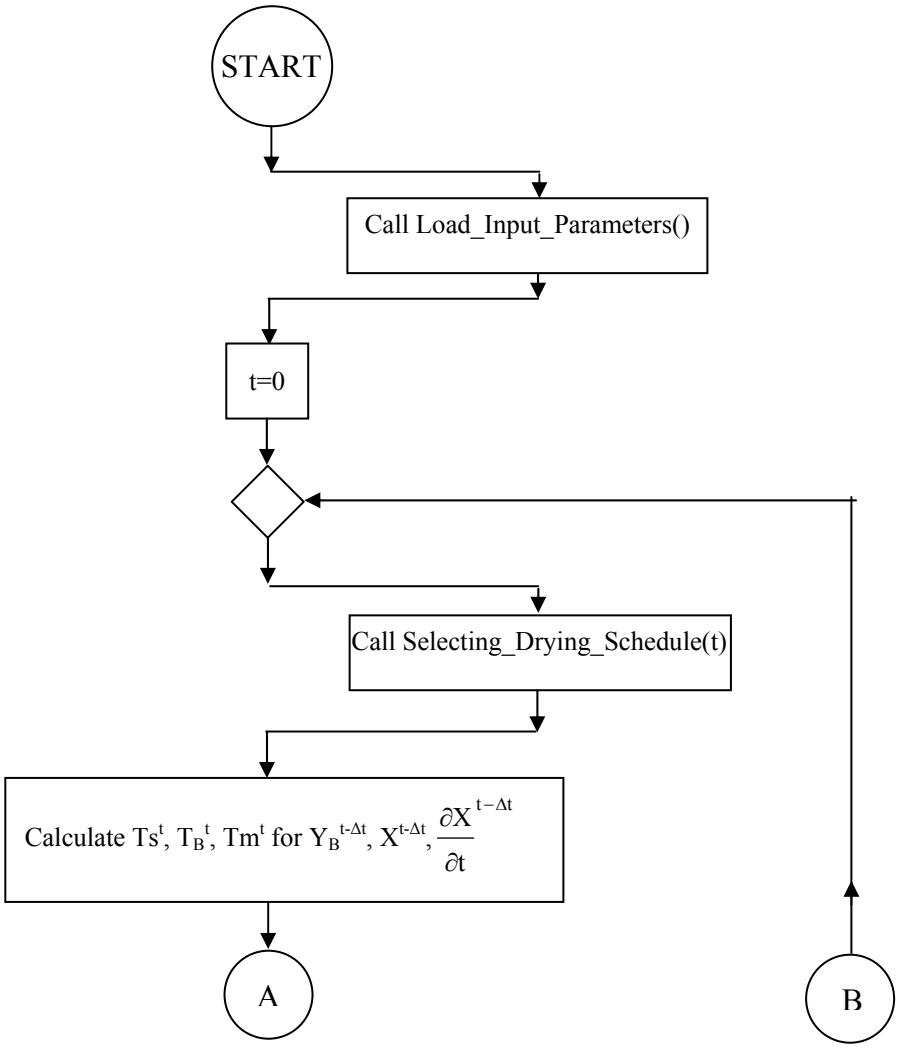

Figure 4.1 The algorithm used in modeling.

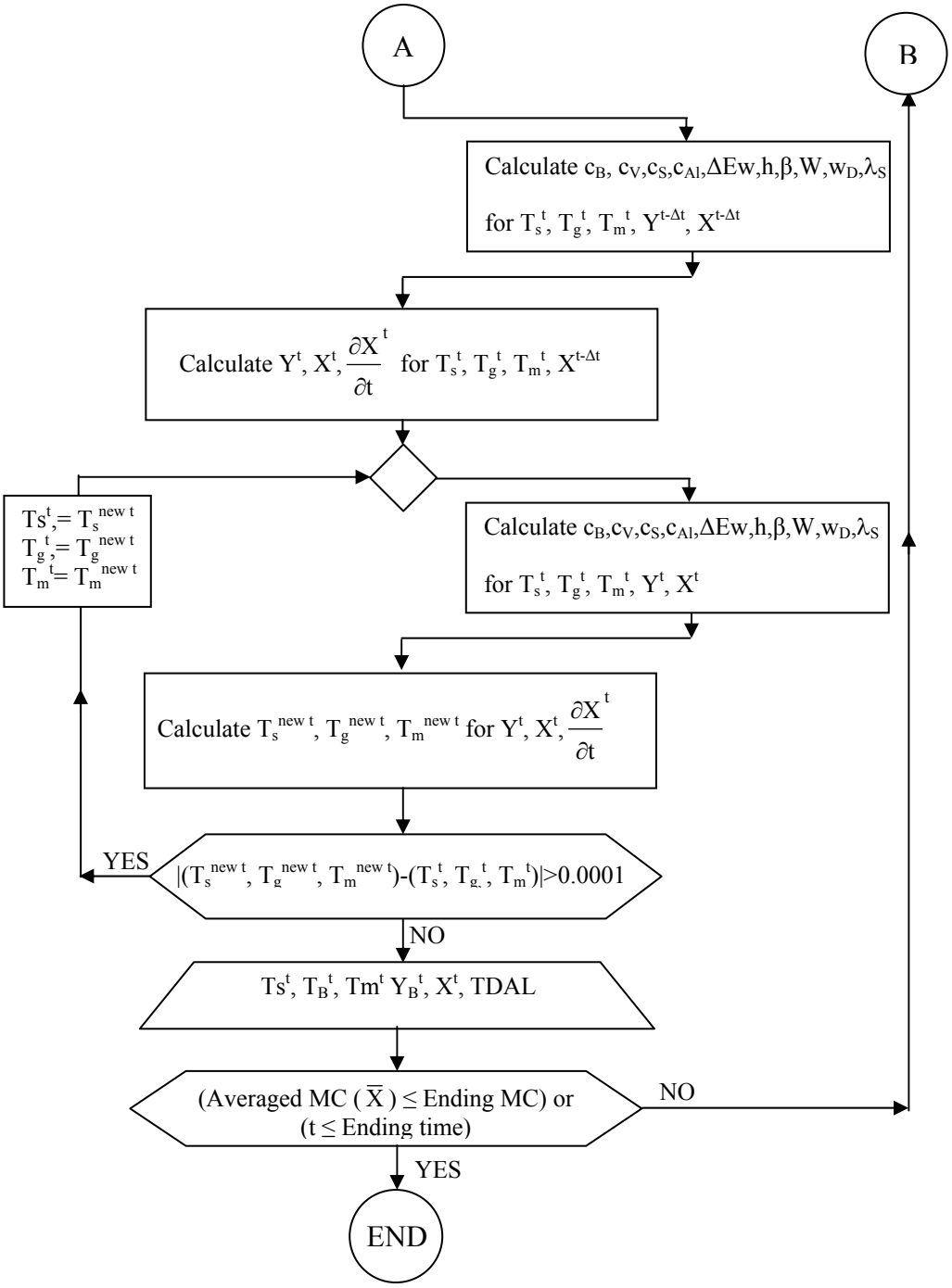

Figure 4.1 (Continued) The algorithm used in modeling.

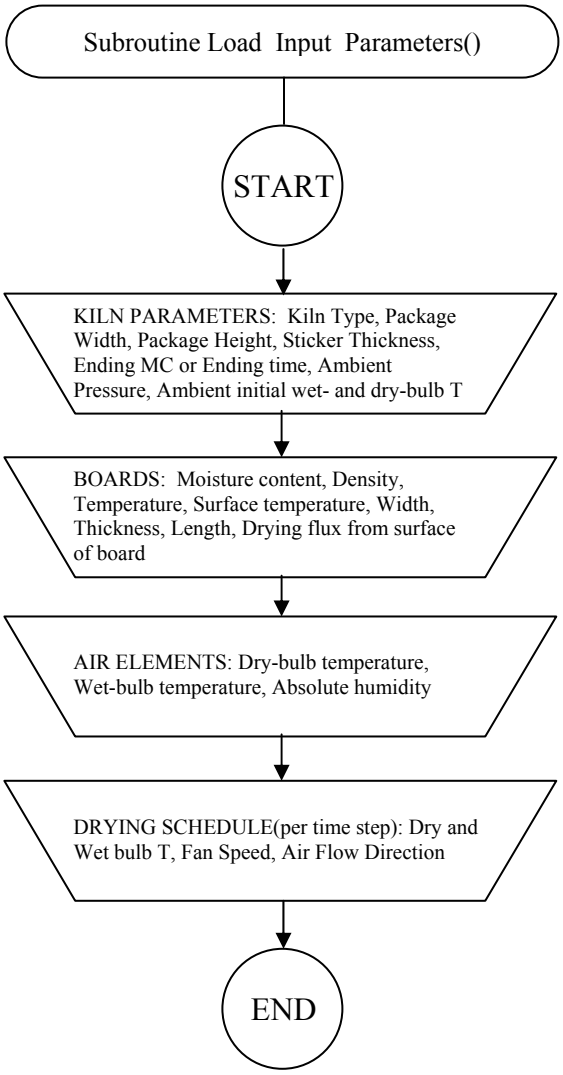

Figure 4.1 (Continued) The algorithm used in modeling.

The reading algorithm consists of several steps:

a) Setting a link between a Visual Basic and Excel environment

b) Reading the data

c) Close a connection

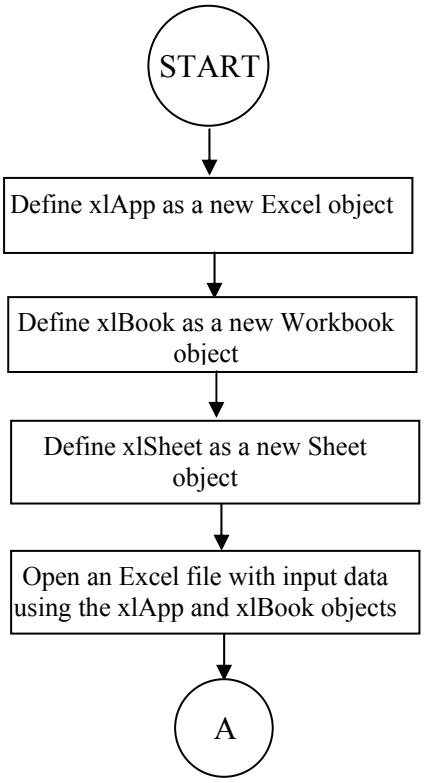

Figure 4.2 The algorithm used for reading data from an Excel sheet.

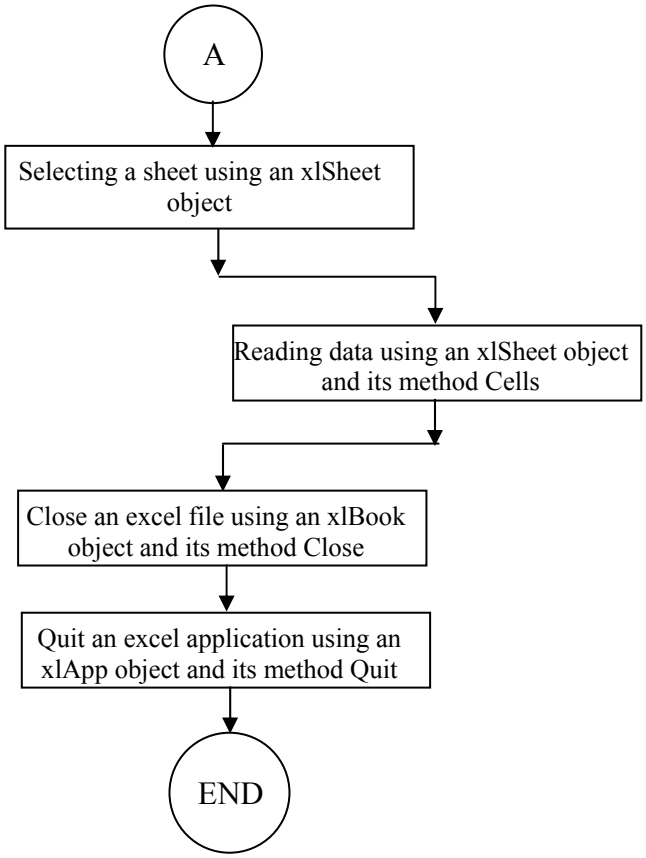

Figure 4.2 (Continued) The algorithm used for reading data from an Excel sheet.

5. Materials and methods

5.1 Introduction

The data from two experiments were used to test the model. In the first, the drying rate for hemlock lumber was determined as a function of wood moisture content and air temperature and humidity. This provided the characteristic drying rate function for the model. In the second, full packages of lumber were dried and the results were compared to the simulation results to validate the model.

5.2 Obtaining a drying rate function

5.2.1 Experiments

Existing published and unpublished data were used for determining the drying rate function. The data came from 23 charges of western hemlock *(Tsuga heterophylla)* lumber that were dried to measure the volatile organic compounds released. Moisture content versus time, the drying curve needed as model input, was developed for each charge as these experiments were conducted. They were conducted using a range of temperatures and humidities typical of those seen in industry.

The hemlock used in the experiments was all dimension lumber with a 2" nominal thickness and nominal widths of 4", 6", 8", or 10". The actual green thickness was approximately 1.65" to 1.7" (4.19 to 4.32 cm) and the actual width was slightly less than the nominal width.

The wood was obtained in 4-foot (1.22-m) lengths from various locations in western Oregon and Washington, at various seasons of the year. The samples were

taken from normal production prior to drying so the wood should be typical of that dried commercially.

The boards were either dried immediately upon arriving at the laboratory, refrigerated for up to 10 days until being dried, or frozen and thawed prior to drying. The boards were wrapped in plastic during shipping and storage to prevent moisture loss.

Approximately 500 boards were dried in the 23 charges. Prior to drying each board was weighed. They were then stacked in the kiln in a stack that was one, two, or three boards wide, depending on the width of the lumber. The stack was 10 or 11 courses high and a charge consisted of 14 to 33 boards.

The dry-bulb temperature ranged from 130°F to 228°F (54.4°C to 108.9°C) and the wet-bulb temperature ranged from 115°F to 192°F (46.1°C to 88.9°C). These are just the boundary values and most of the data used for obtaining the drying rate function were in the dry-bulb range of 160°F to 224°F (71.1°C to 106.7°C) and wet-bulb temperature range of 120°F to 182°F (48.9°C to 83.3°C) (Table 5.2.1.1).

The air velocity was 750 ft/min (3.81 m/s). The schedules were typical of those in industry with a 2- to 8-hour warm-up period followed by a constant or increasing dry-bulb temperature and a decreasing relative humidity.

The typical initial wet-bulb depression was 10-20°F (5.5-11.1°C). The drying conditions were recorded ever three minutes. These included the dry- and wet-bulb temperatures and airflow into the kiln.

Each board was weighed after drying. They were then placed in an oven at 217.4°F (103°C) until a constant weight was attained and reweighed. The full procedure for this data collection can be found in Milota and Mosher (2006).

Table 5.2.1.1 Drying schedules for 23 charges of hemlock for obtaining the drying rate function

Charge [#]	Drying schedule [Figure #]	Reference
1, 2	5.2.1.1	Milota and Mosher, 2006
3	5.2.1.2	
4	5.2.1.3	
5	5.2.1.4	Milota, 2007
6	5.2.1.5	Milota and Mosher, 2006
7	5.2.1.6	
8, 9	5.2.1.7	Milota, 2007
10	5.2.1.8	Milota and Mosher, 2006
11	5.2.1.9	
12	5.2.1.10	
13, 14, 15	5.2.1.11	
16, 17, 18	5.2.1.12	
19, 20, 21, 22, 23	5.2.1.13	

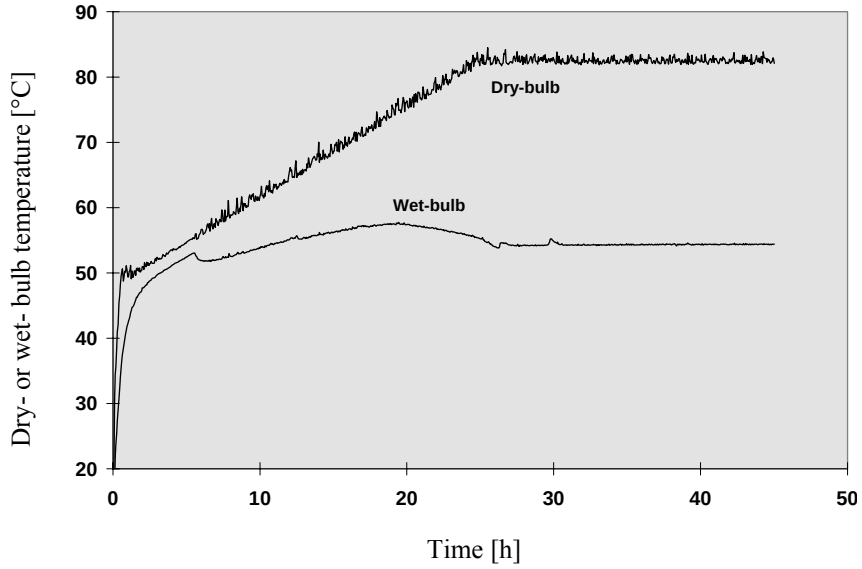

Figure 5.2.1.1 Dry- and wet-bulb temperatures and drying time used for small charges of hemlock (Charge 1 and 2).

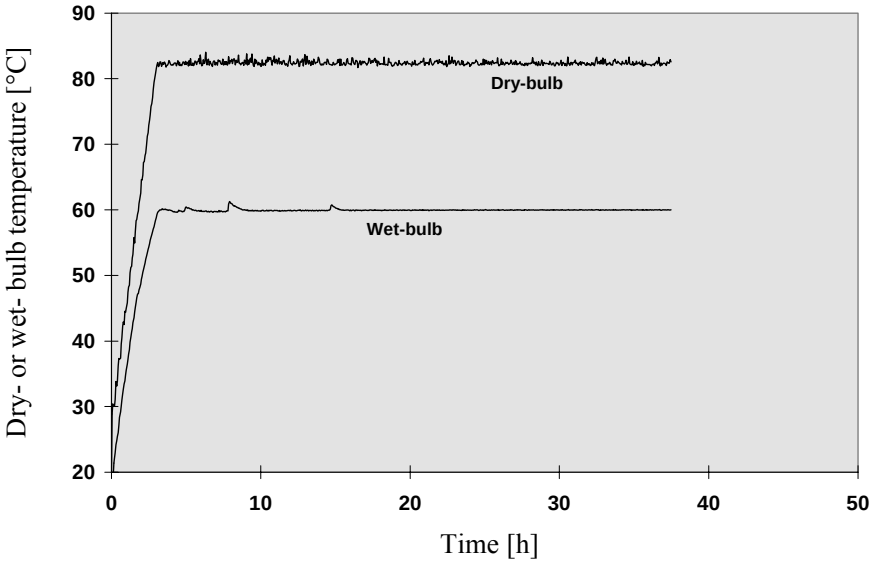

Figure 5.2.1.2 Dry- and wet-bulb temperatures and drying time used for small charges of hemlock (Charge 3).

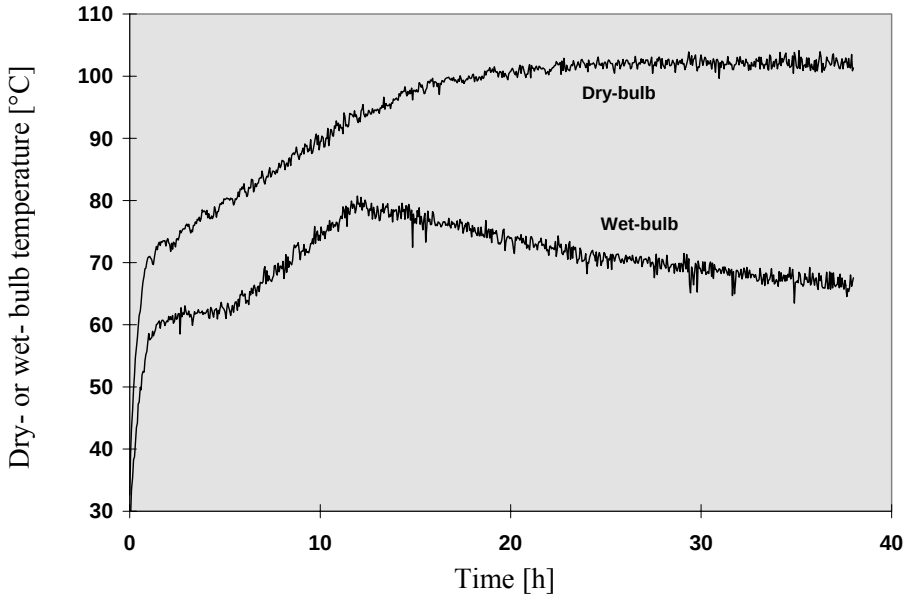

Figure 5.2.1.3 Dry- and wet-bulb temperatures and drying time used for small charges of hemlock (Charge 4).

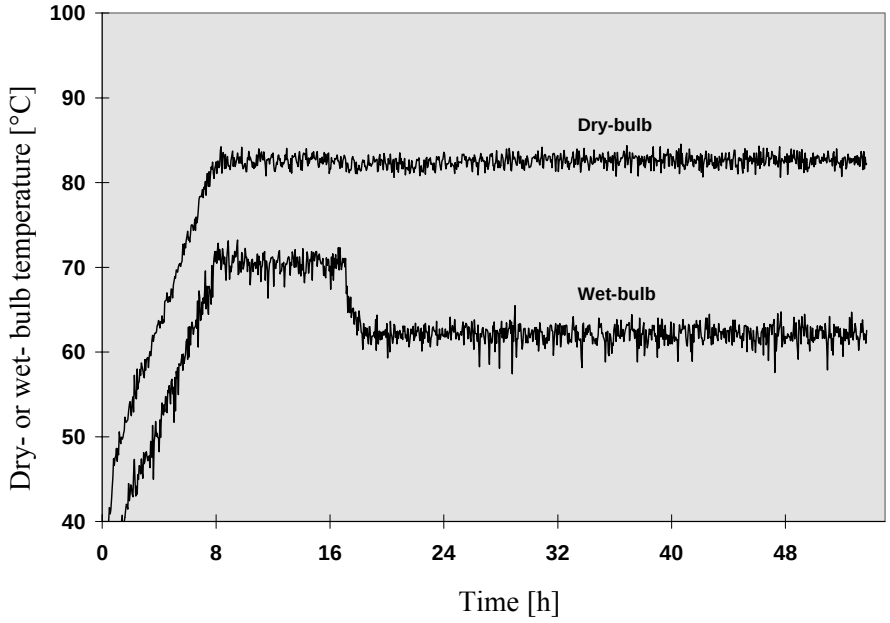

Figure 5.2.1.4 Dry- and wet-bulb temperatures and drying time used for small charges of hemlock (Charge 5).

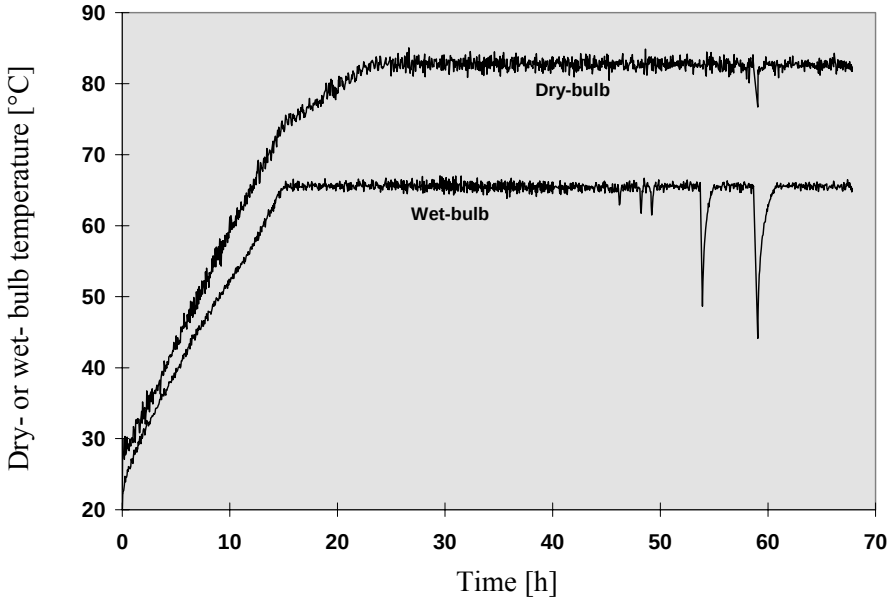

Figure 5.2.1.5 Dry- and wet-bulb temperatures and drying time used for small charges of hemlock (Charge 6).

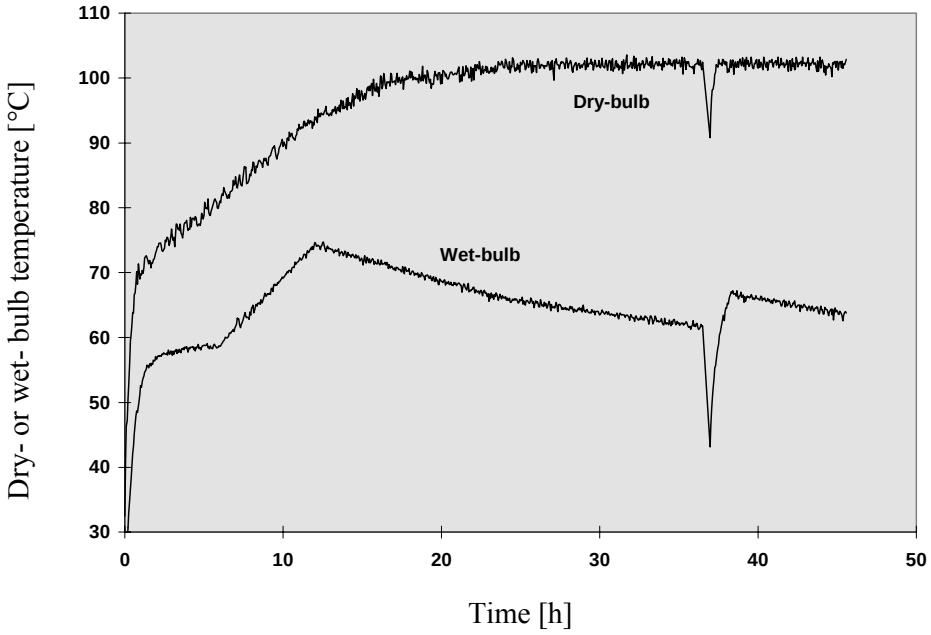

Figure 5.2.1.6 Dry- and wet-bulb temperatures and drying time used for small charges of hemlock (Charge 7).

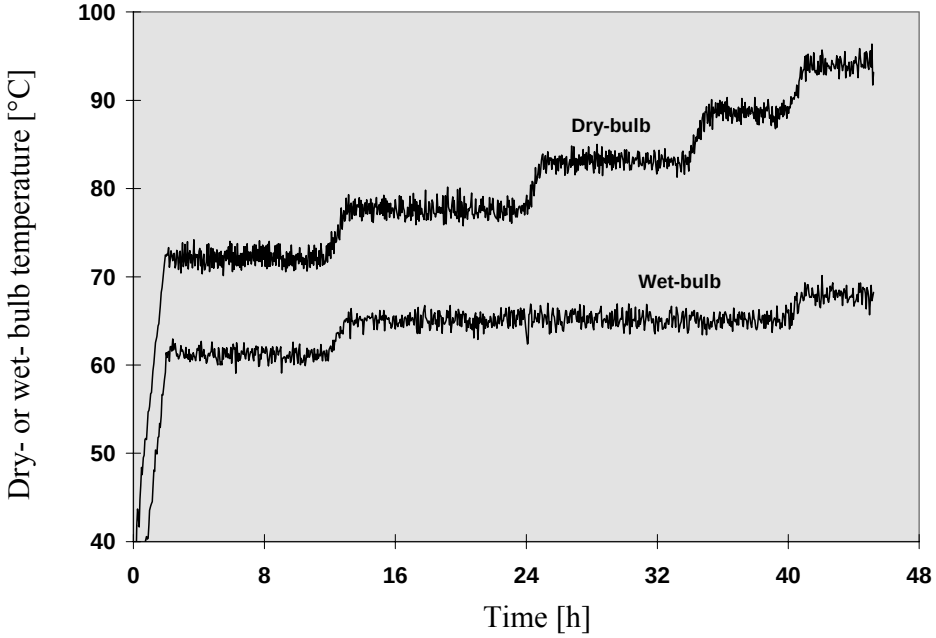

Figure 5.2.1.7 Dry- and wet-bulb temperatures and drying time used for small charges of hemlock (Charge 8 and 9).

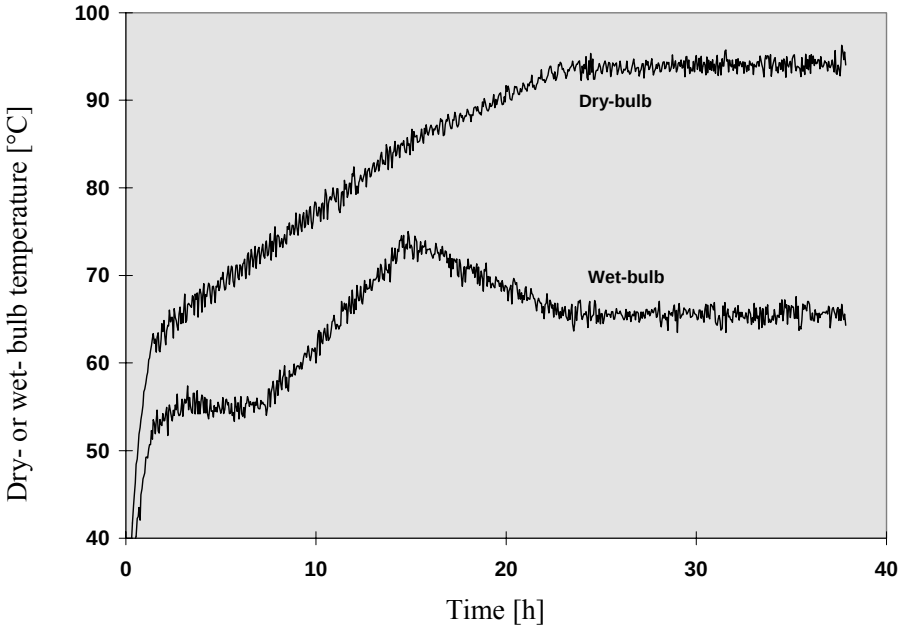

Figure 5.2.1.8 Dry- and wet-bulb temperatures and drying time used for small charges of hemlock (Charge 10).

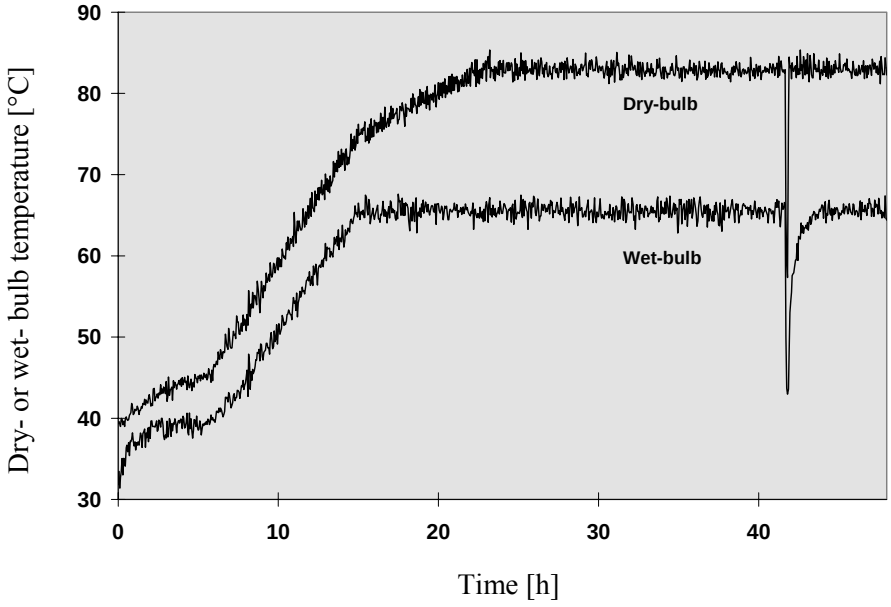

Figure 5.2.1.9 Dry- and wet-bulb temperatures and drying time used for small charges of hemlock (Charge 11).

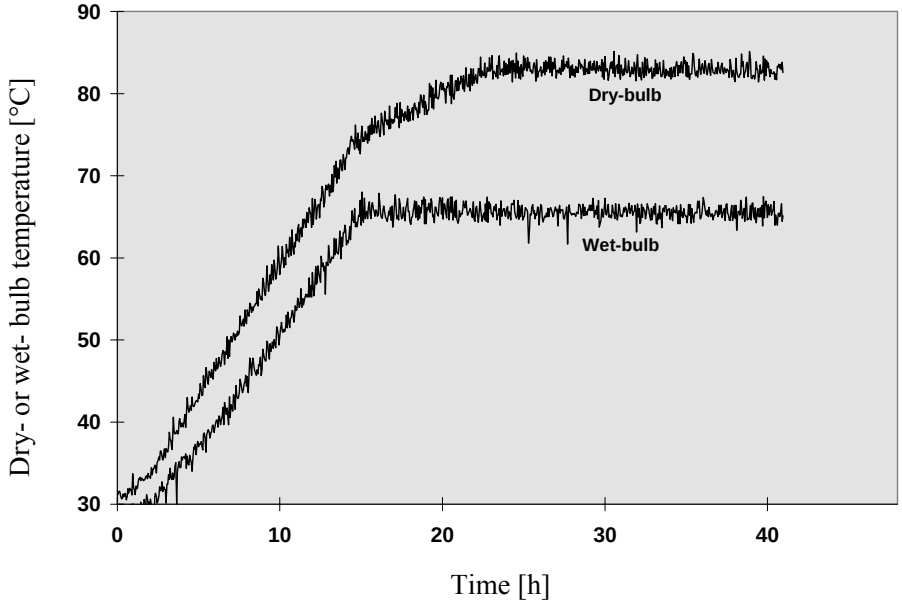

Figure 5.2.1.10 Dry- and wet-bulb temperatures and drying time used for small charges of hemlock (Charge 12).

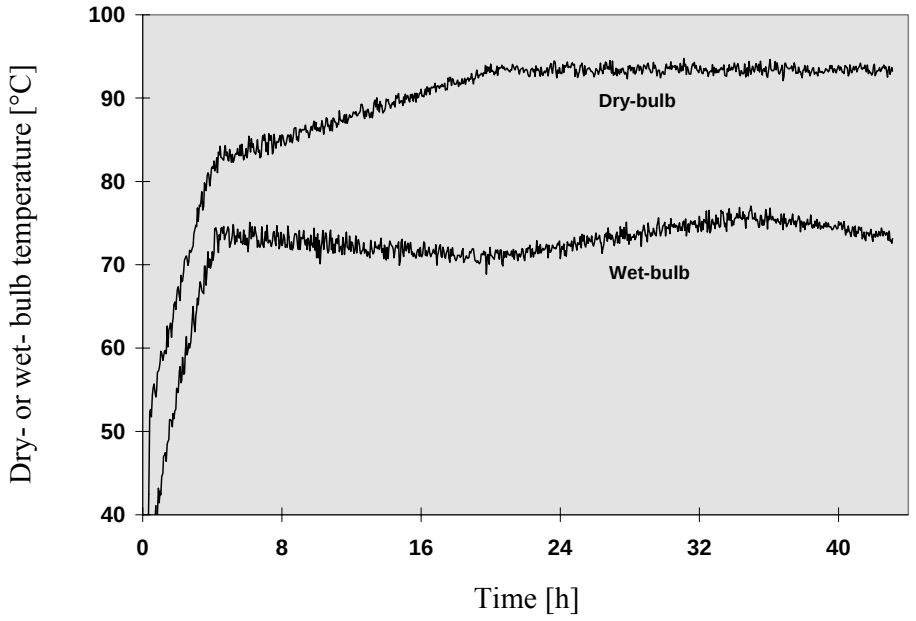

Figure 5.2.1.11 Dry- and wet-bulb temperatures and drying time used for small charges of hemlock (Charge 13, 14, and 15).

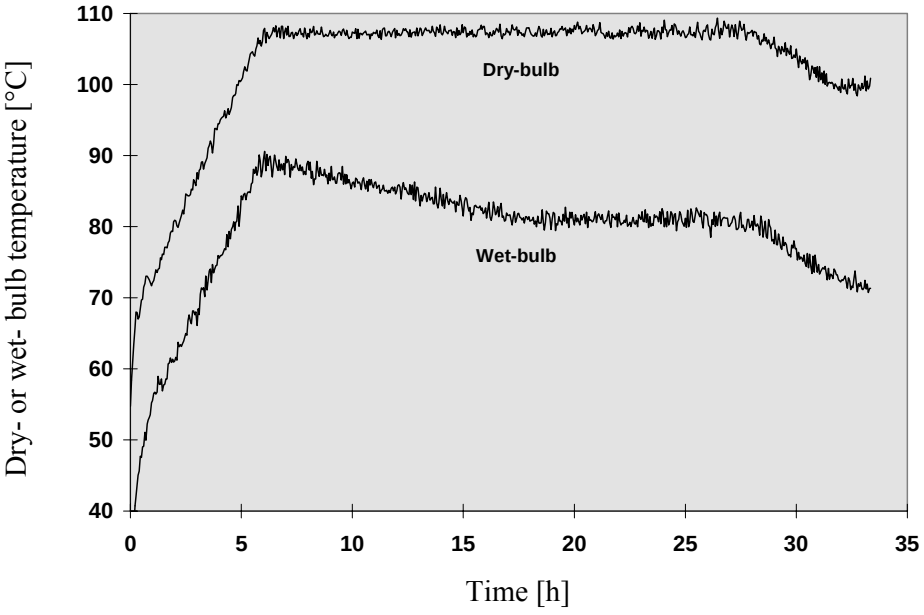

Figure 5.2.1.12 Dry- and wet-bulb temperatures and drying time used for small charges of hemlock (Charge 16, 17, and 18).

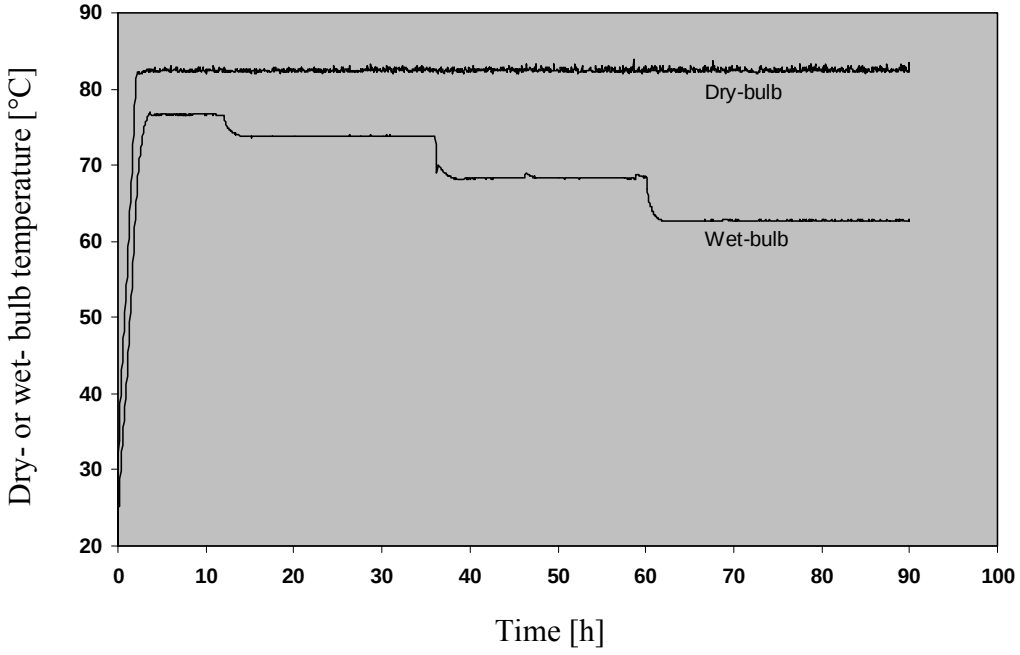

Figure 5.2.1.13 Dry- and wet-bulb temperatures and drying time used for small charges of hemlock (Charge 19, 20, 21, 22, and 23).

5.2.2 Data analysis

The initial and final wood moisture content for each charge were calculated based on the initial, kiln-dry, and oven-dry board weights. The amount of water leaving the kiln was calculated from the dry-bulb temperature, wet-bulb temperature, and gas flow using standard psychrometric relationships. The drying curve, moisture content as a function of time, was constructed by calculating the wood moisture content at each 3-minute time interval based on the initial wood moisture content and the water removed from the kiln. If the kiln-dry moisture content calculated by psychrometric relationships did not agree with the kiln-dry moisture content based on the oven-dry method, the moisture content at each three-minute interval was adjusted up or down to make the drying curve agree with the oven-dry moisture content both before and at the end of drying. The adjustment was proportional to time so that the

moisture contents early in drying were adjusted slightly and the moisture content later in drying were adjusted more. The full procedure for the moisture content calculation can be found in Milota and Mosher (2006).

Because the drying rate didn't change much within a drying interval shorter than one hour, the drying cycle was divided into one-hour time intervals. The drying flux for each time interval was obtained by dividing the amount of the removed moisture during the interval by the length of interval and the surface area of the boards. The fluxes were expressed as $kg_{H2O}/m^2 \cdot s$. Time intervals during the initial period were not used because of the unsteady-state nature of the data.

The fluxes were divided by the wet-bulb depression which is the main driving force during the constant rate period (Chapter 2.1). In that way it was possible to see if the constant rate period occurred, separate the constant from the falling rate period, and obtain the critical moisture content. The critical moisture content is the point at which the constant rate period ends and falling rate period starts.

After the constant rate period was separated from the falling rate period, the fluxes obtained for the constant rate period were correlated as a function of the wet-bulb depression (Eq. 5.2.1.1). The dependent variable was the flux and the independent variable was the wet-bulb depression. Values for the coefficients a and b were obtained by applying a linear regression on the experimental data.

$$Flux_{cr} = a \cdot (T_{db} - T_{wb}) + b \qquad (5.2.1.1)$$

It was impossible to correlate the drying fluxes to the drying air velocity using the experimental data because all the experimental drying fluxes were obtained for a single velocity of 750 ft/min. Therefore, it was assumed that the drying flux in the

constant rate period depends on the square root of velocity (Chapter 2.1). A ratio of the square root of velocity used in a drying schedule to the square root of velocity used in the experiments was used as a velocity correlation factor (5.2.1.2).

$$f = \frac{\sqrt{v}}{\sqrt{750}} \qquad (5.2.1.2)$$

A final form of a function describing the flux in the constant rate period (Eq. 2.1.3) was calculated as a product of a function correlating the drying rates to wet-bulb depression and the velocity correlation factor (5.2.1.2):

$$Flux_{cr} = [\, a \cdot (T_{db} - T_{wb}) + b \,] \cdot f$$

The fluxes obtained in the falling rate period were correlated as a function of difference between moisture and equilibrium moisture content (Eq. 5.2.1.3). The dependent variable was the slope (St) whereas the independent variable was the difference between the moisture content of the board and the equilibrium moisture content of wood for the air properties.

$$Flux_{fr} = St \cdot (X - X_{eq}) \qquad (5.2.1.3)$$

where the slope (St) was a function of dry-bulb temperature (Eq. 2.1.2)

All the data from the falling rate period were sorted based on the value of the dry-bulb temperature used in the experiments due to the temperature dependence of the slope (St). The dependent variable was the slope (St) and the independent was the dry-bulb temperature (T_{db}). The constant S_0 and the activation energy (Ea) were

calculated by an exponential regression (Eq. 5.2.1.4) applied on the data set for each temperature.

$$St=S_0 \cdot \exp[-Ea/(R \cdot T_{db})] \quad (5.2.1.4)$$

where R is the universal gas constant.

The next step was to make a smooth transition between the functions for the constant and falling rate period (Eq. 5.2.1.1 and 5.2.1.3). It was accomplished using the function described by Equation 5.2.1.5. The dependent variable was the drying flux (w_D) and the independent variables were the slope (St), the wet-bulb depression and the drying flux for the constant rate period (w_{Dcr}). The coefficient n was obtained by applying a non-linear regression over all the experimental data.

$$w_D = \{[St \cdot (X - X_{eq})]^{-n} + (w_{D_{cr}})^{-n}\}^{-\frac{1}{n}} \quad (5.2.1.5)$$

5.3 Experiments for validation

5.3.1 Experiments

Three charges, each containing 168 pieces (2688 board feet) of nominal 2"x6" (5.08x15.24cm) hemlock dimension lumber, were dried in a laboratory kiln. The average board thickness was 1.664" (4.226cm) and width was 5.851" (14.861cm). The pieces were 16' (4.9 m) in length and stacked in a 21-board high and 8-board wide package on ¾-inch (1.9 cm) stickers spaced two feet apart. The lumber was obtained from Georgia Pacific in Philomath, OR.

Each board was weighed as the kiln was loaded. The thickness and width of each board in columns C and F (Fig. 5.2.2.1) were measured with digital calipers. Approximately 45 lb/ft^2 (0.31 MPa) of toploading was applied with concrete blocks.

Four load cells were located in the kiln and weighed the wood, stickers, concrete, and cart. This was recorded at six-minute intervals.

The board centerline temperature was measured in two boards, 10C and 10F in the first and second charges and boards 10A and 10B for the third charge. They were located as shown in Fig. 5.2.2.1. During stacking, two 0.31-cm-diameter holes were drilled in the edge of each board to a depth of approximately 2-13/16" (7.1 cm) (Fig. 5.2.2.2). The holes were centered between the board faces and were approximately 5 feet (1.5 m) from each end of the board. A type T thermocouple was placed in each hole and the hole was plugged with wood splinters to insulate the thermocouple sensor from the drying air influence.

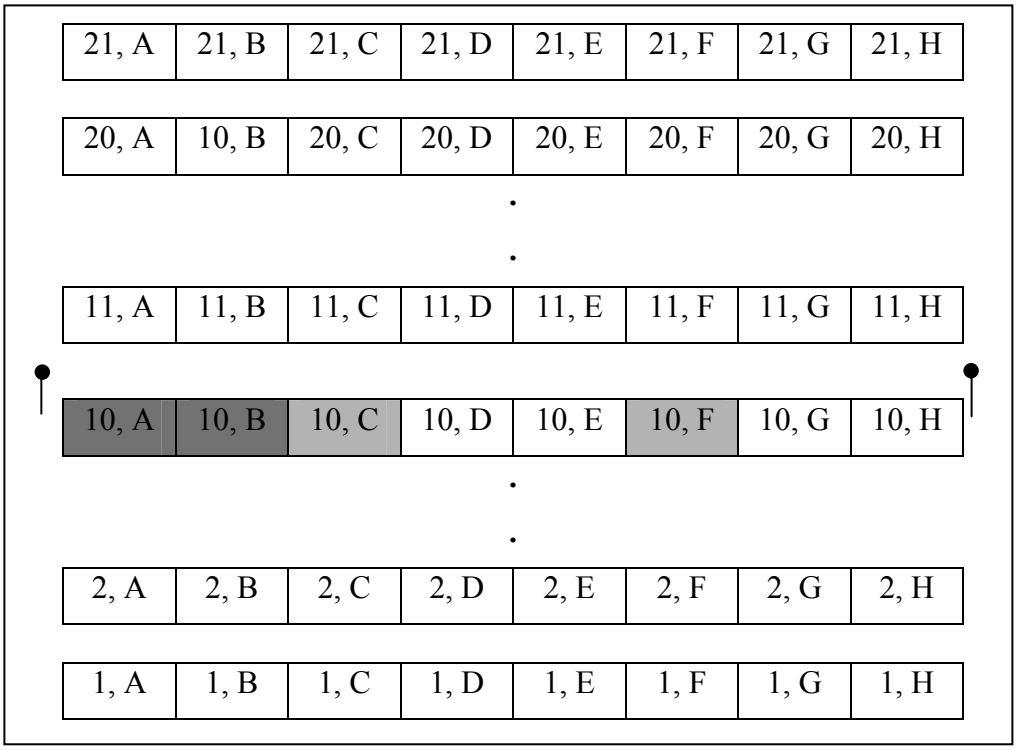

Fig. 5.2.2.1 End view of stack showing the numbering of the boards and the thermocouple placement (T) for measuring gas temperature.

The temperature of the air entering and leaving the package was measured at one-minute intervals by placing two type T thermocouples on each side of the stack. After the kiln was loaded they were mounted at the sticker openings in the slot above the row ten, the row with the boards containing thermocouples. Temperature drop through the package was calculated as the difference of the average the temperature on each side of the package.

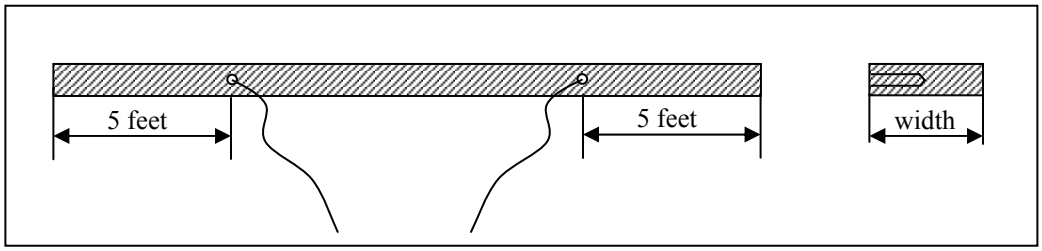

Fig. 5.2.2.2 Side and end view of board with mounted thermocouples

The drying schedules for the three charges are shown, respectively, in Tables 5.2.2.1, 5.2.2.2, and 5.2.2.3. The controlled values were ramped between the times shown. A fan reversal occurred after the first 1.5 hours of drying, then every three hours. The kiln controller recorded temperature and other information related to the kiln operation throughout the cycle at 6-minute intervals.

After drying, each board was weighed. The moisture content of each board was measured at two locations, approximately 3.5 feet from the ends. This was measured with a Wagner 612 hand-held, capacitance-type moisture meter. It was set to correct for the specific gravity of western hemlock.

If the two readings differed by more than 5% moisture content, then a third reading was taken near the center of the board. The thickness and width were again measured in the same locations as before drying.

Table 5.2.2.1 Schedule for the first charge used for the model validation

Step	Time	T_{db}	T_{wb}	Fan Speed
[#]	[h]	[°F]	[°F]	[ft/min]
1	0	90	80	1068
2	2	230	205	1068
3	24	230	195	1068
4	28	230	180	712

Table 5.2.2.2 Schedule for the second charge used for the model validation

Step	Time	T_{db}	T_{wb}	Fan Speed
[#]	[h]	[°F]	[°F]	[ft/min]
1	0	90	80	1068
2	12	170	160	1068
3	18	170	160	890
4	96	170	135	712

Table 5.2.2.3 Schedule for the third charge used for the model validation

Step	Time	T_{db}	T_{wb}	Fan Speed
[#]	[h]	[°F]	[°F]	[ft/min]
1	0	90	80	1068
2	2	180	170	1068
3	6	180	170	1068
4	18	180	165	1068
5	54	180	145	712

5.3.2 Analysis

The final weight and moisture content of the boards were used to calculate the ovendry weight for each board (Eq. 5.3.2.1). The initial and ovendry weights were then used to calculate the initial moisture content for each board (Eq. 5.3.2.2).

$$w_{OD}=w_f / (1+(X_f / 100)) \quad (5.3.2.1)$$

$$X_i=(w_i-w_{OD}) / w_{OD} \quad (5.3.2.2)$$

The initial average moisture content of the package was calculated using sum of the initial weight of each board and the sum of the calculated oven-dry weight of each board (Eq. 5.3.2.3):

$$X_{i,package} = \frac{\sum_{j=1}^{168} w_{i,j} - \sum_{j=1}^{168} w_{OD,j}}{\sum_{j=1}^{168} w_{OD,j}} \quad (5.3.2.3)$$

The average moisture content of the package versus time was obtained using the sum of the initial weight of each board, the water loss during drying based on the loads cells, and the calculated oven-dry weight of each board (Eqn. 5.3.2.4):

$$X = \frac{\sum_{j=1}^{168} w_{i,j} - \text{weight change from load cells} - \sum_{j=1}^{168} w_{OD,j}}{\sum_{j=1}^{168} w_{OD,j}} \quad (5.3.2.4)$$

The temperature drop through the package for each charge (TDAL) was calculated as the difference between the average entering and exiting temperature as measured by the pair of thermocouples on each side of the load.

The internal board temperature for each charge was calculated from the average of the two thermocouples in the board.

6. Results and Validation

6.1 Experimental

6.1.1 Drying Rate Function

After the fluxes have been divided by wet-bulb depression, the values for flux at moisture contents greater than 80% were scattered, but relatively constant (Fig. 6.1.1.1). For moisture contents less than 80% to the equilibrium moisture content, the flux decreased in a linear relationship (Fig. 6.1.1.1). Based on this behavior, the regression function for the constant rate period was based on the data in the moisture range above 80% while for the falling rate period on the data from 80% to the equilibrium moisture content.

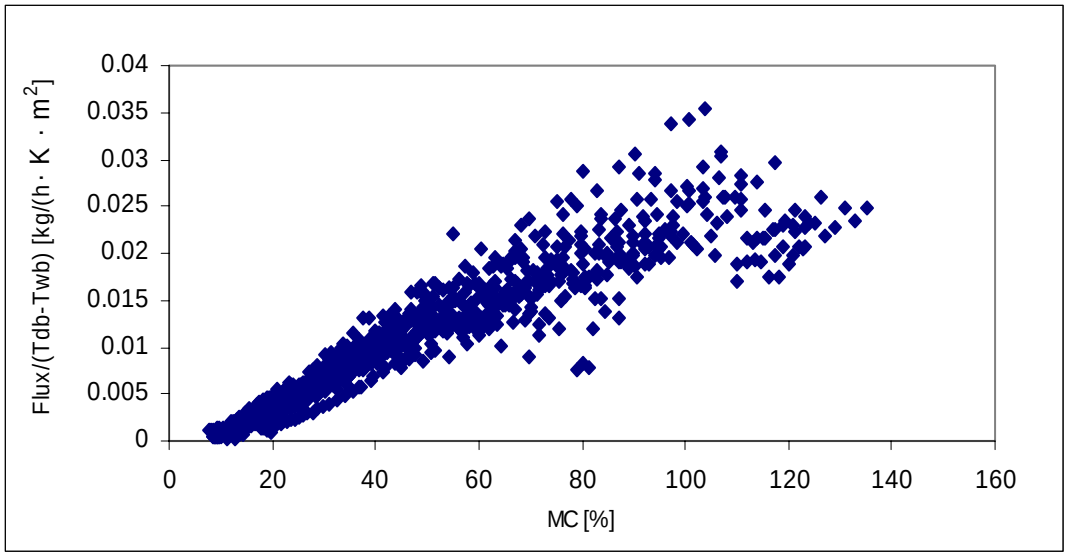

Fig. 6.1.1.1 Flux divided by wet-bulb depression versus moisture content for all data.

After the regression functions for the constant and falling rate period were obtained, the assumed value for the critical moisture content, 80%, was checked for the range of dry-bulb and wet-bulb temperatures (Table 5.2.1.1). The calculations yielded 77% as the average value of the critical moisture content with a range of 71% to 91% which justified the assumption.

The regression for flux versus (T_{db}-T_{wb}) for the constant rate period resulted in Equation 6.1.1.1. The fitted line and actual values are shown in Figure 6.1.1.2.

$$\text{Flux}_{cr} = 0.0157 \cdot (T_{db} - T_{wb}) + 0.0663 \qquad (6.1.1.1)$$

The coefficient of determination (R^2) was equal to 0.65 which means that 65% of variability in the drying flux is explained by wet-bulb depression.

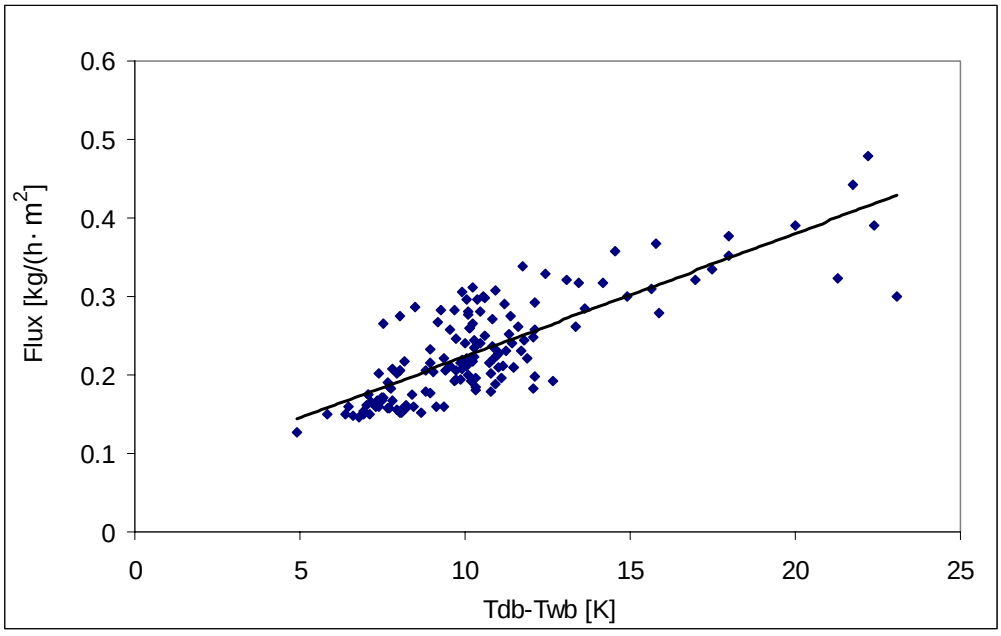

Figure 6.1.1.2 Drying fluxes versus wet-bulb depression for a constant rate period.

The data for flux versus MC-EMC at different drying temperatures is shown in Figures 6.1.1.3, 6.1.1.4, 6.1.1.5, and 6.1.1.6. The regression equation for flux versus MC-EMC is also shown on each plot.

At each temperature the coefficient of determnation exceeded 0.9 which means that more than 90% of the variability in flux can be explained difference between moisture content and equilibrium moisture content at a given temperature.

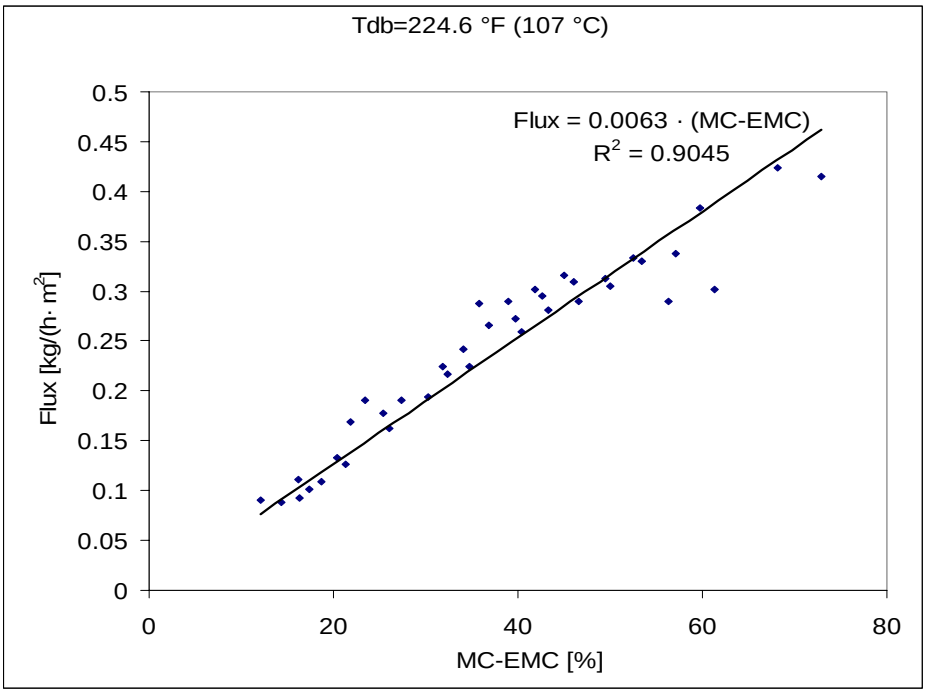

Fig. 6.1.1.3 Drying fluxes versus difference between moisture and equilibrium moisture content for a falling rate period (Tdb=224.6ºF).

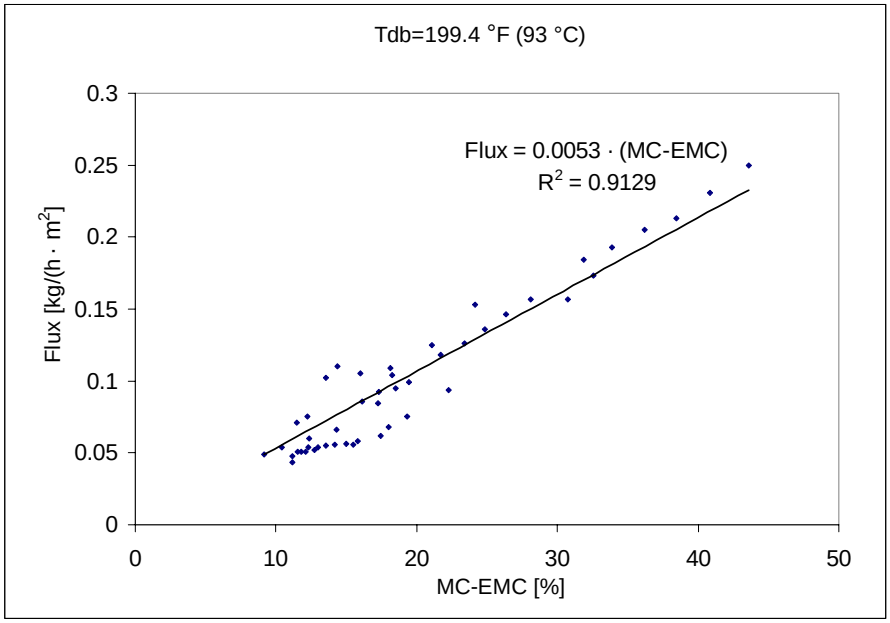

Fig. 6.1.1.4 Drying fluxes versus difference between moisture and equilibrium moisture content for a falling rate period (Tdb=199.4ºF).

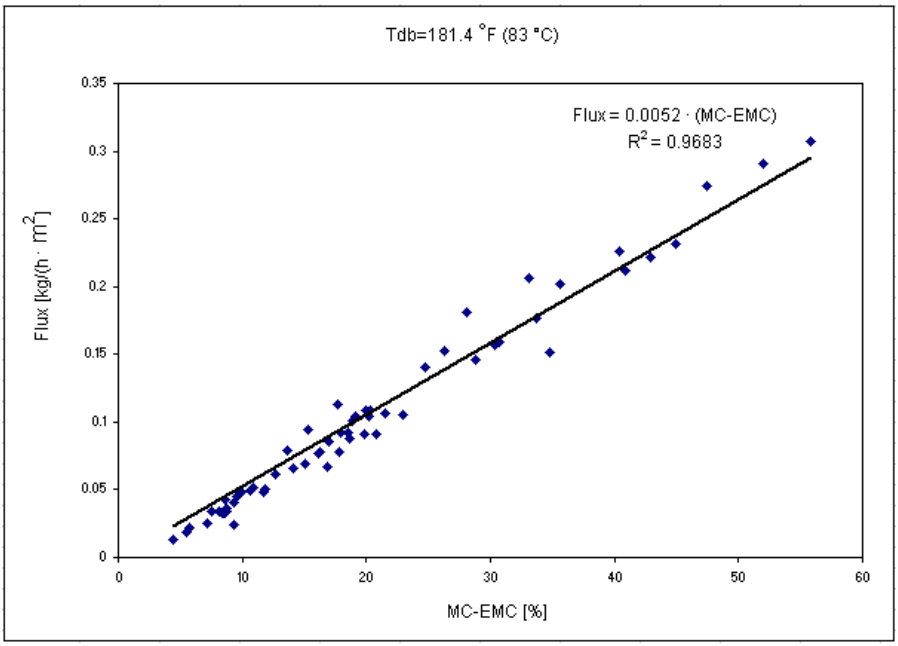

Fig. 6.1.1.5 Drying fluxes versus difference between moisture and equilibrium moisture content for a falling rate period (Tdb=181.4ºF).

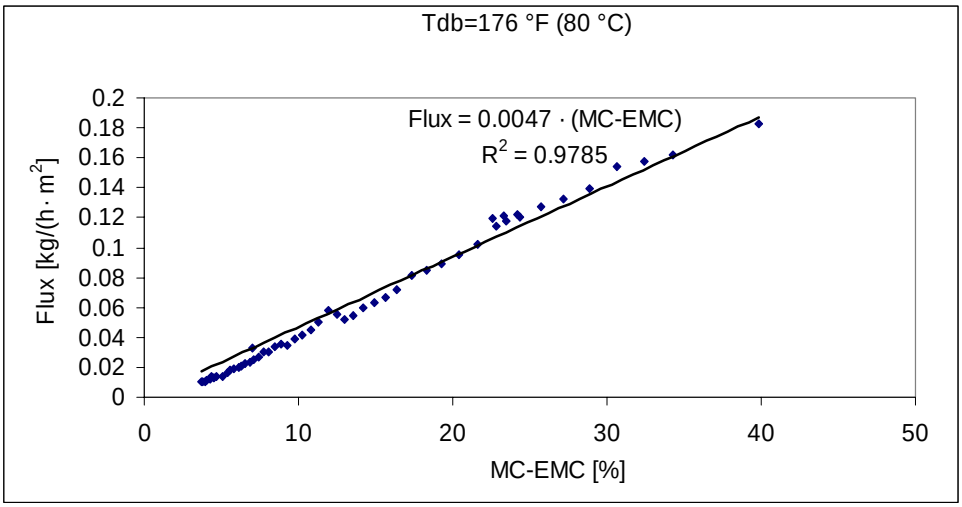

Fig. 6.1.1.6 Drying fluxes versus difference between moisture and equilibrium moisture content for a falling rate period (Tdb=176ºF).

It can be seen from the Figures 6.1.1.3, 6.1.1.4, 6.1.1.5, and 6.1.1.6 that the temperature affects the slope (St) of the linear relationships between the flux and moisture and equilibrium moisture content difference. The equation obtained by an exponential regression where the dry-bulb temperature was independent and the constant (S_0) and activation energy (Ea) (Eq. 2.1.2) dependent variables, was as follows:

$$St = 3.6033 \cdot \exp[-2404.2/T_{db}] \qquad (6.1.1.2)$$

The correlation coefficient for this relationship was 0.3. The regression equation for calculating the drying fluxes in the falling rate period then became (Eq. 6.1.1.3):

$$Flux_{fr} = 3.6033 \cdot \exp[-2404.2/T_{db}] \cdot (X - X_{eq}) \qquad (6.1.1.3)$$

It was necessary to check how predicted data by Equation 6.1.1.3 matched experimental data due to low correlation factor of 0.3. Figure 6.1.1.7 shows the values predicted by equation 6.1.1.3 plotted against the experimental values all data in the falling rate period. The slope of fitted line was 0.94 with R^2=0.8 which indicated a good agreement between calculated and measured drying fluxes. The equation showed especially good agreement for the lower drying fluxes whereas it showed greater deviations for the higher values of drying fluxes. The reason might be in the fact that pits become aspirated as drying progresses. Different level of aspiration due to different moisture levels caused by variability in drying properties, resulted in different drying fluxes between boards in a stack. As the boards were drying more pits became aspirated. When the boards reached the moisture level when most of the pits got aspirated then the diffusion remained the main driving force for a moisture movement (Forest Products Laboratory 1999). At that time the drying fluxes of the boards start becoming equal.

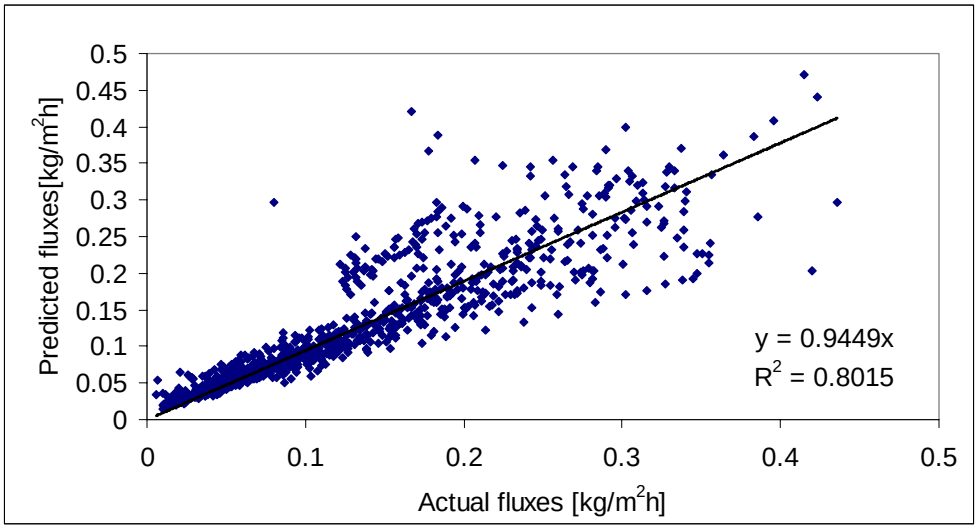

Fig. 6.1.1.7 Predicted versus actual fluxes for the falling rate period.

After a non-linear regression procedure with n as dependent and drying fluxes as independent variables was applied over all the data for both the constant and falling rate periods using the calculated drying fluxes (Eq. 6.1.1.1 and 6.1.1.3.) and those experimental, n was found to be 16.64 with R^2 equal to 0.9.

As it can be seen from the Figure 6.1.1.8, the variable n affects the sharpness of transition between the constant and falling rate period. The value of variable n has a high impact on the shape for the values up to 10. The shape doesn't change much for the values beyond 10. This means that the last two digits of obtained n value (16.64) were not very significant.

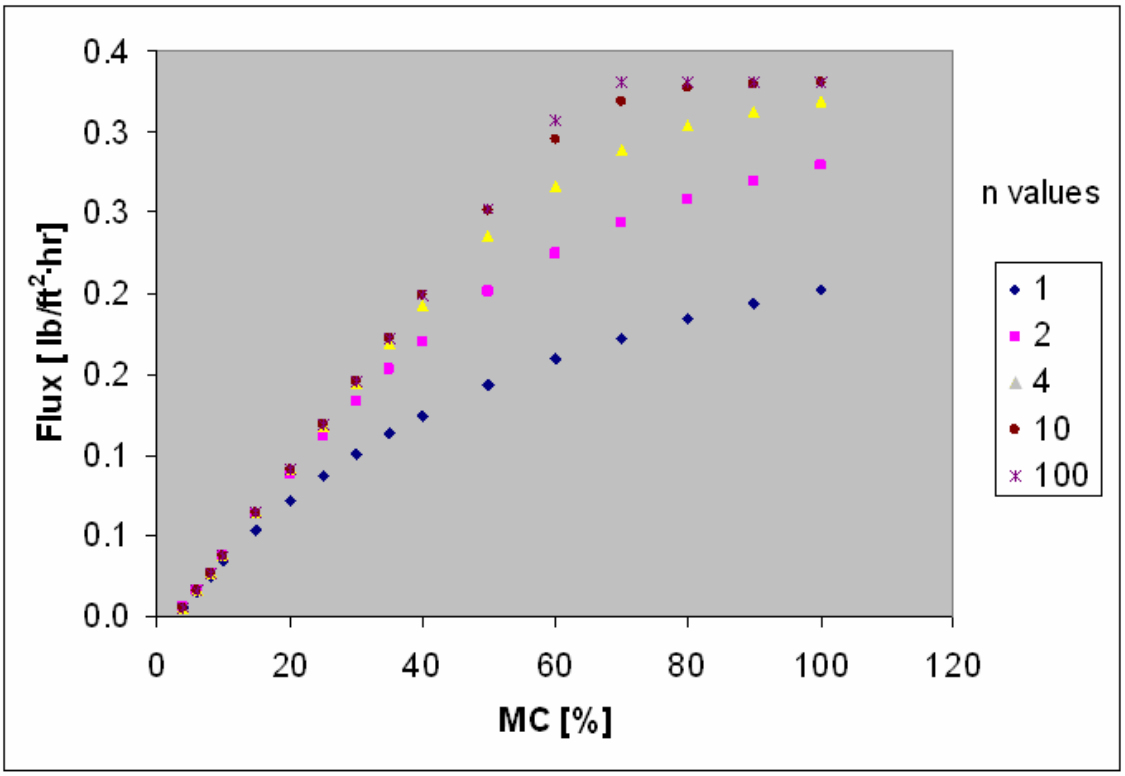

Fig. 6.1.1.8 Impact of the variable n on the shape of the drying rate function curve.

The drying rate function describing the flux for both the constant and falling rate period was obtained to be as follows:

$$w_D = \{[(3.6033 \cdot e^{(-2404.2/T_{db})}) \cdot (X - X_{eq})]^{-16.64} + \\ +(0.0157 \cdot (T_{db} - T_{wb}) + 0.0663)^{-16.64}\}^{-\frac{1}{16.64}} \quad (6.1.1.4)$$

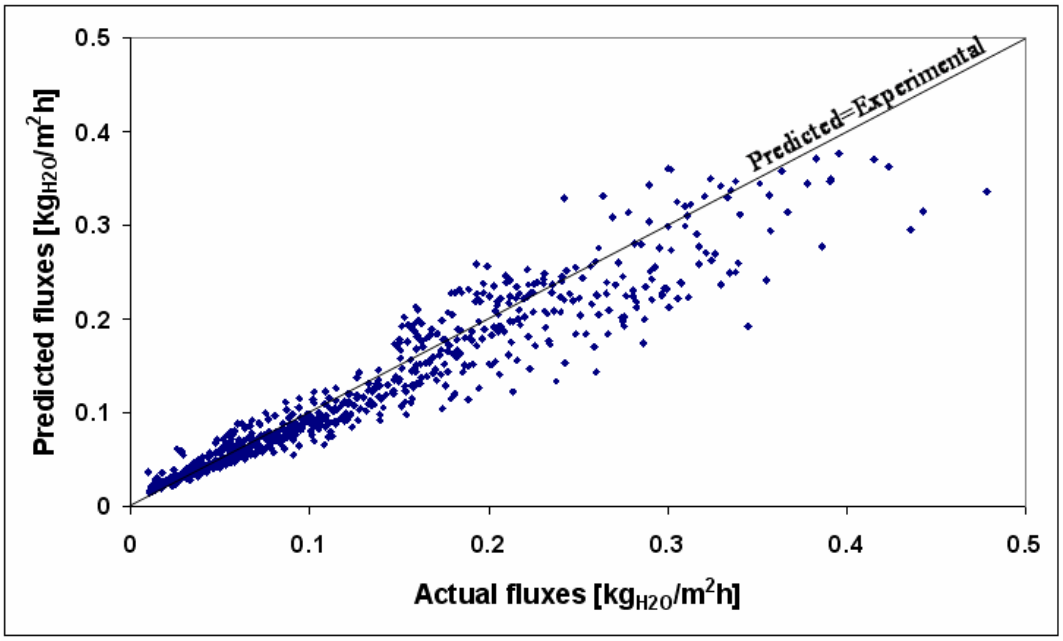

Fig. 6.1.1.9 Comparison of drying fluxes for both drying periods predicted by drying rate function to that measured.

A very good correlation with R^2 equal to 0.9 between predicted (Eq. 6.1.1.4) and experimental data was obtained (Fig. 6.1.1.9). It provided a good base for the simulation because the mass transfer was an important calculation part besides the heat transfer calculations.

6.1.2 Package drying

6.1.2.1 Charge 1

The Figure 6.1.2.1.1 shows a temperature drop through the package, the Figure 6.1.2.1.2 shows the average moisture content of the package versus time while the Figure 6.1.2.1.3 shows a board-by-board comparison of ending moisture content between predicted and experimental results.

During the experiment the acquisition system broke and therefore board temperatures could not be measured. Temperature drop through the package was measured as the difference between a temperature of entering and exiting air measured by kiln sensors (Figure 6.1.2.1.1). The difference between experimental and predicted values was somewhat greater in this case because the kiln sensors were placed around 12” (0.3m) away from the entering and exiting side of a package thereby measuring a higher temperature drop.

The parameters obtained by measuring the boards of the first charge are given in the Table 6.1.2.1.1. From the measured values (Table 6.1.2.1.1), the mean of specific gravity was calculated to be 0.44 while the volumetric shrinkage was 7.4 percent.

Table 6.1.2.1.1 Parameters of the boards measured before and after drying (Charge 1).

	Green				Dry			
	Weight	MC	Width	Thickness	Weight	MC	Width	Thickness
	[lb]	[%]	[in]	[in]	[lb]	[%]	[in]	[in]
Mean	56.1	114.3	5.861	1.667	29.8	12.9	5.584	1.620
St. dev.	11.6	46.5	0.052	0.065	3.6	4.4	0.147	0.081

The Figures 6.1.2.1.1 and 6.1.2.1.2 show the temperature drop through the package and the moisture content versus time, respectively. Peaks that can be seen in Figure 6.1.2.1.1 occurred due to hot check at 21st hour (time when the kiln was turned off and the wood moisture content checked manually) and 31st hour due to a steam shutdown. For the same reasons, the moisture content drops can be observed at the same times in Figure 6.1.2.1.2.

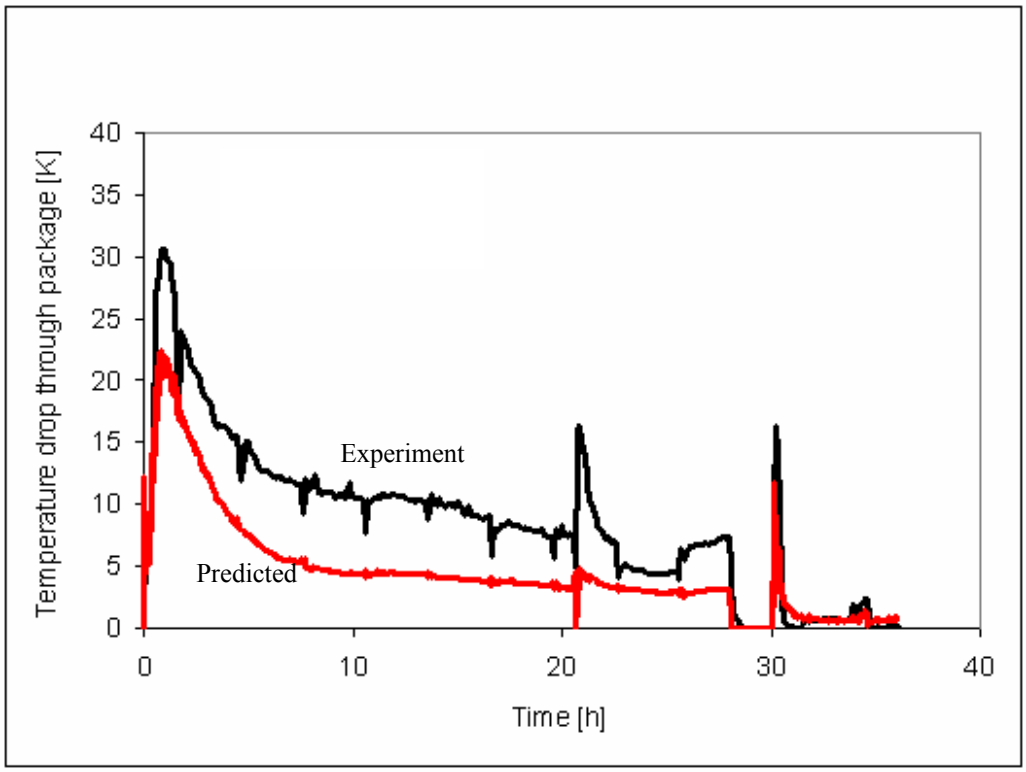

Figure 6.1.2.1.1 Temperature drop through the package as measured and as predicted by the model (Charge 1).

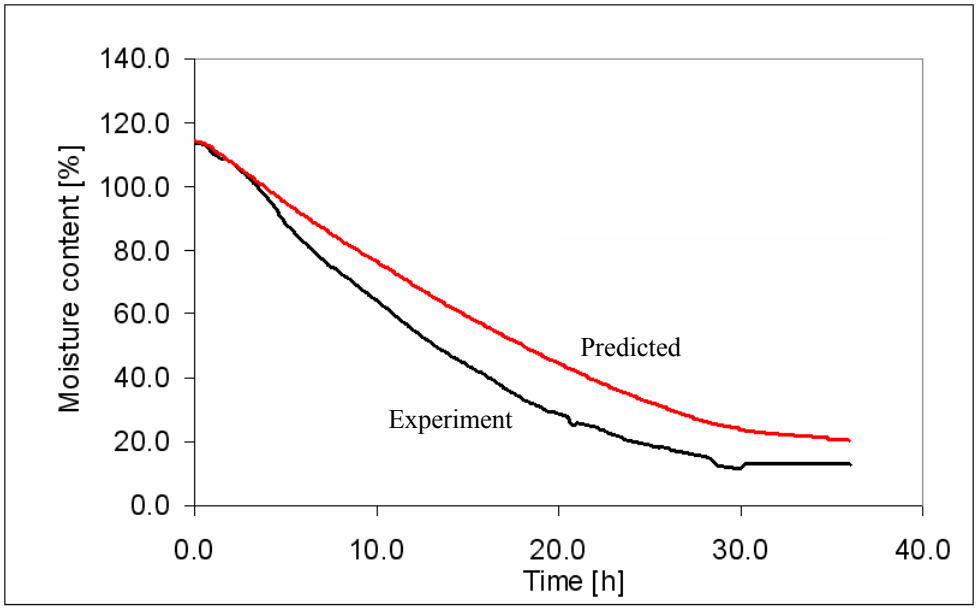

Figure 6.1.2.1.2 Average moisture content of the package as measured and as predicted by the model (Charge 1).

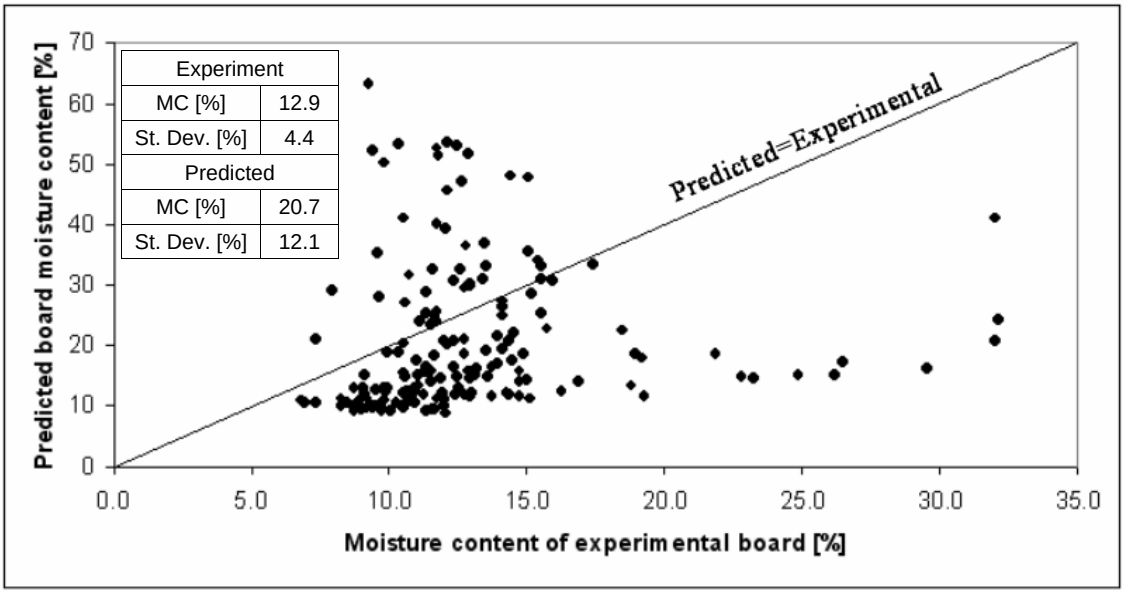

Figure 6.1.2.1.3 Board-by-board comparison of ending moisture content distribution predicted by the model to that measured (Charge 1).

6.1.2.2 Charge 2

The Figures 6.1.2.2.1 and 6.1.2.2.2 show the board centerline temperatures for two boards from the middle row of the stack. The Figure 6.1.2.2.3 shows a temperature drop through the package, the Figure 6.1.2.2.4 shows the average moisture content of the package versus time while the Figure 6.1.2.2.5 shows a board-by-board comparison of ending moisture content between predicted and experimental results.

The board temperature drop occurred at 64^{th} hour due to hot check whereas the temperature drop due to a steam shutdown occurred at 87^{th} hour of drying (Fig. 6.1.2.2.1 and 6.1.2.2.2). The hot check and steam shutdown can be observed in Figure 6.1.2.2.3 (temperature drop through the package) as two peaks.

In Figure 6.1.2.2.4 (average moisture content of the package versus time), it can be observed that the hot check caused a stagnation in drying (straight line) while the steam shutdown caused the boards to pick up some water because the conditioning process was under way and the equilibrium moisture content for the kiln conditions was higher than the current moisture contents of boards.

Due to lower dry- and wet-bulb temperatures, wet-bulb depressions, and the lower fan speed used for the longer time, a lower temperature drop through the package (Fig. 6.1.2.1.1 and 6.1.2.2.3) can be observed for the first charge compared to the second charge.

This charge also took more time to dry (Fig. 6.1.2.1.2 and 6.1.2.2.4) due to lower moisture fluxes fromh boards caused by the milder drying schedule compared to the schedule used for the first charge.

The parameters obtained by measuring the boards of the second charge are given in the Table 6.1.2.2.1.

From the measured values (Table 6.1.2.2.1), the mean of specific gravity was calculated to be 0.44 while the volumetric shrinkage was 6.6 percent.

Table 6.1.2.2.1 Parameters of the boards measured before and after drying (Charge 2).

	Green				Dry			
	Weight	MC	Width	Thickness	Weight	MC	Width	Thickness
	[lb]	[%]	[in]	[in]	[lb]	[%]	[in]	[in]
Mean	57.2	116.5	5.859	1.668	29.7	11.9	5.617	1.625
St. dev.	10.9	41.2	0.087	0.038	2.9	3.5	0.115	0.044

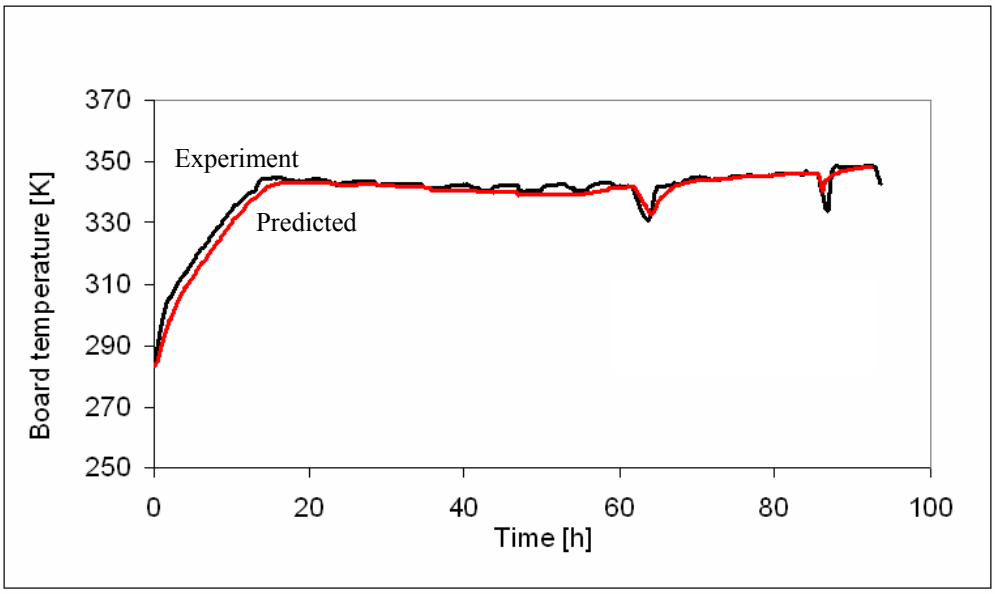

Figure 6.1.2.2.1 Centerline temperature for a board (10, C) as measured and as predicted by the model (Charge 2).

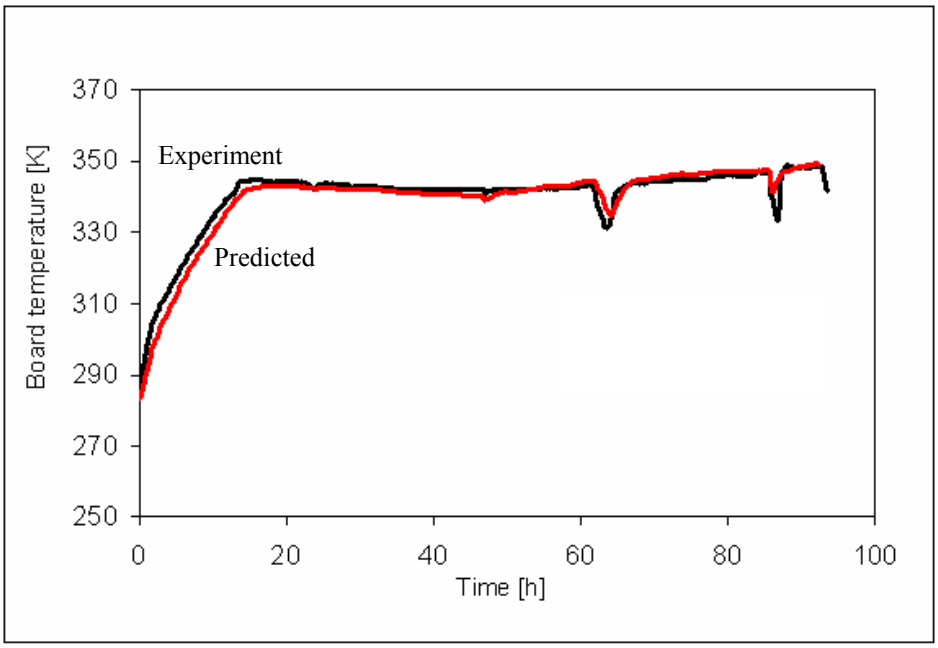

Figure 6.1.2.2.2 Centerline temperature for a board (10, F) as measured and as predicted by the model (Charge 2).

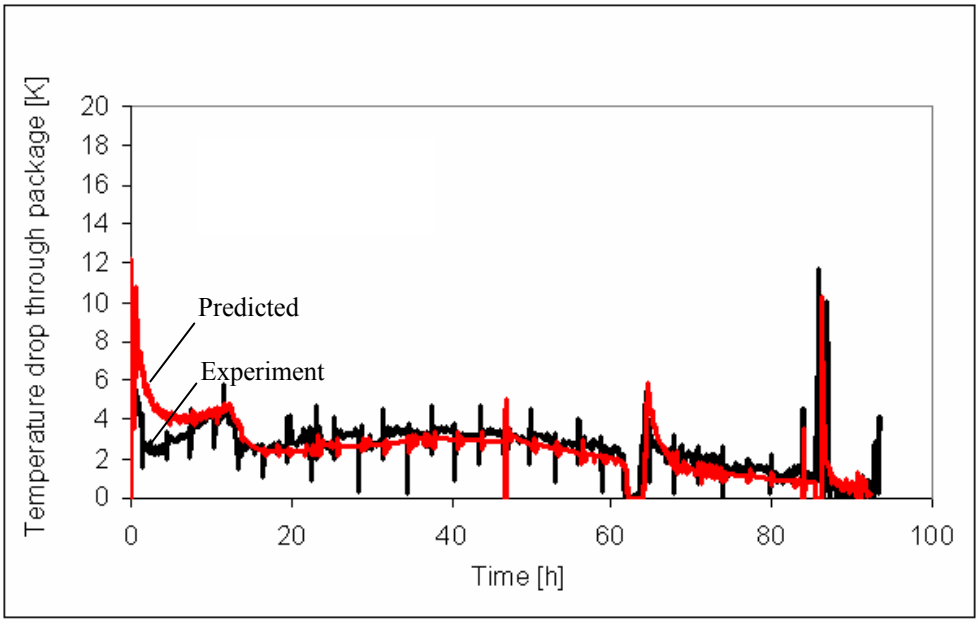

Figure 6.1.2.2.3 Temperature drop through the package as measured and as predicted by the model (Charge 2).

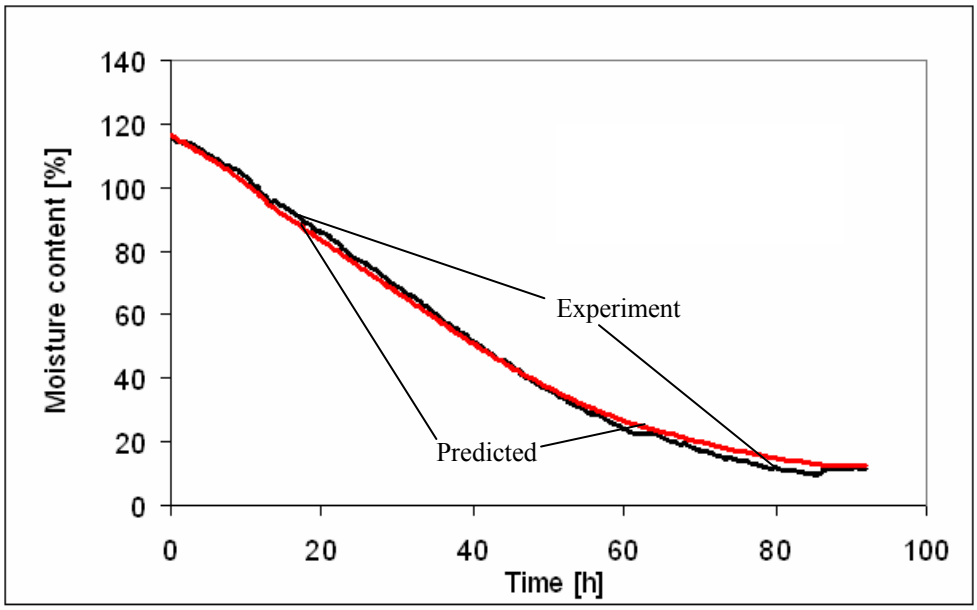

Figure 6.1.2.2.4 Average moisture content of the package as measured and as predicted by the model (Charge 2).

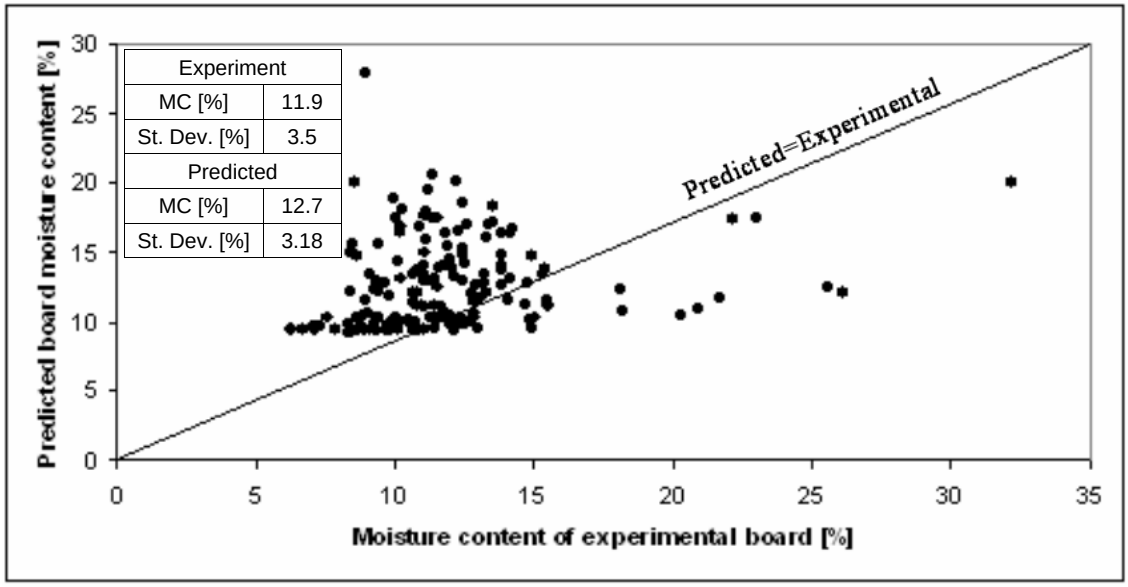

Figure 6.1.2.2.5 Board-by-board comparison of ending moisture content distribution predicted by the model to that measured (Charge 2).

6.1.2.3 Charge 3

The Figures 6.1.2.3.1 and 6.1.2.3.2 show the board centerline temperatures for two boards from the middle row of the stack. The Figure 6.1.2.3.3 shows a temperature drop through the package, the Figure 6.1.2.3.4 shows the average moisture content of the package versus time while the Figure 6.1.2.3.5 shows a board-by-board comparison of ending moisture content between predicted and experimental results.

The board temperature drop occurred at 43rd hour due to hot check whereas the temperature drop due to a steam shutdown occurred at 63rd hour of drying (Fig. 6.1.2.3.1 and 6.1.2.3.2). The hot check and steam shutdown can be observed in Figure 6.1.2.3.3 (temperature drop through the package) as two peaks.

In Figure 6.1.2.3.4 (average moisture content of the package versus time), it can be observed that the hot check caused a stagnation in drying (straight line) while the steam shutdown caused the boards to pick up some water because the conditioning process was under way and the equilibrium moisture content for the kiln conditions was higher than the current moisture contents of boards.

Due to higher dry- and wet-bulb temperatures, wet-bulb depressions, and the higher fan speed used for the longer time, this charge took less time to dry (Fig. 6.1.2.2.4 and 6.1.2.3.4) than it took the second charge. For the same reason, the board temperatures for the third charge were slightly higher (Fig. 6.1.2.2.1, 6.1.2.2.2, 6.1.2.3.1, and 6.1.2.3.2).

The parameters obtained by measuring the boards of the second charge are given in the Table 6.1.2.3.1. From the measured values (Table 6.1.2.3.1), the mean of specific gravity was calculated to be 0.44 while the volumetric shrinkage was 5.7 percent.

Table 6.1.2.3.1 Parameters of the boards measured before and after drying (Charge 3).

	Green				Dry			
	Weight	MC	Width	Thickness	Weight	MC	Width	Thickness
	[lb]	[%]	[in]	[in]	[lb]	[%]	[in]	[in]
Mean	57.4	122.4	5.852	1.658	29.5	14.0	5.618	1.629
St. dev.	10.5	41.1	0.048	0.042	3.4	4.4	0.068	0.047

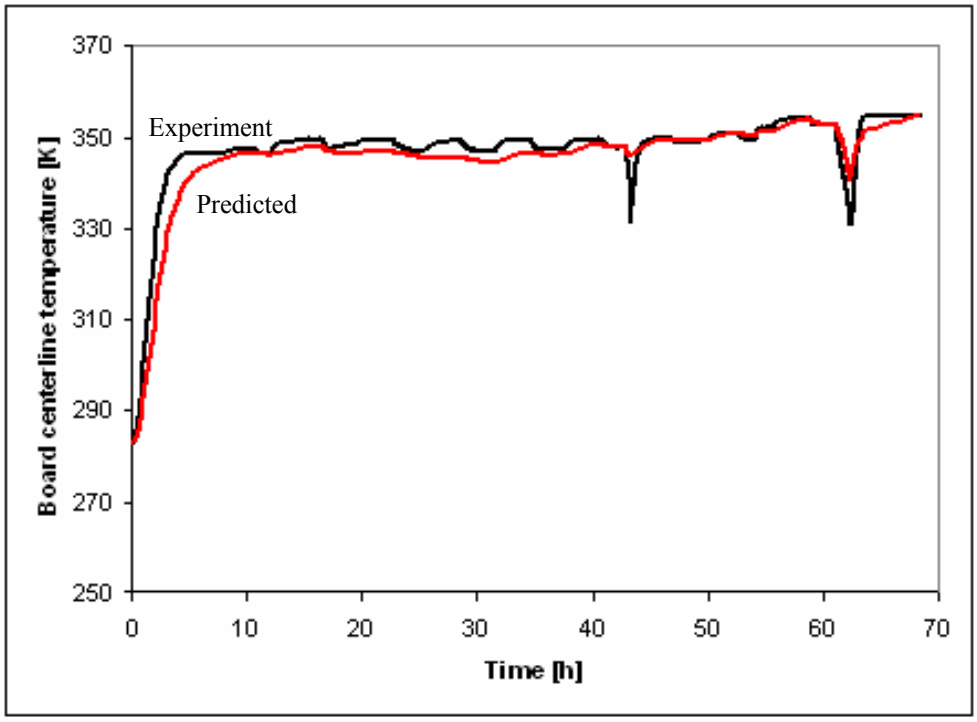

Figure 6.1.2.3.1 Centerline temperature for a board (10, A) as measured and as predicted by the model (Charge 3).

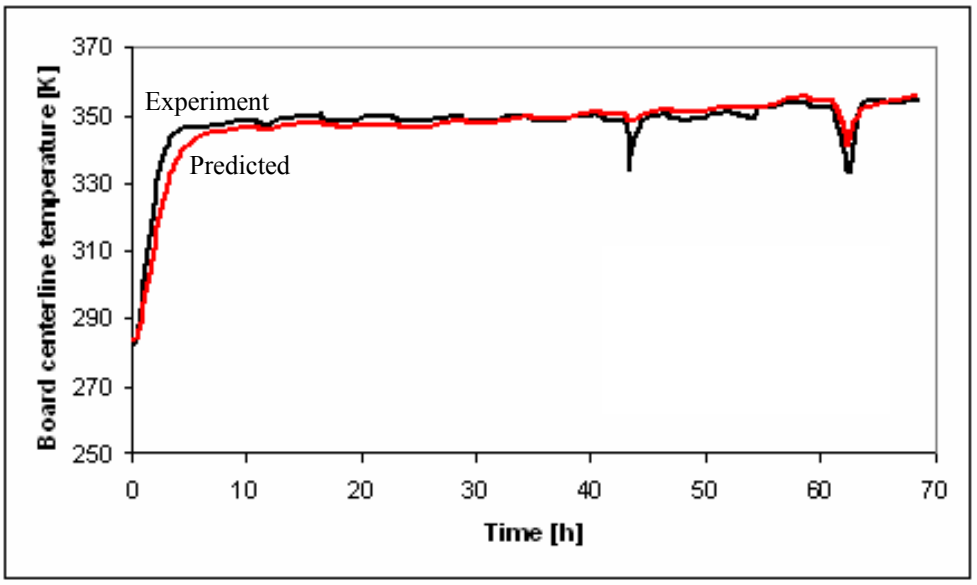

Figure 6.1.2.3.2 Centerline temperature for a board (10, B) as measured and as predicted by the model (Charge 3).

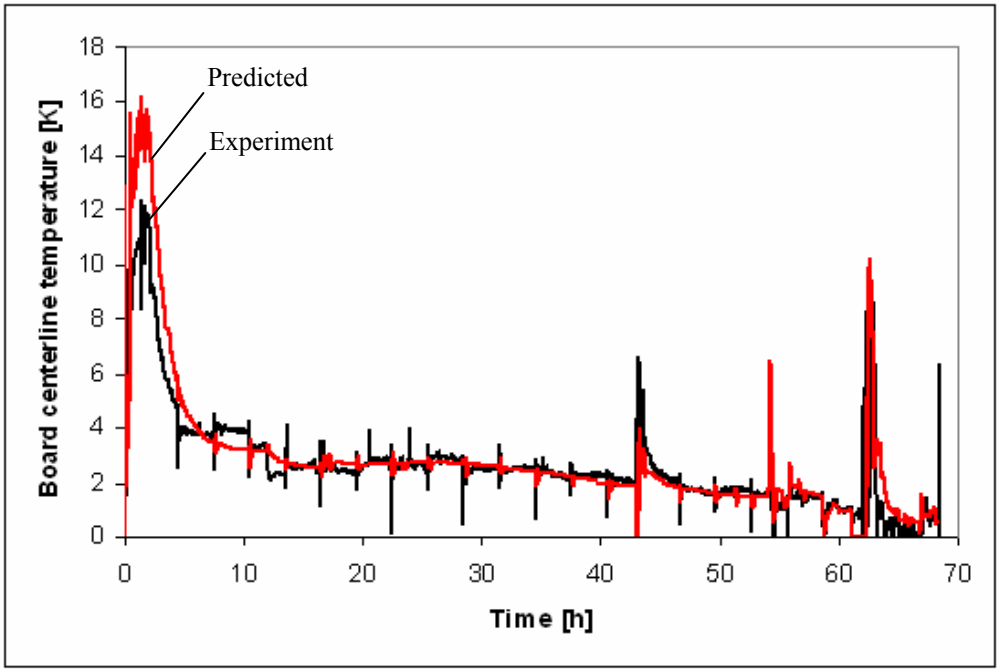

Figure 6.1.2.3.3 Temperature drop through the package as measured and as predicted by the model (Charge 3).

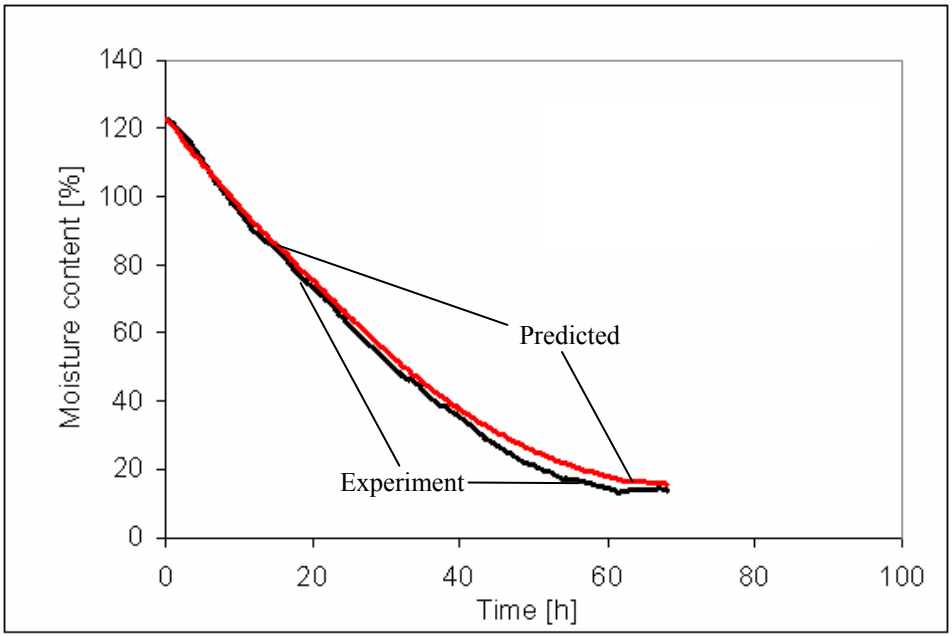

Figure 6.1.2.3.4 Average moisture content of the package as measured and as predicted by the model (Charge 3).

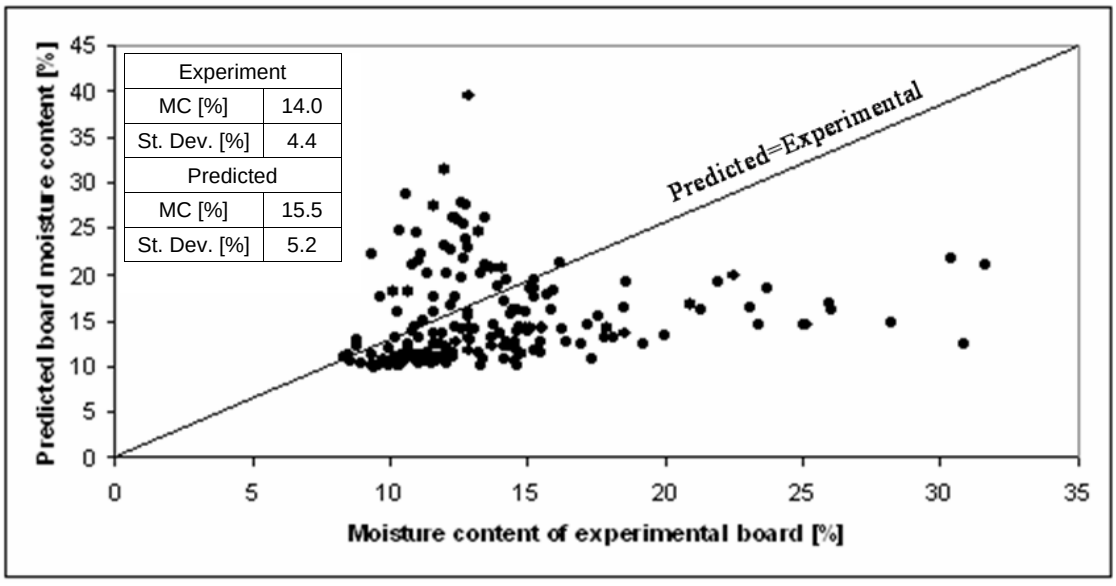

Figure 6.1.2.3.5 Board-by-board comparison of ending moisture content distribution predicted by the model to that measured (Charge 3).

6.1.2.4 Comparisons

From the measured data from all three charges (Tables 6.1.2.1.1, 6.1.2.2.1, and 6.1.2.3.1) and the fact that the mean oven-dry weights were almost equal, the boards of a charge with the higher initial moisture content were also higher in green weights.

Specific gravities of all three charges were the same. This was expected since they were all the same species.

The second charge was dried best in terms of the targeting ending moisture content which was 12% moisture content. It had also the lowest deviation in moisture contents between boards.

6.2 Validation

In the early phase of development, the model was validated using published data on loblolly pine. It was then validated using the drying rate function developed for hemlock and the hemlock data from the package drying. The validation consisted of substituting the drying rate function into the model, obtaining the simulation results and comparing the results to those measured experimentally.

6.2.1 Loblolly pine

The full-package experimental data presented here are loblolly pine drying data obtained from Milota and Tschernitz (1994). The drying rate function on loblolly pine obtained by Milota and Tschernitz (1990) was used in the model. The parameters in the model were set to match the experiments of Milota and Tschernitz (1994) as closely as possible. Physical dimensions of the package and stickers, the initial moisture content, temperature, density, thickness, width and length of each board were set to match those measured (Table 6.2.1.1). The model was run in 30-second steps.

6.2.1.1 Values of the parameters used in the simulation (Loblloly pine).

Parameter	Value
Package height [# of boards]	13
Package width [# of boards]	18
Sticker thickness [in]	0.7
Initial moisture content [%]	130
Initial air dry-bulb temperature [ºF]	90
Initial air wet-bulb temperature [ºF]	70
Initial wood temperature [ºF]	69.5
Wood density[lb/ft^3]	28.1
Board length [ft]	8
Board thickness [in]	1.49
Board width [in]	3.54

The solid lines in the Figures 6.2.1.1, 6.2.1.2, and 6.2.1.3 represent the predicted values from the model and the dashed lines are results obtained from the experiments.

The exact values of average moisture content with time, board centerline temperature, and temperature drop through the package measured in the experiments were not published. Therefore the validation was based on the visual assessment from the comparative charts (Fig. 6.2.1.1, 6.2.1.2, and 6.2.1.3).

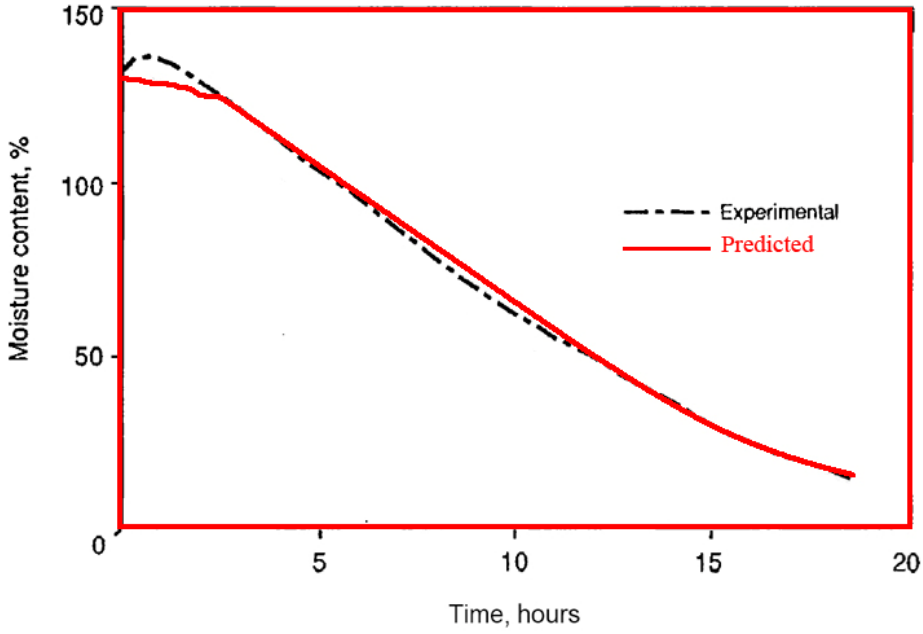

Figure 6.2.1.1 Average moisture content of the package as measured (Milota and Tschernitz 1994) and as predicted by the model.

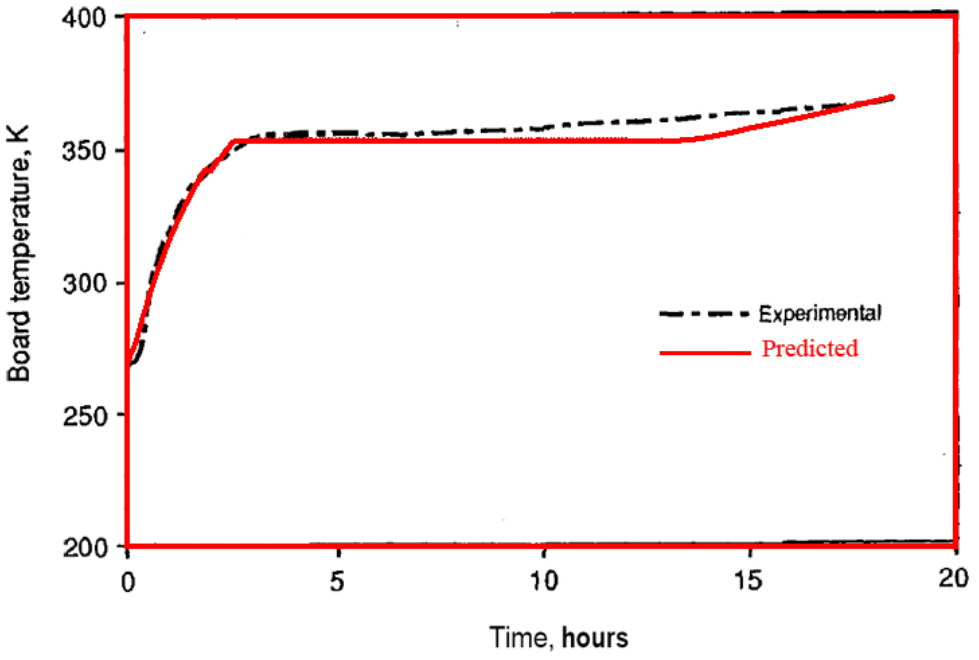

Figure 6.2.1.2 Centerline temperature for center board in the uninterrupted drying experiment as measured (Milota and Tschernitz 1994) and as predicted by the model.

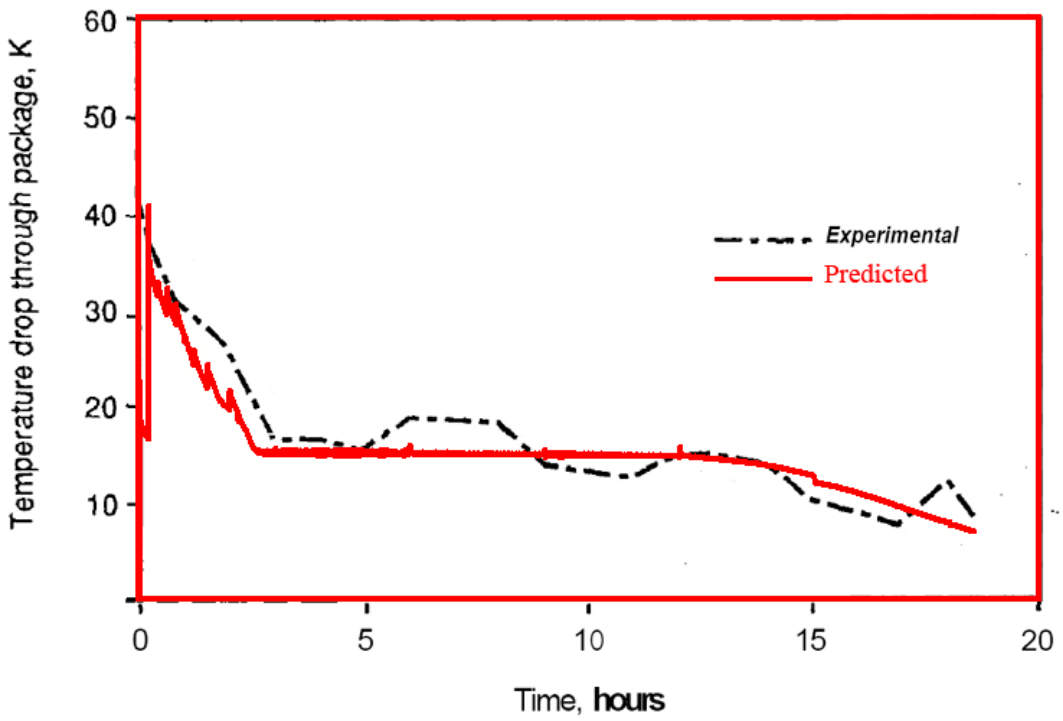

Figure 6.2.1.3 Temperature drop through the package for the uninterrupted drying experiment as measured (Milota and Tschernitz, 1994) and as predicted by the model.

6.2.1.1 Mass Transfer

The predicted and measured average moisture contents showed excellent agreement except at the beginning of the drying process when condensation happened (Fig. 6.2.1.1). The model predicted condensation; however, the parameter c (Eq. 3.5.3) was set so that all the condensed water would run off the wood This is why there the model did not "accumulation" of water or increase in the moisture content of package (Sec. 3.5).

There is also a small deviation from the measured values occurring approximately from 6^{th} to 10^{th} hour of drying. Explanation of this may be in the fact that Milota and Tschernitz (1990) assumed one falling rate period and described it as a

linear function of the difference between the current moisture content and equilibrium moisture content. More advanced drying theory predicts two falling rate periods. Since the two falling rate periods are difficult to describe mathematically it is usually approximated by just one (Chapter 2.1). In general, the model prediction of the average moisture content was quite good and accurate. Regarding the drying time, at 18.55 hours the package was at 12.7% moisture content, which the model predicted would be attained at 18.15 hours which. It gives an error of 2% in the drying time estimation. It can be seen from these results that the model showed a good agreement in both the average moisture content and the drying time.

6.2.1.2 Heat Transfer

The board temperature predicted by the model rose as fast initially as measured and they were in a very good agreement during the whole initial period (Fig. 6.2.1.2). After the first initial period, the board reached T_{wb} for the current drying air condition.

The predicted and measured temperature showed an excellent agreement except a little deviation between 8 and 16 hours when the measured drying rate became greater then predicted one. It happened around 5 hours from the beginning of drying. The greater drying rate resulted lower moisture content which caused the measured board temperature to rise. In spite of that, the deviation of the predicted temperature was not great. When the drying rates became equal which happened around 14 hours from the beginning of drying, the predicted temperature started reaching the measured one.

The agreement between the measured air temperature change through the package (Milota and Tschernitz 1994) and that predicted by the model (Fig. 6.2.1.3) was very good. The peaks on the predicted line during the first three hours of drying were at times when a change in the drying schedule occurred. The system of

governing equations presents an ideal system while the kiln is a real system. At schedule changes, the entering air temperature in the model changes instantly whereas in the kiln it takes some time due to the response time for the heating coils and kiln structure.

The peaks occurring after the initial period occurred when a fan reversal occurred. As with the initial period, due to the ideal nature of the mathematical model a temperature change occurred instantly whereas in the kiln it takes several minutes.

The good agreement in the measured and predicted temperature change along the package helps to verify the overall energy balance around the package and accuracy is also important because many lumber dry kilns use temperature drop along the package as an indicator of moisture content (Milota and Tscchernitz 1994).

6.2.2 Hemlock

For the first charge, the temperatures measured by the kiln controller were used for the entering air temperature. The temperature of the thermocouples placed on the load was used for the other two charges. Physical dimensions of the package and stickers, the initial moisture content, temperature, density, thickness, width and length of each board were set to match those measured (Tables 6.2.2.1, 6.2.2.2, and 6.2.2.3).

The drying rate function obtained from the data analysis in the Chapter 5 was used in the model (Eq. 6.1.4). The model was run in 30-second steps.

6.2.2.1 Values of the parameters used in the simulation (Charge 1).

Parameter	Value
Package height [# of boards]	21
Package width [# of boards]	8
Sticker thickness [in]	0.75
Initial moisture content [%]	Variable (Measured)
Initial air dry-bulb temperature [ºF]	90
Initial air wet-bulb temperature [ºF]	70
Initial wood temperature [ºF]	50
Wood density[lb/ft^3]	26.2
Board length [ft]	16
Board thickness [in]	1.667
Board width [in]	5.861

6.2.2.2 Values of the parameters used in the simulation (Charge 2).

Parameter	Value
Package height [# of boards]	21
Package width [# of boards]	8
Sticker thickness [in]	0.75
Initial moisture content [%]	Variable (Measured)
Initial air dry-bulb temperature [ºF]	90
Initial air wet-bulb temperature [ºF]	70
Initial wood temperature [ºF]	50
Wood density[lb/ft^3]	26.2
Board length [ft]	16
Board thickness [in]	1.668
Board width [in]	5.859

6.2.2.3 Values of the parameters used in the simulation (Charge 3).

Parameter	Value
Package height [# of boards]	21
Package width [# of boards]	8
Sticker thickness [in]	0.75
Initial moisture content [%]	Variable (Measured)
Initial air dry-bulb temperature [ºF]	90
Initial air wet-bulb temperature [ºF]	70
Initial wood temperature [ºF]	50
Wood density[lb/ft^3]	26.2
Board length [ft]	16
Board thickness [in]	1.658
Board width [in]	5.832

6.2.2.1 Mass transfer

The predicted and measured values of average moisture content of the package showed a very good agreement for the second and third charges (maximum 6% relative difference) (Fig. 6.1.2.2.4 and 6.1.2.3.4) while a greater difference between the predicted and experimental values was observed for the first package (maximum 28% relative difference) (Fig. 6.1.2.1.2). The relative difference was obtained as an absolute value of the ratio of the difference between the measured and predicted values and measured values. The reason for this great difference between the predicted and experimental values for the first package may be that the drying flux equation was based on data for which the dry- and wet-bulb temperatures ranged from 160°F to 224°F and from 120°F to 182°F, respectively. The dry-bulb temperature used in the first charge was 230°F and wet-bulb temperature ranged from 190°F to 205°F. These

were out of range of conditions used in obtaining the drying rate function. The drying temperatures for the second and third package were within the range of conditions used to obtain the drying rate function, thereby yielding very good agreement between the predicted and experimental average moisture content versus time curves. Regarding the final moisture content of package, the first package showed the worst agreement again. After the entire drying period set by drying schedules, the absolute difference in predicted and experimental moisture contents were 7.7% for the first, 0.8% for the second and 1.5% moisture content for the third package.

The model assumes that drying behavior does not vary among boards as a result of wood characteristics. Since the model is deterministic, rather than stochastic, the predicted and actual final moisture contents were compared board by board (Fig. 6.1.2.1.3, 6.1.2.2.5, and 6.1.2.3.5). Considering the variability of wood properties (Tables 6.1.2.1.1, 6.1.2.2.1, 6.1.2.3.1) and the fact that the model uses the drying rate function representing an average drying behavior of 14 to 33 boards, the agreement was good. According to the Figures 6.1.2.1.3, 6.1.2.2.5, and 6.1.2.3.5, the model results showed the best agreement with the experimental for the third package.

The relative differences between the standard deviations of the predicted moisture contents and the standard deviations of those measured varied between the charges. For the first charge the relative difference was 63.4%, for the second 10.3% whereas for the third the difference was 15.1%. The relative difference for the first package proves that the drying rate function could not capture the values of drying fluxes for the drying range beyond a range the drying rate function was defined for. The relative difference for the second package was lower than that for the third charge. Based on this and the figures 6.1.2.2.5 and 6.1.2.3.5 it can be concluded that the charge 3 had more boards that were drying very slowly (points spread out to the right horizontally). The points spread out above the line for which predicted values equal experimental, indicate the boards that were drying very fast. The model cannot predict

these abnormal behaviors because the drying rate function is based on the average board behavior. Thus, to model this species and capture the true final moisture content variability, some boards would have to be assigned a different drying rate function or a set of drying rate functions is needed. This might also be true for some of the factors that vary naturally in lumber, such as the amount of heartwood and sapwood in the board.

6.2.2.2 Heat transfer

For the charges 2 and 3, the board centerline temperatures predicted by the model rose almost as fast initially as the measured temperature and they were in good agreement during the whole initial period (Fig. 6.1.2.2.1, 6.1.2.2.2, 6.1.2.3.1, and 6.1.2.3.2). Better agreement in the initial period was reached for the second package where the temperature increase rate deviated just for the first 3 hours while for the third charge it deviated for almost 10 hours until it reached the wet-bulb temperature. After the first initial period, the boards did reach T_{wb} for the current drying air condition. The predicted and measured temperatures showed an excellent agreement. The small deviations could be observed, though. For the second package the greatest absolute deviation was 2ºK (3.6ºF) and it was around 3ºK (5.4ºF) for the third package. They were caused by difference between the experimental and predicted moisture content versus time curves (Fig. 6.1.2.2.4, 6.1.2.3.4). The difference between those curves yielded different experimental and predicted board moisture contents which resulted in different heat capacities for the boards. Therefore the same amount of energy transferred to the board didn't result in the same experimental and predicted board temperature. The model also predicted the temperature drop due to a steam shutdown at 87th hour for the second and 63rd hour of drying for the third charge and due to hot checks at 64th hour for the second and 43rd hour of drying for the third charge (times when the kiln was turned off and the wood moisture content checked

manually). The greater temperature drop in the experimental board temperature compared to the predicted occurred also due to the lower moisture content and heat capacity at those times in the experimental charge.

The measured air temperature change through the package compared favorably to that predicted by the model (Fig. 6.1.2.2.3 and 6.1.2.3.3) in charges two and three. In the first charge (Fig. 6.1.2.1.1), where the drying temperatures used in the experiment were out of range for which the drying rate function was obtained, the agreement was not very good. The absolute difference for that charge was up to 8ºK (14.4ºF). In the case of the second and third charge, there were deviations, too, but they were less. For the second package the maximum absolute difference was 2ºK (3.6ºF) whereas for the third it was 3.3ºK (5.94ºF). But these differences occurred only during the initial periods. As soon as this period ended the absolute differences went down to 0.5ºK (0.9ºF) and less. These differences between the predicted and experimental temperature drops through the package were caused by deviation between the predicted and measured moisture content versus time curves (Fig. 6.1.2.2.4, 6.1.2.3.4).

The peaks that can be noticed on the predicted as well as experimental line during drying were spots when a fan reversal occurred. The predicted line appears noisy because the measured values of drying air obtained directly from the kiln controller were used in the model. Using these, however, enabled the model to simulate the drying process as closely as possible.

From a closer analysis of the charts for the second charge, it can be seen that the same deviation between the predicted and experimental moisture content versus time curve (Fig. 6.1.2.2.4) had a different impact on the difference between experimental and predicted board temperatures (Fig. 6.1.2.2.1 and 6.1.2.2.2) and

temperature drop through the package (Fig. 6.1.2.2.3). The same thing was observed for the third charge.

Due to lower value of the heat capacity of humid air than that of moist wood, humid air and thereby the temperature drop through a package is more sensitive to drying rate value. Both humid air and moist wood are proportional to it but with the difference in the values of the heat capacity as the proportional coefficient. The different values of the heat capacities imply that the same energy applied or taken away will result in different drop or rise of board and air temperature. Therefore, greater deviations can be observed between experimental and predicted values of temperature drop through the package than that of board temperatures.

This is very useful to know when validating the model because beside deviations caused by a model imperfection, errors can also arise when processing the experimental data.

7. Discussion

The model showed a good agreement with the experimental results. However, certain assumptions were made in model developments. To test the sensitivity of the model to the assumptions as well as to some drying parameters the model will be run by changing a certain parameter and keeping all other parameters the same.

The first parameter that will be tested is the coefficient (c) used in the Equation 3.5.3 as fraction of water condensed from drying air when it comes across a board that is at a temperature lower than a dew point. Simulating the condensation is problematic because it is difficult to predict how much of the condensed water will go into the boards and how much will run off.

Due to all these difficulties and the fact that the period during which the condensation occurs is short and happens most often at the beginning of the drying process, the simulation of condensation was simplified. It was assumed that all the condensed water would run off the boards thereby setting a “condensation” coefficient (c) to zero. This assumption caused deviations between predicted and experimental curves (Fig. 6.2.1.1).

To see an impact of parameter (c), its value was changed and a comparative chart was plotted in Figure 7.1 for c ranging from 0 to 0.3.

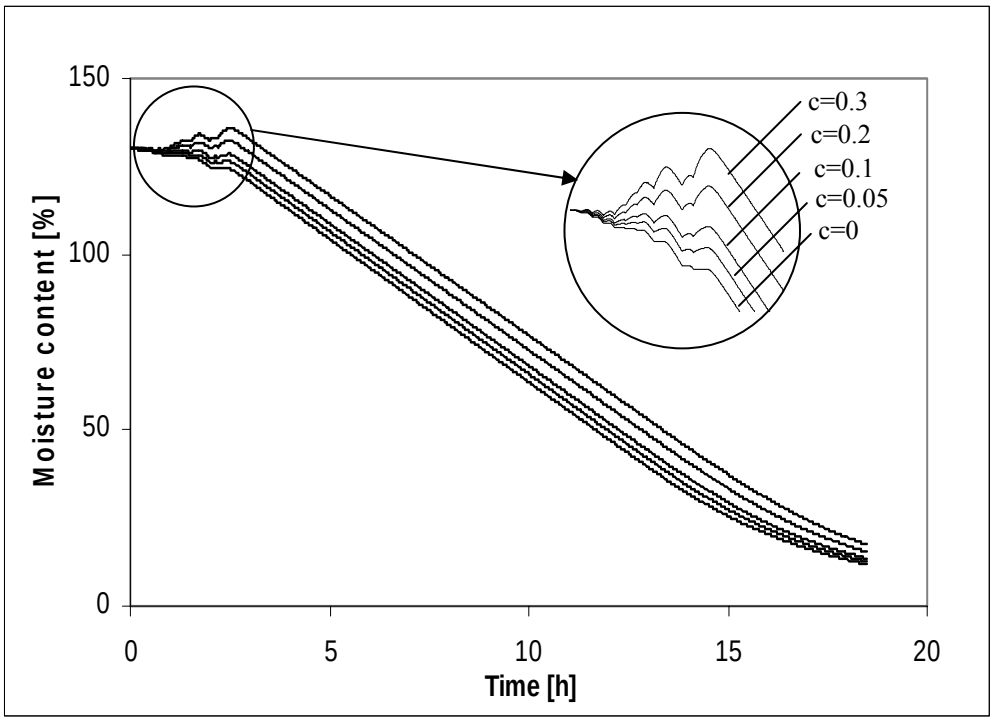

Figure 7.1 Effect of the condensation coefficient on average moisture content prediction.

The lowest line (c=0) is a predicted line in Figure (6.2.1.3). A greater value for the condensation factor yielded a greater response of the model to the condensation. The wave-like lines occurred due to different dry- and wet-bulb temperatures used in the initial period. The moisture level in the initial period did rise but the moisture content level of the entire stack rose as well (2.4% moisture content for each 0.05 step). Therefore, a greater value for condensation coefficient would cause greater deviations between the experimental and predicted lines in a later period of drying. It is likely that the majority of condensed water runs off the boards whereas just a small amount of it goes into the boards.

From these results, it can be concluded that besides the water coming into the boards the problem is also a simulation of the water that does not go into the boards

but moves through the stack. It is hard to simulate because its movement through a stack depends on parameters such as velocity of the drying air, roughness of the boards and size of the drying channels. The effects of the accumulated condensed water in the drying channels on the heat and mass transfer processes makes the simulation of condensation even harder because it can also vaporize during its movement through a stack.

The solution may be in treating the water that does not go into the boards as a moving fluid with heat and mass exchange with the surroundings (boards and drying air) during its movement between boards through a stack. The appropriate simulation of the condensed water accumulated in drying channels between boards would yield an increase in the moisture content level of the entire package but as soon as the condensation stops the moisture level would start decreasing because the condensed water would be taken away by drying air flowing between the boards. It would yield parabolic-like behavior of the average moisture content as it happened in the experiments (Fig. 6.2.1.1).

Beside this, there is one more thing to consider about the condensation. If the package oven-dry weight is around 5000 lbs which was the average weight of the hemlock charges, just one percent moisture content change due to condensation is around 50 lbs of water which is a great amount of water. Therefore, if load cells are used for measuring the average moisture content of the package, there might be possibility that the expansion of wood during the initial warm-up period causes interaction of the package with the surroundings (kiln construction) and thereby applying the additional force to the load cells. The additional force will cause the load cells to indicate an increase in moisture content which may be confused with the condensation.

There were more assumptions made in the modeling (Sec. 3). However, it was hard to test them because either new equations or a new approach in how board and air elements are treated had to be introduced into the model which would require making changes in the main algorithm.

The time step (Δt) was changed to examine for how sensitive the model is in terms of execution time and accuracy. The absolute execution time depends on a computer hardware specification. The relative execution time depends on the main loop defined by the algorithm. Considering that the time step is the counter within the main loop, the execution time increases or decreases inversely with the time step.

Regarding the influence of the time step on accuracy of the model, two parameters were observed, the board temperature and average moisture content of the package (Eq.3.3.2 and 3.5.2). The both equations incorporate the time step within the accumulation term.

From the Figure 7.2, it can be seen what influence a value of the time step has on accuracy of the model. The trend shown during testing was that the greater time step caused the higher average moisture content of the package. The maximum relative difference was around 1.3% with each 15 minute increase of the time step.

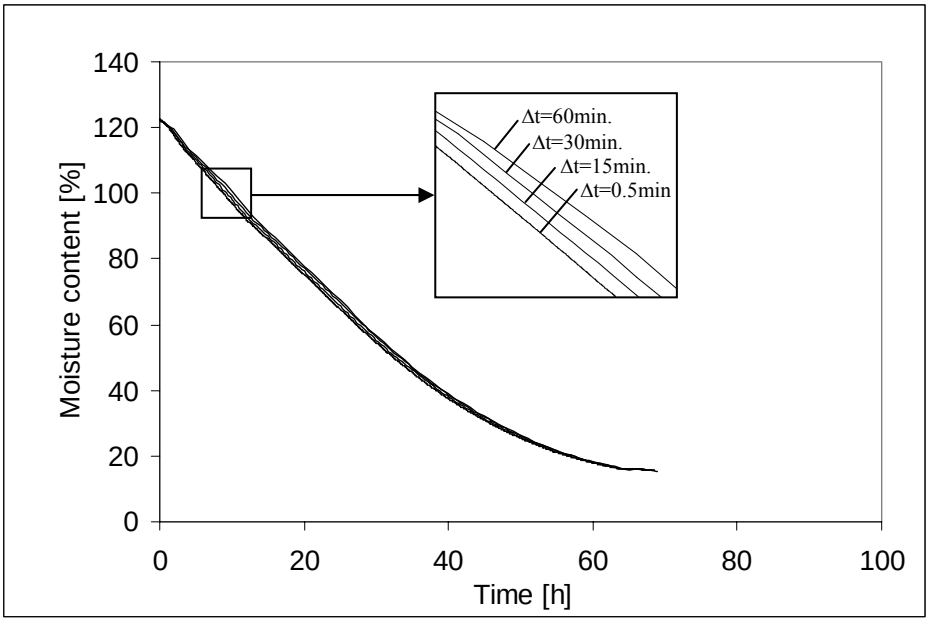

Figure 7.2 Influence of the time step on accuracy of the average moisture content prediction.

The influence of the time step on the board temperature is shown in Figure 7.3. It can be seen that the noticeable difference occurred during the unsteady drying periods. Those periods happened at the beginning of the drying process (up to 10 hours) and when the temperature drops occurred (43^{rd} and 63^{rd} hour of the drying process). This was expected because the time step has an influence on the accumulation term ($\partial T/\partial t$) which greatly changes during the warm-up or cool-down period. It can be also seen that the greater time step yielded the lower rate of temperature increase (Fig. 7.3). This happened because the calculated moisture content levels (Fig. 7.2) were higher for the higher values of the time step causing the heat capacity of the boards to increase. The maximum average relative difference was around 1.3% for each 15 minute increase of the time step.

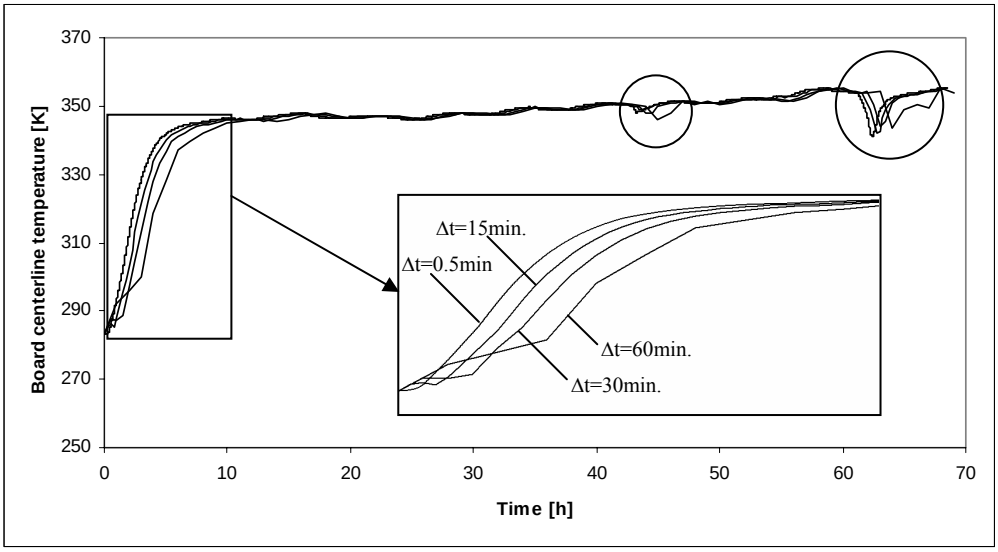

Figure 7.3 Influence of the time step on accuracy of the board temperature prediction.

The next test was how changing the air velocity affected the average moisture content of the package. The drying schedule for the third charge (Table 5.2.2.3) was used where the air velocity for each drying step was changed from the original value to a 60% greater value in 20% steps (Fig 7.4). This relatively small step was used to check how sensitive model is to a velocity change. The first thing that can be observed from the Figure 7.2 is that the model works well in terms of a physical model used in modeling. As expected, the higher velocities yielded greater drying fluxes.

After calculations on drying fluxes and drying times were performed it was found that the 20% velocity increase caused the drying flux to increase by around 3% thereby making the curves steeper. The drying times decreased by around 1.7 hours for each 20% step velocity increase.

The main parameters affected this difference were the convective heat and mass transfer coefficients (h and β). Both of them are functions of the air velocity. A greater

value of the heat transfer coefficient resulted in greater board temperatures which caused the higher drying rate. A grater value of the mass transfer coefficient directly caused the greater drying rate.

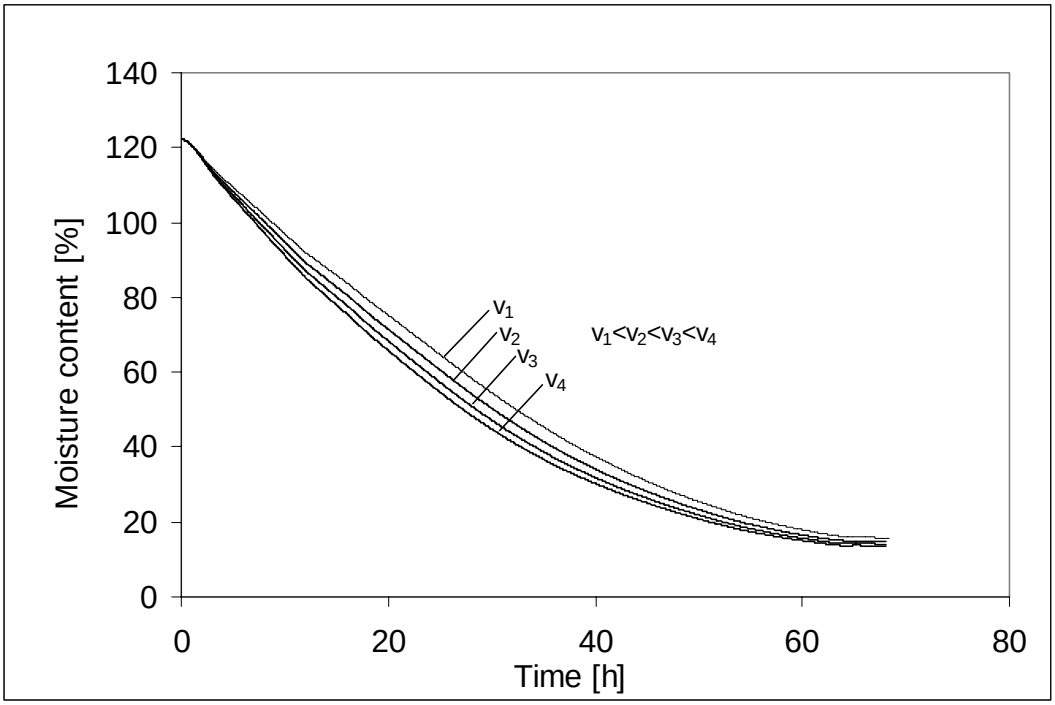

Fig 7.4 Effect of the velocity on average moisture content of the package during drying

Fan reversal times play a big role in wood drying, especially in terms of moisture variability from one side of package to the other. Again, the drying schedule for the third package (Table 5.2.2.3) was used for testing how the model responses to change of fan reversal time. The fan reversal time was changed from 1 to 3 hours by one hour steps. A unidirectional airflow was also used as the extreme case of drying where the drying air does not change a flow direction throughout entire drying process. The ending average moisture contents of each row (21 boards) were plotted versus horizontal board position (Fig. 7.5).

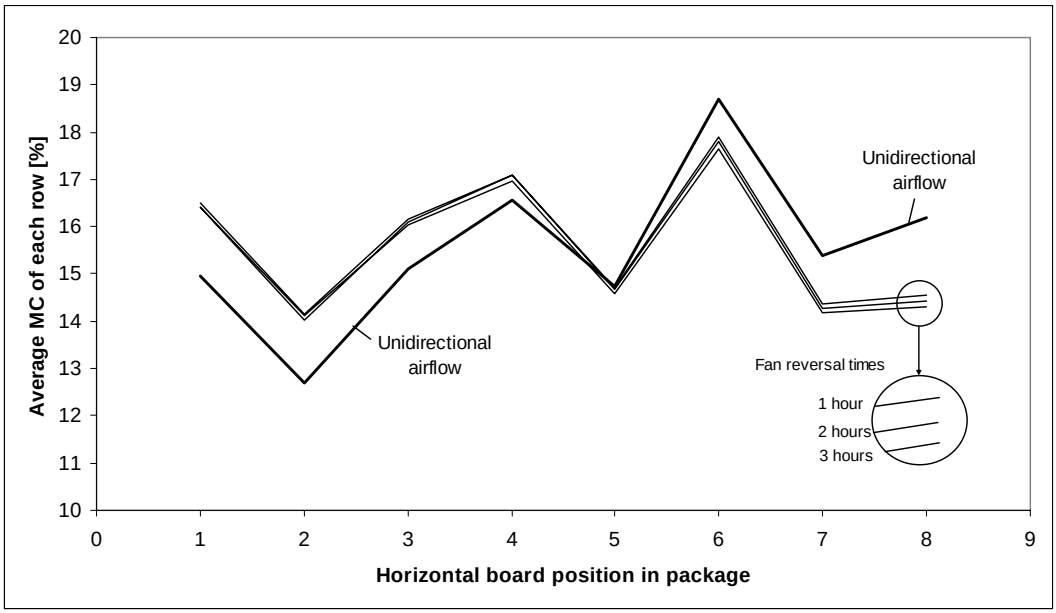

Figure 7.5 Effect of fan reversal times on the average moisture content from one side of the package to the other. Initial airflow was from left to right

There was just a slight difference between the moisture distributions across the stack for one, two, and three hour fan reversal intervals. It was expected that way because the stack was only eight boards wide. It resulted in that the drying air did not increase in absolute humidity much across the stack as well as the temperature drop through the stack was not so high except for the very short initial period (6.1.2.3.3).

So, the boards at the entering and exiting sides of the package were exposed to almost the same external conditions.

As opposed to the case with the different fan reversal times, in the case of the unidirectional airflow the drying air did not change the flow direction thereby exposing the boards at the entering and exiting side of the package to the different

external conditions. Those external conditions did not differ much but 68 hours of exposure to them caused the entering end boards to decrease in the moisture level by around 1.5% moisture content and the exiting end boards to increase by 1.5% as well.

The problem that was observed when comparing the experimental and predicted data (Fig. 6.1.2.1.3, 6.1.2.2.5 and 6.1.2.3.5) was the variability in the drying behavior among boards in a stack due to the variable wood properties (Tables 6.1.2.1.1, 6.1.2.2.1, and 6.1.2.3.1). The issue is that the model uses the same drying rate function for every board. The drying rate function is dependent on the external conditions such as dry- and wet-bulb temperature, the velocity of the drying air as well as moisture content of boards but it represents averaged values of drying fluxes of all the experimental boards. Therefore the drying rate function does not account for the differences in the drying flux between each board caused by variability in wood properties.

The solution may be in defining an additional coefficient that will represent a unique drying feature for each board. This coefficient will account for the difference in a drying flux due to different wood properties caused by knots, grain direction, specific gravity, number of rings per inch and different amount of heartwood and sapwood. However, the model has to be modified to allow introduction and usage of additional coefficient. The moisture variability within a package is very important indicator in terms of quality of drying process and therefore the future work will be mostly focused on solving this problem.

One, at the first glance, not so obvious problem can arise if the inappropriate algorithm is used when modeling. Namely, all the main variables are dependent on each other. Whenever one variable changes all other have to be recalculated. For example, an amount of humidity coming out of a board that air can hold is dependent

on a temperature and pressure of air. Further, a drying rate depends on the air temperature and humidity but also on the board temperature and the board temperature is dependent on the drying rate and air temperature. Therefore, all the governing equations are coupled and all the variables are calculated iteratively as it can be seen from the Figure 4.1. Within each iteration the model checks for how much the variables' values have changed compared to the previous iteration. If the change is lower than the certain predefined value (coupling criterion) then the model performs the next calculation step defined by the algorithm. This is the only way to preserve physics of the drying process. This is very important aspect of the algorithm to ensure that a model can be used for any set of drying conditions.

The value of the coupling criterion used for running the model was 0.0001. Regarding accuracy, the number of the digits after the decimal point determines the number of significant digits in the calculations. It means that for 0.0001 three digits after the decimal point are significant. The simulation was run using the values for the coupling criterion from 0.1 to 0.00000001. No difference was noticed in the accuracy of the model between these runs. However, the value of the coupling criterion should be less than one.

Regarding the execution time, no huge difference was noticed for a range from 0.1 to 0.00000001. The difference in the execution time could not be measured because exporting output data to Excel that is performing during the execution of the simulation takes much more time than time it takes one calculation cycle to couple all the equations thereby masking the time it takes for coupling the governing equations.

As it can be seen, there are good and weak spots and problems that arose in modeling. Of course, wood itself makes modeling even harder with its very complex structure. But even then it is still possible to predict a wood behavior pretty closely to that real. The model predicts all the major drying variables accurately thereby enabling to examine wood drying behavior.

8. Conclusions

The fact and conclusion that the simulation results showed a good agreement with experimental results is not enough because making a simulation is not a goal itself. Therefore from all the comparisons between experimental and simulation results the following conclusions can be made:

a) The wood drying behavior in small charges can be scaled to a full package. Success at this makes it likely that the drying rate function will work in a commercial kiln because the commercial kiln is made up of packages similar in size to what was dried in the lab.

b) The main advantage of the simulation is to enable a user to make conclusions based on its results without needing to conduct time-consuming and expensive experiments. The results from this simulation can be used for the following purposes:

   - Predicting temperature and moisture content of boards accurately during drying which was shown by applying the model on four charges of lumber (Fig. 6.1.2.2.1 to 6.1.2.2.13 and 6.2.1.1 to 6.2.1.3)

   - Revealing how different drying schedules (temperatures, velocities and fan reversal times) affect a wood drying (Fig. 6.1.2.2.1 to 6.1.2.2.13, 6.2.1.1 to 6.2.1.3, 7.2 and 7.3). Since the model does not calculate stresses set up within wood during drying, the schedules should be ones that were already used and tested in terms of stresses.

- Calculating the amount of energy required for heating the drying air that is required for drying a stack of lumber based on the temperature drop through the package (Fig. 6.1.2.2.3 and 6.1.2.3.3) and when this amount of energy s added to amounts of other forms of energy loss within a kiln the total energy required for running the kiln can be calculated (Bogner and Vasiljević 1986)

- Optimizing the drying process in terms of energy used for running fans. This can be done by evaluating how different velocities affect the length of the drying process (Fig. 7.2) and power consumption of the fans

- Choosing the fan reversal time that will provide the best uniformity in drying of the package from both sides (Fig. 7.3)

- Improving the lumber presorting process by estimating the drying time of different boards

- Estimating the impact of the stack geometry change on the drying behavior using the same drying schedules

c) It is impossible to capture different drying properties of each board due to natural variability within a stack by using the drying rate function. Improving the simulation in terms of the variability problem will increase a range of simulation use substantially.

d) A programming language as a part of computer science is a powerful tool in solving the problem of wood drying. However, only a good mathematical

model resulted from sciences such as mathematics, wood science, physics and thermodynamics will ensure that a simulation will give results in a good agreement with experimental results.

Based on the conclusions, the future work will determine how to apply the same simulation for different species accounting for defects and anisotropic nature of wood. This work includes developing of an approach where the simulation is able to "learn" how certain wood species dries based on data already available or data that are easy to obtain such as raw kiln data.

In this way, first, there will be no need to conduct expensive and time consuming controlled experiments where a researcher has to control certain conditions to be able to make valid conclusions. There also will be no need for processing data statistically to obtain a convenient form of the drying rate function used in the simulation because the simulation will be capable of using raw data. In this way, it will be able to treat every board within a stack differently during drying thereby being able to predict variability in moisture content among boards caused by variability in wood properties.

A simulation feature to "learn" how certain material dries based on raw data opens up a possibility for using the same model for simulating the drying process of other materials such as food, building materials or other industrial products that have to be dried prior to use.

From this entire work, it can be concluded that a purpose of simulation is not just to present that it is possible to simulate a certain process in nature by using science laws. It also presents a connection between science and industry which helps in improving the technology level of society. Therefore the simulation must be made and adapted in the way that both science and industry can take advantage of it.

Nomenclature

Symbols:

A - Area of board surface [m^2]

a - Flux parameter [$kg_{H20}/m^2 \cdot s$]

a – Slope of a regression line [$kg/(h \cdot m^2 \cdot K)$]

b - Board thickness [m]

b - Flux parameter [$kg_{H20}/m^2 \cdot s$]

b - Intercept of a regression line [$kg/(h \cdot m^2)$]

c - Specific heat capacity [$J/(kg \cdot K)$]

c - Condensation coefficient [-]

C - Concentration of moisture [kg/m^3]

D - Diffusion coefficient [m^2/s]

D_0 - Constant in Arrhenius relation ($1/s^2$)

E - Energy [J]

$\dot{E}$ - Energy flux [J/s]

Ea – Activation energy [J/mol]

ΔE_w - Heat of sorption [J/kg]

F - Drying rate [kg_{H20}/s]

f - Velocity correlation factor [-]

f – Dimensionless relative drying rate [-]

h - Convective heat transfer coefficient [$W/m^2 \cdot K$]

ΔH - Latent heat of vaporization [J/kg]

i - Specific enthalpy [J/kg]

k - Drying rate constant [h^{-1}]

m - Mass [kg]

N, n - Empirical constants [-]

Nu - Nusselt number

p - Pressure [Pa]

Pr - Prandtl nmber [-]

q - Heat transfer [W]

R - Universal gas constant (8.314 J/mol K)

R_v – Water vapor gas constant (461.5 J/(kg·K))

Re - Reynolds number [-]

Sc - Schmidt number [-]

Sh - Sherwood number [-]

St - Slope of w_D-X curve as X tends to Xeq [$kg_{H2O}/m^2/s/(kg_{H2O}/kg_{OD})$]

ST - Sticker Thickness [m]

S_0 - Constant in Arrhenius relation ($1/s^2$)

T - Temperature [K]

t - Time [s]

V - Volume [m^3]

v - Velocity [m/s]

W - Mass flow rate [kg/s]

w - Weight [kg]

w_D - Drying flux from surface of board [$kg_{H20}/m^2 \cdot s$]

X - Absolute moisture content [kg_{H20}/kgBDS]

x - x axis [m]

Y - Absolute humidity [kg_{H20}/kgDryAir]

Greek symbols:

β – Convective mass transfer coefficient [m/s]

Π - Production term [$kg/(m^3 \cdot s)$]

λ - Thermal conductivity [W/m·K]

μ - Dynamic viscosity [kg/m·s]

μ - Mean [-]

ν - Kinematic viscosity [m^2/s]

ρ - Density [kg/m3]

σ - Standard deviation [-]

Subscripts:

ACC- Accumulated

Al - Liquid water

a - Ambient

B - Dry air

c - Critical

cr – Constant rate

cond - Conduction

conv - Convection

eq - Equilibrium

f - Final

fr – Falling rate

fsp - Fiber Saturation Point

G - Green

g - Gas

GEN - Generated

IN - Input

i - Initial

l – Lower surface

m - Moist solid

OUT - Output

OD - Oven-dry

S - Dry solid

s - Surface

sat – Saturation

u – Upper surface

v - Water vapor

W - Wet bulb

x - x axis

Supercripts:

t - Current time step

Δt – Time period between current and previous time steps

Bibliography

Alvear, M., W. Broche, C. Salinas, and R. Ananias. 2003. Drying Kinetic Of Chilean Coigüe: Study of the Global Drying Coefficient. *In:* Proc. of the IUFRO Wood Drying Conference, Faculty of Wood Industry, Brasov. pp 383-387.

Awadalla, F., F. El-Dib, A. Mohamad, M. Reuss, and S. Hussein. 2004. Mathematical Modeling and Experimental Verification of Wood Drying Process. Energy Conservation and Management. 45(2):197-207.

Baronas, R., F. Ivanauskas, I. Juodeikiene, and A. Kajalavicius. 2001. Modeling of Moisture Movement in Wood during Outdoor Storage. Nonlinear Analysis: Modeling and Control. 6(2):3-14.

Baronas, R.,F Ivanauskas, and M. Sapagovas. 1999. Modeling of Wood Drying and an Influence of Lumber Geometry on Drying Dynamics. Nonlinear Analysis: Modeling and Control. 4(2):11-22.

Belhanri, A. 2003. Characterization of the First Falling Rate Period during Drying of a Porous Material. Drying Technology. 21(7):1235–1252.

Berger, D. and Pei D. 1972. Drying of Hygroscopic Capillary Porous Solids-A Theoretical Approach. International Journal of Heat & Mass Transfer. 16(1):293-302.

Bramhall, G. 1978. Mathematical Model for Lumber Drying. I. Principles Involved. Wood Science. 12(2):14-21.

Bogner, M. and B. Vasiljević. 1986. Drying Theory Basics. Procesna Tehnika. 1(2):77-85.

Bowyer, J., R. Shmulsky, and J. Haygreen. 2003. Forest Products and Wood Science. Iowa State Press, Ames, IA. 568 pp.

Cadiergues, R. 1977. Thermodynamic Properties of Moist Air : Choice Justification. Etudes Thermiques et Aerauliques. 8(2):70-88.

Chen, G., R. Keey, and J. Walker. 1996. Moisture Content Profiles in Sapwood Boards on Drying. *In:* Proc. of the International Drying Symposium, Krakow. pp. 679-687.

Cronin, P., K. Abodayeh , and J. Caro-Corrales. 2002. Probabilistic Analysis and Design of the Industrial Timber Drying Process. Drying Technology. 20 (2):307-324.

Cronin, P., P. Baucour., K. Abodayeh, and A. Barbot Da Silva. 2003. Probabilistic Analysis of Timber Drying Schedules. Drying Technology. 27(8):1435-1458.

Davis, C., C. Carrington, and Z. Sun. 2002. The Influence of Compression Wood on the Drying Curves of Pinus radiata Dried in Dehumidifier Conditions. Drying Technology. 20(10):2005–2026.

Forest Products Laboratory. 1999. Wood handbook—Wood as an engineering material. Gen.Tech. Rep. FPL–GTR–113. Madison, WI: U.S. Department of Agriculture, Forest Service, Forest Products Laboratory. 463 p.

Elustondo, D. and S. Avramidis. 2005. Comparative Analysis of Three Methods for Stochastic Lumber Drying Simulation, Drying Technology. 23(1&2):131-142.

Erriguible, A., P. Bernada, F. Couture , and M. Roques. 2005. Modeling of Heat and Mass Transfer at the Boundary between a Porous Medium and its Surroundings, Drying Technology. 23(3):455-472.

Hart, A. 1964. Principles of Moisture Movement in Wood. Forest Product Journal. 14(5):207-214.

Hashimoto, A., S. Stenstrom, and T. Kameoka. 2003. Simulation of Convective Drying of Wet Porous Materials, Drying Technology. 21(8):1411–1431.

Incropera, F. and D. Dewitt. 1996. Introduction to Heat Transfer. John Wiley and Sons, New York. 801 pp.

Kanevce, G., Lj. Kanevce, G. Dulikravich, and H. Orlande. 2002. Estimation of Thermophysical Properties of Moist Materials under Different Drying Conditions. Inverse Problems in Science and Engineering. 13(4):341 – 353.

Kayihan, F. 1982. Simultaneous Heat and Mass Transfer with Local Three-phase Equilibria in Wood Drying. *In*: Proc. International Drying Symposium. Proc. No. 3. Birmingham. pp. 123-134.

Kayihan, F. 1985. Stochastic Modeling of Lumber Drying in Batch Kilns. *In:* Proc. Drying. Washington: DC. pp. 368-375.

Keey, R. and Asworth J. 1979. The Kiln Seasoning of Softwood Timber Boards. Chemical Engineering. 1(347/8):593-598

Liu, J., W. Simpson, and S. Verrill. 2000. An Inverse Moisture Diffusion Algorithm for the Determination of Diffusion Coefficient. Drying Technology. 19(8):1555–1568.

Luikov, A. 1975. Systems of Differential Equations of Heat and Mass Transfer in Capillary-Porous Bodies (Review). International Journal of Heat & Mass Transfer. 18(1):1-14.

Meel, D. 1958. Adiabatic Convection Batch Drying with Recirculation of Air. Chemical Engineering Science. 9(1):36-44.

Meroney, R. 1969. The State of Moisture Transport Rate Calculations in Wood Drying. Wood and Fiber. 1(1):64-74.

Milota, M. and P. Mosher. 2006. Emissions from western hemlock Lumber During Drying. Forest Product Journal. 56(5):66-70.

Milota , M. 2007. Personal Communication.

Milota, M. and L. Tschernitz. 1990. Correlation of loblolly pine Drying Rates at High Temperatures. Wood and Fiber Science. 22(3):298-313.

Milota, M. and L. Tschernitz. 1994. Simulation of Drying in a Batch Lumber Kiln from single-board test. Drying Technology. 12(8):2027-2055.

Mujumdar, A. and Devahastin S. 2000. Practical Guide to Industrial Drying. Exergex Corporation, Montreal. 187 pp.

Pang, S. 2002. Investigation of effects of wood variability and rheological properties on lumber drying: application of mathematical models. Chemical Engineering Journal. 86(1&2):103–110.

Pang, S., B. Keey, and G. Langrish. 1992. Modeling the Temperature Profiles within Boards during the High-temperature Drying of Pinus radiata timber: the Influence of Airflow Reversals, Heat Mass Transfer Journal. 38(2):189-205.

Pang, S. 2005. Development, Validation and Practical Application of Mathematical Models for Wood Drying. *In:* Proc. of the IUFRO Wood Drying Conference. Faculty of Wood Science and Technology, Nanjing, pp. 39-49.

Pang, S. and A. Haslett. 1997. High-Temperature Kiln Drying of Softwood Timber: The Role of Mathematical Modeling. *In:* Mathematical Modeling and Numerical Techniques in Drying Technology. Marcel Dekker, New York. pp. 179-219.

Patankar, S. 1980. Numerical heat transfer and fluid flow. McGRAW-HILL Book Company, New York. 197 pp.

Perre, P. and I. Turner. 1997. The Use of Macroscopic Equations To Simulate Heat And Mass Transfer In Porous Media: Some Possibilities Illustrated by A Wide Range of Configurations that Emphasize the Role of Internal Pressure. *In:* Mathematical Modeling and Numerical Techniques in Drying Technology. Marcel Dekker, New York. pp. 83-156.

Perre P. and I. Turner. 1999. A 3-D version of TransPore: a comprehensive heat and mass transfer computational model for simulating the drying of porous media. International Journal of Heat and Mass Transfer. 42(24):4501-4521

Perre, P. and I. Turner. 2002. A Heterogeneous Wood Drying Computational Model That Accounts for Material Property Variation Across Growth Rings. Chemical Engineering Journal. 86(1&2):117–131.

Perre, P., I. Turner, and J. Passard. 1999. 2-D Solution for Drying with Internal Vaporization of Anisotropic Media. AIChE Journal. 45(1):13-26.

Pinheiro, C., T. Raad, and M. Yoshida. 1998. Model of a Process for Drying Eucalyptus spp at High Temperatures. Chemical Engineering Journal. 15(4):382-395.

Plumb, O. and L. Gong. 1996. Modeling the Effect of Heterogeneity on Wood Drying. *In:* Mathematical Modeling and Numerical Techniques in Drying Technology. Marcel Dekker, New York. pp. 221-258.

Raisul, I., J. Ho, and A. Mujumdar. 2003. Convective Drying with Time-Varying Heat Input: Simulation Results. Drying Technology. 21(7):1333–1356.

Rohsenow, M. and P. Hartnett. 1973. Handbook of Heat Transfer. McGraw-Hill, New York, 1344 pp.

Skaar, C. 1991. Heats of transfer and activation energy for bound water diffusion in wood. Wood Science and Technology. 25(3):193-202.

Spencer, H. 1969. A Mathematical Simulation of Grain Drying. Journal of Agricultural Engineering Research. 14(3):226-235.

Stamm, A. and Nelson R. 1961. Comparison Between Measured and Theoretical Drying Diffusion Coefficients for Southern Pine. Forest Products Journal. 11(1):536-543.

Stanish, A., S. Schajer, and F. Kayihan. 1986. A Mathematical Model of Drying for Hygroscopic Porous Media. AIChE Journal. 32(8):1301-1311.

Sun, F., G. Carrington, C. Davis, Q. Sun, and S. Pang. 2005. Mathematical Modeling and Experimental Investigation of Dehumidifier Drying of Radiata pine Timber. Maderas. Ciencia y Technologia. 7(2):87-98.

Thomas, H., Lewis R. and Morgan K. 1980. An Application of the Finite Element Method to the Drying of Timber. Wood and Fiber. 11(4):237-243.

Treybal, R.1980. Mass-Transfer Operations. McGraw-Hill, New York. 784 pp.

Welty, J., C. Wicks, and R. Wilson. 1984. Fundamentals of Momentum, Heat, and Mass Transfer. John Willey & Sons, New York. 803 pp.

Yaws, L. 1999. Chemical Properties. McGraw-Hill, New York. 779 pp.

Yrjola, J. and J. Saastamoinen. 2002. Modelling and Practical Operation Results of a Dryer for Wood Chips. Drying Technology. 20(6):1077–1099.

Zhang, J. and A. Datta. 2004. Some Considerations in Modeling of Moisture Transport in Heating of Hygroscopic Materials. Drying Technology. 22(8):1983–2008.

Zhang, Z., S. Yang, and D. Liu. 1999. Mechanism and Mathematical Model of Heat and Mass Transfer during Convective Drying of Porous Materials. Scripta Technica. Heat Trans Asian Res. 28(5):337-351.